The influence of meltwater on the thermal structure and flow of the Greenland Ice Sheet

Kristin Poinar

A dissertation
submitted in partial fulfillment of the
requirements for the degree of

Doctor of Philosophy

University of Washington

2015

Reading Committee:

Ian R. Joughin, Chair

Michelle R. Koutnik

Benjamin E. Smith

Edwin D. Waddington

Program Authorized to Offer Degree:
Earth and Space Sciences

University of Washington

Abstract

The influence of meltwater
on the thermal structure and flow of the Greenland Ice Sheet

Kristin Poinar

Chair of the Supervisory Committee:
Senior Principal Engineer Ian R. Joughin
Applied Physics Laboratory

As the climate has warmed over the past decades, the amount of melt on the Greenland Ice Sheet has increased, and areas higher on the ice sheet have begun to melt regularly. This increase in melt has been hypothesized to enhance ice flow in myriad ways, including through basal lubrication and englacial refreezing. By developing and interpreting thermal ice-sheet models and analyzing remote sensing data, I evaluate the effect of these processes on ice flow and sea-level rise from the Greenland Ice Sheet.

I first develop a thermal ice sheet model that is applicable to western Greenland. Key components of this model are its treatment of multiple phases (solid ice and liquid water) and its viscosity-dependent velocity field. I apply the model to Jakobshavn Isbræ, a fast-flowing outlet glacier. This is an important benchmark for my model, which I next apply to the topics outlined above.

I use the thermal model to calculate the effect of englacial latent-heat transfer (meltwater refreezing within englacial features such as firn and crevasses) on ice dynamics in western Greenland. I find that in slow-moving areas, this can significantly warm the ice, but that englacial latent heat transfer has only a minimal effect on ice motion ($<$10%). By contrast, in fast-flowing regions, which contribute most ($>$60%) of the ice flux into the ocean, evidence of deep englacial warming is virtually absent. Thus, the effects of

englacial latent heat transfer on ice motion are likely limited to slow-moving regions, which limits its importance to ice-sheet mass balance.

Next, I couple a model for ice fracture to a modified version of my thermal model to calculate the depth and shape evolution of water-filled crevasses that form in crevasse fields. At most elevations and for typical water input volumes, crevasses penetrate to the top $\sim$200–300 meters depth, warm the ice there by $\sim$10°C, and may persist englacially, in a liquid state, for multiple decades. The surface hydrological network limits the amount of water that can reach most crevasses. We find that the depth and longevity of such crevasses is relatively robust to realistic increases in melt volumes over the coming century, so that we should not expect large changes in the englacial hydrological system under near-future climate regimes. These inferences put important constraints on the timescales of the Greenland supraglacial-to-subglacial water cycle.

Finally, I assess the likelihood that higher-elevation surface melt could deliver water to regions where the bed is currently frozen. This hypothetical process is important because it could potentially greatly accelerate the seaward motion of the ice sheet. By analyzing surface strain rates and comparing them to my modeled basal temperature field, I find that this scenario is unlikely to occur: the conditions necessary to form surface-to-bed conduits are rarely found at higher elevations ($>\sim$1600 meters) that may overlie frozen beds.

TABLE OF CONTENTS

Page

List of Figures v

List of Tables vii

Chapter 1: Introduction 1
1.1 Scientific and societal motivation 2
1.2 Research approaches and tools 3
1.3 Glossary 5
1.4 Organization of the dissertation 7
1.5 Expertise 8

Chapter 2: Ice temperatures and deformational motion of Jakobshavn Isbræ . . . 9
2.1 Polythermal ice systems 10
2.2 Description of polythermal model for englacial temperature 11
2.2.1 Horizontal velocity field 12
2.2.2 Vertical velocity field 13
2.2.3 Shear heating and basal shear stress 15
2.2.4 Flow law parameter, including water content 17
2.2.5 Polythermal mode 18
2.3 Model Evaluation and Tuning 27
2.3.1 Vertical velocity 27
2.3.2 Deformational heating 29
2.4 Application to Jakobshavn Isbræ 30
2.5 Conclusion 33

Chapter 3: The contribution of englacial latent heat transfer to seaward ice flux in western Greenland 35

3.1 Introduction . . . 36
3.2 Study Area in Western Greenland . . . 40
3.3 Methods . . . 42
3.3.1 Temperature model without englacial latent heat transfer . . . 42
3.4 Results . . . 48
3.4.1 Model results from Jakobshavn Isbræ . . . 48
3.4.2 Model results from Pâkitsoq . . . 51
3.5 Scaling over western Greenland . . . 58
3.5.1 Time spent in the ablation zone . . . 58
3.5.2 Weighting for ice flux . . . 61
3.6 Discussion . . . 62
3.6.1 Latent heat transfer in firn . . . 62
3.6.2 Englacial temperatures in Pâkitsoq . . . 64
3.6.3 Context for field measurements of cryo-hydrologic warming . . . 66
3.6.4 Ice-sheet-wide interpretation . . . 67
3.7 Conclusion . . . 68

Chapter 4: Constraints on the storage of surface meltwater in Greenland crevasses 69
4.1 Introduction . . . 70
4.2 Methods . . . 71
4.2.1 Characteristics of the Swiss Camp study area . . . 72
4.2.2 Model for crevasse depth and shape . . . 74
4.2.3 Thermal model for englacial refreezing rates . . . 75
4.2.4 Englacial refreezing rates informed by field observations . . . 76
4.3 Results . . . 78
4.3.1 Sensitivity tests . . . 78
4.3.2 Annual freeze-up . . . 80
4.3.3 Englacial water storage . . . 80
4.3.4 Full-thickness penetration . . . 82
4.3.5 Depth of typical crevasses . . . 83
4.3.6 Effect on ice temperature . . . 85
4.4 Discussion . . . 85
4.5 Conclusion . . . 88

4.6 Model Details . . . 89
4.6.1 Elastic component of the model . . . 89
4.6.2 Effect of creep closure on crevasse depth . . . 90
4.6.3 Thermal component of the model . . . 91
4.7 Inferred englacial refreezing rates in the Swiss Camp region . . . 92
4.8 Crevasse depths at higher and lower elevations . . . 93

Chapter 5: Limits to future expansion of surface-melt-enhanced ice flow into the interior of western Greenland . . . 96
5.1 Introduction . . . 97
5.2 Extent of Wet Bed . . . 98
5.3 Expansion of Surface Melt . . . 98
5.4 Variations in Supraglacial Lakes and Streams with Elevation . . . 99
5.5 Variation of Strain Rate with Elevation . . . 100
5.6 Discussion . . . 101
5.6.1 Limitation to High-Elevation Hydrofracture . . . 102
5.6.2 Effect of New Meltwater at the Bed . . . 103
5.7 Conclusions . . . 103
5.8 Supporting Information . . . 106
5.8.1 Methods . . . 106
5.8.2 Model for the thermal state of the bed . . . 106
5.8.3 Climatological analysis of the change in surface melt extent . . . 108
5.8.4 Inland migration distance of the ELA . . . 111
5.8.5 Identification of surface features . . . 111
5.8.6 Strain rate dataset . . . 113

Chapter 6: Synthesis and Conclusion . . . 120
6.1 Summary of research contributions . . . 121
6.2 Generalization and pattern of my scientific contributions . . . 123
6.3 Application of methods to other geophysical research areas . . . 124
6.3.1 Thermodynamics of mantle melts . . . 124
6.3.2 Mechanics of mantle plumes and dikes . . . 125
6.3.3 Phase changes in permafrost . . . 127
6.4 Potential questions for further research . . . 129

6.4.1 Explanation of warm basal ice in Southwest Greenland 129
6.4.2 The timescale of cryo-hydrologic warming 130
6.4.3 Moulin formation on a drastically different Greenland Ice Sheet . . . 131
6.4.4 Why do moulins form where they do? 132
6.4.5 What is the subsurface character of a moulin? 134
6.5 Thesis summary 135
6.6 Relevance to Greenland Ice Sheet hydrology 136

LIST OF FIGURES

Figure Number Page

2.1 Vertical velocities . . . 14
2.2 Driving stress and basal shear stress along the centerline of Jakobshavn Isbræ 16
2.3 Schematic of polythermal ice thermodynamics . . . 20
2.4 Bisection scheme used to locate the CTS . . . 24
2.5 Isochrones in Pâkitsoq . . . 28
2.6 Convergent flow in Jakobshavn Isbræ . . . 31
2.7 Modeled temperatures in Jakobshavn Isbræ . . . 33

3.1 Study area and flow regimes in central western Greenland . . . 41
3.2 Illustration of boundary conditions and prescribed temperatures . . . 43
3.3 Boundary conditions versus surface elevation . . . 45
3.4 Model results for Jakobshavn Isbræ . . . 50
3.5 Model results for higher-elevation Pâkitsoq sites . . . 52
3.6 Model results for lower-elevation Pâkitsoq sites . . . 53
3.7 Maps of time spent in the ablation zone . . . 59
3.8 Cumulative histogram of ice flux through central western Greenland . . . 61

4.1 Crevasse fields in western Greenland . . . 73
4.2 Evolution of a water-filled crevasse . . . 77
4.3 Englacial drainage regimes versus meltwater influx and time . . . 81
4.4 Volumetric influx as a function of englacial refreezing rate . . . 84
4.5 Englacial drainage regimes for high-elevation ice . . . 94
4.6 Englacial drainage regimes for low-elevation ice . . . 95

5.1 Locations of supraglacial lakes and modeled wet-bedded areas . . . 98
5.2 Annual surface melt and surface mass balance vs. elevation . . . 99
5.3 Surface hydrologic features at various elevations from satellite images . . . 100
5.4 Strain rates in map view, as histograms, and as a function of elevation . . . 101

5.5 Lakes and streams in southwestern Greenland in Landsat imagery 115
5.6 Stream length as a function of elevation 116
6.1 Similarity of thermal systems: polythermal ice and mantle melts 126
6.2 Similarity of mechanical systems: water-filled crevasses 127
6.3 Similarity of mechanical systems: magma-filled dikes 128
6.4 Schematic of moulin formation regions 133

LIST OF TABLES

Table Number Page

3.1 Model parameters and results for Jakobshavn and Pâkitsoq boreholes 49

4.1 Sensitivity of crevasse depth to various parameters 79

ACKNOWLEDGMENTS

I am grateful my advisor, Ian Joughin, for his support over the years. He has been so very generous with his time and ideas. As a supervisor, he has walked the fine line between pushing me toward rigor while also encouraging me that I was capable of the work, even when I wasn't so sure I believed so. Ian has also been an excellent role model. I aspire to his level of critical thinking and hard work.

I would like to thank my committee for their work in preparing me as a scientist and for their academic support.

Ben Smith has been an excellent office neighbor – an expert in many special topics, Ben is always jovial through his open door.

Ed Waddington taught me glaciology from square one and stressed the importance of thinking through all the details of numerical modeling. He also encouraged me to keep developing myself as a teacher and, to that end, gave me annual chances to experiment with his undergraduate glaciology class.

Michelle Koutnik, in particular, has given me great support, especially during these past few months when I needed it most. Her willingness to really ask how it's going has led to many helpful and pleasant conversations, and her mindset as a young asker of big questions has greatly influenced my own development as a young researcher.

Twit Conway has also encouraged me in my work, but unfortunately, my December defense date precluded his presence on my final committee.[1]

[1]Twit spends Northern Hemisphere winters in Antarctica with incredible consistency.

I was fortunate to be surrounded by an excellent cadre of fellow graduate students during my time here at the University of Washington.

My glaciology cohort, Brooke Medley and T.J. Fudge, over the years have given me equal parts of pleasant collaboration (Olympic National Park field work, NASA applications) and the sort of teasing that only siblings should get away with.

My many officemates, Max Stevens, Emily Newsom, Jessica Lundin, Aurora Burd, Dave Shean, David Lilien, Laura Kehrl, and Daniel Shapero, have made work academically interesting and fun, even on days when the work itself may have kept me away.

Regina Carns and I have spent many AGUs together and, more recently, I have enjoyed her company over the midnight oil in Benjamin Hall.

I would also like to thank Emma Kahle, a late but treasured addition to my glaciology network and my nationally competitive frisbee family.

Though most of them may never read this document, I also owe thanks to the members of the Seattle ultimate frisbee community. From our department team the Red Hot Igneous Intrusions through the friendly faces of Boom and Barrel of Monkeys, the aptly named Seattle Freeze, and the driven women of Seattle Underground and Seattle Mint, this sport has given me thousands of hours of enjoyment and has improved me as an athlete, goal setter, and citizen. I'd like to acknowledge Washington Element and Toolbox in particular as the teams that have meant the most to me and whom I will most miss.

Finally, I would like to acknowledge and thank the National Science Foundation Graduate Research Fellowship Program, the Center for Remote Sensing of Ice Sheets, and the University of Washington Program on Climate Change for providing funding that made my work possible.

DEDICATION

To my family,
Kay, Tom, Melanie, and Mark,
who always thought I would do something good,

and Kate and Denny,
who have been like a family in Seattle.

Chapter 1

INTRODUCTION

Meltwater and ice flow interact in Greenland, making interesting systems to study. Greenland ice loss translates directly to sea-level rise, which affects us all.

1.1 Scientific and societal motivation

The Greenland Ice Sheet has been a major focus within the global climate community over the past decade (e.g., IPCC, 2007, 2014) due to its potential near-term contribution to global sea level (e.g., Csatho et al., 2014). The ice sheet contributes approximately 0.7 mm to global sea levels each year (van den Broeke et al., 2009), through both melting and calving. These processes have long contributed approximately equally to the mass balance, but there is now evidence that the relative proportion of mass loss by surface melt is increasing (Enderlin et al., 2014; Tedesco et al., 2013). Record melt in 2012 made headlines worldwide, bringing the Greenland Ice Sheet even more into public awareness[1].

Surface melting is important in its own right. Interestingly, though, surface melt may form feedbacks with ice dynamics. In such a scenario, if increased surface melting enhanced ice speeds, this would increase dynamic mass loss, which would further lower the ice-sheet elevation. The higher temperatures found at lower elevations would, in turn, accelerate the rate of surface melt, and the processes would grow in step.

The potential positive feedback between melt and ice dynamics would need a trigger: a mechanism by which increased melt could initially enhance ice speeds. Previous workers have identified a number of potential mechanisms. One is the lubrication of dry (or, equivalently, frozen) beds – cold ice that is stuck to its bed often does not move as quickly as warm ice that can slide across the bed.[2] If surface melt were to reach the bed in a frozen area, the latent heat could warm the bed to the melting point, permitting faster sliding and setting off the positive feedback.

A second mechanism whereby surface melt could trigger faster ice motion is "cryo-

[1]With the perspective of the years following 2012, though, it seems that the 2012 melt rates were an anomaly rather than indicative of a particular new trend (Bennartz et al., 2013).

[2]Of course, there are interesting edge cases – for example, local "sticky spots" within an otherwise slippery bed can gain traction on the ice above it and, through deformation of the overlying ice column, cause the ice at the ice-sheet surface to flow faster than the surrounding ice, which is in plug flow. Similarly, the ice-sheet surface above Antarctic subglacial lakes, which are well-lubricated patches in a field of high basal friction, moves more slowly. But over larger-than-local scales, a wet bed almost always enhances ice motion.

hydrologic warming". This concept also involves the latent heat of meltwater, but in this case the energy transfer is *within* the ice sheet rather than beneath it. Surface melt is hypothesized to enter the ice sheet through crevasses, where it can refreeze and warm the ice. Like honey, ice has a temperature-dependent constitutive relation – that is, the warmer it is, the softer it is. Pouring cold honey is difficult, while warmer honey flows more freely; it is the same for ice sheets. An increase in the magnitude or extent of cryo-hydrologic warming (which I also call "englacial latent heat transfer" in this thesis) may also trigger the positive feedback between melt and ice motion. We have already seen that surface melt is increasing, and in fact, shifting flow patterns appear to have increased the number and extent of crevasses on some areas of the ice sheet surface (e.g., Colgan et al., 2011).

These two processes – latent heat transfer to the bottom of the glacier, and latent heat transfer within the glacier – were recently identified by the IPCC (2014) as current unknowns with possible implications for the stability of the Greenland Ice Sheet and thus global sea level. My work has been to investigate these processes and to evaluate their potential to contribute to the mass balance of the ice sheet in the coming decades to millennia. Latent heat transfer is not the only process that affects the mass balance of the ice sheet, but it is my focus here.

1.2 Research approaches and tools

I approach these problems from a physical perspective. The scientific community understands certain things very well – the nature of heat transfer, for instance, or the physical processes that contribute to observable motion of a continuum – and has understood them for a very long time. Thus, not only are the concepts well established, but many tools for applying the concepts (e.g., numerical methods) have already been developed. Standing on the shoulders of giants, who themselves are atop the giants who came before them, is an appealing way to do science.

Observational data motivate the problem – for instance, unexpectedly warm temper-

atures measured in a borehole. What heat source is responsible? How long has that heat source likely been in operation? These questions lend themselves well to simple models that incorporate well-understood physical processes.

I also rely on remote-sensing and field observations to implement the model. Boundary conditions for the models are an obvious place where data are required; using observations to constrain the output of the model are another.

My models are intentionally as simple as the problem allows. Such models are sometimes termed "process-scale", in contrast to "systemic" models that incorporate all the processes within, say, the system of ice-sheet surface mass balance. While I do not discount the value of systemic models, my contributions have been on the process scale. Studies such as mine of these new processes pave the way for incorporation into large-scale ice-sheet models.

1.3 Glossary

ABLATION ZONE: The portion of a glacier or ice sheet where the net loss of mass exceeds the mass gained by snowfall, on average, each year. The mass loss is usually due to melting, but sublimation can also contribute. The ablation zone occupies the lower reaches of the glacier.

ACCUMULATION ZONE: The portion of a glacier or ice sheet where the average annual mass change is positive; that is, where snowfall exceeds melting and sublimation.

CALVING: The process by which solid ice flows into the ocean. Calving occurs on outlet glaciers and produces icebergs.

COLD ICE: Ice whose temperature is below the melting point.

CREVASSE: A brittle fracture, usually vertical or near-vertical, in an ice sheet. Crevasses are usually much narrower (centimeters to meters) than they are long (kilometers) or deep (tens to hundreds of meters). Crevasses can form on the top surface (surface crevasses, which this thesis primarily addresses) or subglacially (basal crevasses).

CREVASSE FIELD: Multiple surface crevasses that occupy the same region of the ice sheet. Tens to hundreds or more surface crevasses may make up a crevasse field, which can span up to some kilometers.

ENGLACIAL: Within a glacier or ice sheet. Contrast with *subglacial* and *supraglacial*.

EQUILIBRIUM LINE: The location on the surface of the ice sheet where average accumulation is equal to average ablation. Also referred to as "equilibrium line altitude" or ELA.

FIRN: An icy substance on the continuum between snow (low density) and glacier ice (high density). Firn consists of densely packed snow grains that have begun to metamorphose into solid ice, but that retains intragranular pore space through which air or water can circulate.

FLOWLINE: The path a parcel of ice will take from its origin on the ice sheet (where it originally fell as snow) to its terminus (either by melting or calving).

ICE SHEET: A continental- or near-continental-scale glacier. The earth currently has three ice sheets: the West Antarctic, East Antarctic, and Greenland Ice Sheets.

MELTING POINT: The temperature where both liquid and solid phases of water / ice can coexist. The melting point is a function of pressure, and thus its temperature is commonly denoted as T_{pmp}, where $_{pmp}$ indicates "pressure melting point." Under 1000 m of ice, for instance, the higher pressure lowers the melting point to $-0.87°C$.

MOULIN: A vertical conduit or shaft in a glacier that hydrologically connects the top surface to the bed.

OUTLET GLACIER: A region along the coast of an ice-sheet where ice funnels and flows more quickly than the "ice-sheet ice" surrounding it.

PERCOLATION ZONE: The area of the ice sheet just above the ELA where surface melt occurs regularly, but where runoff is small or zero. Instead of running off, the melt percolates into the firn, where it refreezes. This area is also sometimes called the "wet snow zone".

RUNOFF: Surface melt that reaches the ocean. This melt figuratively runs off the glacier or ice sheet.

SUBLIMATION: A phase change where the solid turns directly to the vapor, bypassing the liquid phase.

SUPRAGLACIAL: On the upper surface of a glacier or ice sheet; that is, the surface in contact with the atmosphere.

SUPRAGLACIAL LAKE: A body of water that collects in a local depression on the surface of a glacier. Supraglacial lakes are typically $\leq$2 km in diameter and $\leq$10 m deep and form at elevations up to or just above the equilibrium line altitude (ELA).

SUPRAGLACIAL STREAM: A stream that carries meltwater on the surface of the ice sheet. These are usually 1–10 meters wide and a few kilometers long, although they can be as short as 100 meters or as long as 60 km. Also referred to as "supraglacial river."

SURFACE MASS BALANCE: The net gain or loss of ice on the upper surface of a glacier or ice sheet. The sum of all local accumulation and ablation over a specific time period, usually one year.

SURFACE MELT: Ice that turns to liquid water on the upper surface of a glacier or ice sheet. Also referred to as *ablation*.

TEMPERATE ICE: Ice whose temperature is equal to the melting point.

1.4 Organization of the dissertation

My thesis comprises a body of observations and interpretations sourced from a numerical model for ice temperature, which I developed. Although I have outlined this model in broad strokes in scientific journal articles, this dissertation contains a complete description of the model (Chapter 2). An in-depth analysis of the ice in Jakobshavn Isbræ, an important Greenland outlet glacier, accompanies this description. I used this fast-flowing, thermally complex glacier as a benchmark for my thermal model.

In Chapters 3 and 5, I apply this thermal model to contemporary questions in Greenland Ice Sheet hydrology. Each chapter is meant to function as a stand-alone paper. Chapter 5 has been previously published in the journal *Geophysical Research Letters* (February 2015). Chapter 3 is in preparation for submission to a long-format journal, such as the *Journal of Glaciology* (anticipated January 2016).

Chapter 4 builds on the conclusions of Chapter 3. It addresses similar topics but approaches them from a different perspective. It also relies on a new model, which is based on fracture mechanics, coupled to a variant of the thermal model underlying the rest of the thesis. This chapter is also written in the form of a journal article; it is in preparation for submission to a short-format journal, such as *Geophysical Research Letters* (anticipated February 2016).

Chapter 6 contains a short conclusion and synthesis of this work. It also describes other topics in geophysics that are analogous to the ice-sheet systems studied here, and to which my models could have direct application. This chapter also outlines new questions raised by my research and topics that could be explored in the future.

1.5 Expertise

Many glaciologists are interested in supraglacial hydrology of ice sheets – the behavior of meltwater on the surface of a glacier – and a great many more in basal hydrology, which occurs beneath the ice sheet at its interface with the rock. **I am an expert in the englacial hydrology of an ice sheet**, which connects these two systems. Surface water accesses the englacial system through moulins and crevasses, and once inside the ice, the water may refreeze (Chapter 3), persist (Chapter 4), or travel through swiftly to the bed (Chapter 5). Also, due to the entirely separate process of strain heating, a sizable amount of water can be present within ice at the microscopic level, between the grains of fast-deforming ice (Chapter 2).

Like so many things in glaciology, the englacial system has been studied more extensively on alpine glaciers than it has on ice sheets, due to the smaller size and thinner ice of alpine glaciers (e.g., Fountain et al., 2005). We as a community are currently extending this knowledge to the Greenland Ice Sheet, where the ice thickness is an order of magnitude greater ($\sim$1000 m in the ablation zone) and thus too are the cryostatic stresses that must be overcome to keep an englacial conduit open. At the same time, the englacial temperatures of the Greenland Ice Sheet are often 10–20°C cooler than on temperate alpine glaciers. This allows greater volumes of water to refreeze within the ice sheet, giving great importance to the thermal component of the problem.

A secondary area of my expertise is the development of ice-sheet models. I have developed a set of numerical models that physically describe the fracturing of a water-filled crevasse, and the thermodynamics (temperature and refreezing rates) of a two-phase (solid ice and liquid water) englacial system. I sometimes describe these models as having "medium complexity": they contain physics that are relatively off-the-shelf (heat conduction and convection; phase changes and latent heat transfer; conservation of mass; viscous (creep) and elastic deformation), but combine them in novel ways to address the subtleties of new problems.

Chapter 2

ICE TEMPERATURES AND DEFORMATIONAL MOTION OF JAKOBSHAVN ISBRAE

My thesis is built on two models: (1) a polythermal ice sheet model for englacial temperature, and (2) a fracture-mechanics model for crevasse propagation. Here I describe the physics, implementation, and evaluation of the first model. I use this model for Chapter 5 and, with slight modifications, for Chapter 3. The fracture-mechanics model (Chapter 4) couples to a thermal model with a different setup than the one described here. That thermal model is described in detail in Chapter 4.

I developed the polythermal ice sheet model described in this chapter as a base model for my thesis work. It is meant to accurately capture the temperatures in the bottom half of the ice column. I use it to model the basal temperature field (melted vs. frozen) in Chapter 5. I also apply it to investigate processes in the top half of of the ice column, in Chapter 3. Though most of the "interesting" things in that chapter occur well above the basal temperate ice layer, it is the basal ice that has the greatest effect on ice flow, as demonstrated in that chapter.

In this section, I first describe the general setup of the polythermal ice-sheet model. Next I describe the details required to accurately compute the thermal state of a polythermal ice mass such as the Greenland Ice Sheet. Finally I apply the model to a case study of Jakobshavn Isbræ, a polythermal outlet glacier on the Greenland west coast.

2.1 Polythermal ice systems

A polythermal ice mass has distinct sections of cold ice, or ice whose temperature is below the melting point, and temperate ice, or ice whose temperature is at its melting point. The temperate ice usually contains a small fraction of liquid water that exists within the ice structure, at grain triple boundaries (Nye, 1989).The scale of such grain boundaries (microns) compared to the size of the grains themselves (millimeters) means that this water is trapped within the crystal structure of the ice.

Although the liquid water cannot physically escape the tiny pockets within the ice sheet, it can change phase (refreeze) and rejoin the ice structure. Such a phase change occurs when, for example, temperate ice passes into an area of sub-freezing temperature.

My model discretizes this problem and allows for its exploration.

2.2 Description of polythermal model for englacial temperature

The polythermal model solves the heat equation for a two-phase system. That is, it computes both ice temperature (when $T \leq T_{pmp}$) and liquid water content (when $T = T_{pmp}$), where T denotes temperature and T_{pmp} denotes the melting temperature, which is pressure-dependent (hence "pressure-melting-point", or pmp). The model computes these quantities at points along two-dimensional flowlines in the along-flow and vertical dimensions. The model uses a one-dimensional finite-differences scheme, which includes both vertical advection and diffusion, to solve for the temperature of individual ice columns along a flowline. Each column is linked to the column immediately upstream of it via a horizontal advection term. Because horizontal heat diffusion is at least one order of magnitude lower than the next-weakest term, horizontal diffusion is not included in the model. Thus, the heat equation we solve is given by

$$\frac{\partial T}{\partial t} = \kappa \frac{\partial^2 T}{\partial z^2} - \overrightarrow{u} \cdot \overrightarrow{\nabla} T + \frac{W}{\rho C} \tag{2.1}$$

where T is the temperature field, t is time, z is the vertical coordinate, κ is thermal diffusivity, u is the two-dimensional velocity vector, ρ is the density of ice (a constant), C is the temperature-dependent specific heat capacity of ice, and W is the heat generated from internal shearing of the ice.

The boundary conditions of the model are the geothermal flux at the bed (Shapiro and Ritzwoller, 2004) and climate data (surface mass balance, surface temperature, and near-surface firn temperature) at the surface, which we take from the regional climate model RACMO2 (van Angelen et al., 2013), averaged over 1960–2011.

Our model has no mechanical component to determine ice velocity and elevation change; rather, we define the model domain from the observed present-day ice sheet surface (Bamber et al., 2013; Howat et al., 2014), bed (Bamber et al., 2013; Gogineni et al., 2014;

Morlighem et al., 2014), and velocity (Joughin et al., 2010). By doing so, we effectively assume that this part of the ice sheet is in geometric equilibrium. We use radar isochrones, which can bear signatures of past ice-sheet geometries, to investigate the soundness of this assumption in Section 2.3.1.

2.2.1 Horizontal velocity field

The horizontal velocity field is calculated from the modeled temperature-dependent ice viscosity, the depth within the ice, and the modeled basal condition:

$$u(x,z) = u_b(x) + E(x) \cdot \phi(z) \cdot \int_b^z \left(A(x,z') \cdot \tau_b^3 \cdot \left(1 - \frac{z'}{H(x)}\right)^3 \right) dz' \tag{2.2}$$

Here, u_b is the horizontal velocity at the ice sheet bed at the along-flow position x, E is a flow-enhancement factor, A represents the temperature-dependent flow law parameter, which we take from Cuffey and Paterson (2010) (described further in Section 2.2.4), and ϕ is the shape function, which describes the shape of the horizontal deformational velocity curve with z, the height above the bed:

$$\phi(z) = \frac{\int_0^z \left(A(z')(H-z')^3\right) dz'}{\int_0^H \left(A(z)(H-z)^3\right) dz} \tag{2.3}$$

We assume that areas with frozen beds are not sliding ($u_b = 0$) and thus attribute the entirety of the observed surface velocity there to deformation, varying E to make Equation 2.2 match the observed surface velocities. At areas with thawed beds, we assume that any observed velocity exceeding the predicted deformational velocity (the second term in Equation 2.2) is due to slip over a hard, undeformable bed. We use a spatially variant enhancement factor E to approximate the additional deformation allowed by the ice as a result of impurities and strain softening within Jakobshavn Isbræ. The enhancement factor is a free parameter in the model that we tune to best reproduce temperature observations in the deep Jakobshavn boreholes (Iken et al., 1993).

2.2.2 *Vertical velocity field*

We construct a vertical velocity field w from the surface mass balance $\dot{a}$, which we take from RACMO2 (van Angelen et al., 2013), and the basal melt rate $\dot{B}$, which we calculate from basal temperature gradients and basal friction generated by sliding:

$$\dot{B} = \frac{1}{\rho L_f}\left(\tau_b \cdot u_b - k_r \frac{\partial T}{\partial z}\bigg|_r + k_i \frac{\partial T}{\partial z}\bigg|_i\right) \tag{2.4}$$

Here, L_f is the latent heat of freezing, k_r is the thermal conductivity of rock, which we take to be 3.3 W/m/K, a value appropriate for the high-grade metamorphic rocks underlying the Greenland Ice Sheet. Similarly, k_i is the thermal conductivity of ice, which we take as 2.1 W/m/K. The vertical temperature gradients are calculated immediately below the bed within the rock (r) and immediately above the bed within the ice (i).

We define the vertical velocity as a weighted average of the standard Nye model (Nye, 1957) and the Dansgaard-Johnsen formulation (Dansgaard and Johnsen, 1969). The Nye model assumes no horizontal ice deformation and consequently a uniform vertical strain rate:

$$w_{\text{Nye}}(z) = -\left(\frac{z}{H}\dot{a} + \left(1 - \frac{z}{H}\right)\dot{B}\right) \tag{2.5}$$

where H is the thickness of the ice column. The Dansgaard-Johnsen formulation, on the other hand, supposes a constant vertical strain rate only in the upper part of the ice column and prescribes nonlinear vertical deformation in the bottom part of the ice column. Thus, below some kink height h, the vertical velocity decreases quadratically to the basal melt rate at the ice-bed interface:

$$w_{\text{DJ}}(z) = \begin{cases} -\frac{kz^2}{2h} - \dot{B}\left(1 - \frac{z}{H}\right), & 0 \le z \le h \\ -\frac{k}{2}\left(2z - h\right) - \dot{B}\left(1 - \frac{z}{H}\right), & h \le z \le H \end{cases} \tag{2.6}$$
$$\text{for } k = {}^{2\dot{a}}/_{(2H-h)}$$

The Nye formulation is appropriate for ice that is moving entirely by basal sliding;

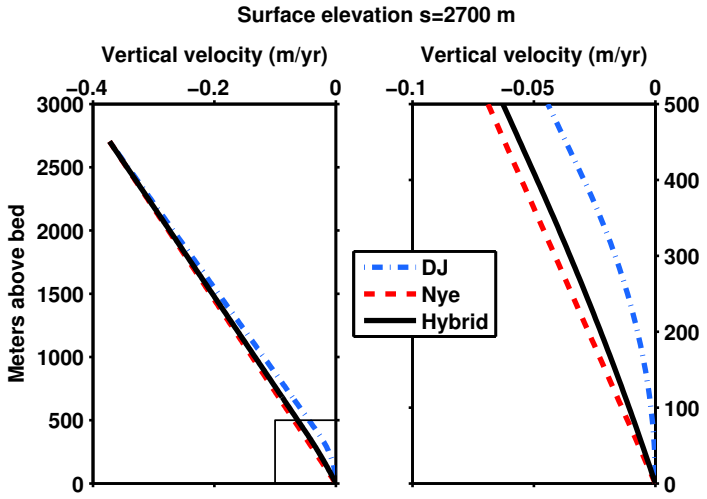

Figure 2.1: Illustration of the various vertical-velocity profiles. Our model uses the hybrid velocity profile (black; Eqn. 2.7), which is a weighted average of the Nye and Dansgaard-Johnsen profiles. In the upper ice column (left), all three profiles are virtually identical. They differ most at the bed (right), where the Nye profile prescribes fast downward motion while the Dansgaard-Johnsen allows ice to slow vertically as it approaches the bed.

that is, ice that is not deforming in vertical shear. The Dansgaard-Johnsen formulation, on the other hand, was developed for use near ice divides, where the ice undergoes considerable vertical shear. Because ice in our flowlines encounters both regimes as it travels downstream, we weight the vertical velocity at a map point based on the relative amount of horizontal deformation experienced by the ice there:

$$w(x,z) = \frac{u_b(x)}{u_s(x)} \cdot w_{\mathrm{Nye}}(x,z) + \frac{u_d(x)}{u_s(x)} \cdot w_{\mathrm{DJ}}(x,z) \tag{2.7}$$

Here, u_s is the observed horizontal velocity of the ice at the ice-sheet surface, u_b is the horizontal basal or sliding velocity of the ice column, and u_d is the deformational component of the horizontal velocity. Thus, $u_b + u_d = u_s$. Near the divide and where the ice is frozen to the bed, u_d/u_s is approximately 1; on fast-moving outlet glaciers, u_d/u_s is commonly less than one percent. Based on comparison of modeled isochrones to isochrones observed in radar data (see Section 2.3.1), we assign a kink height of $h = 0.15H$ to the Dansgaard-Johnsen velocity, a value applicable to ice far from ice divides (Fudge et al., 2014).

2.2.3 Shear heating and basal shear stress

Deformation of the ice as the ice column shears vertically along-flow generates heat. We include such xz shear heating as a source term. We calculate shear heating as follows:

$$W(x,z) = \left(1 - \frac{z}{H}\right) \cdot \frac{\partial u_d(x,z)}{\partial z} \cdot \tau_b(x) \tag{2.8}$$

Here, $u_d(z)$ represents the deformational velocity at the height z, andτ_b represents the basal shear stress underlying the column at point x.

We rely on previous geophysical inversions (Shapero et al., 2015) to constrain the basal shear stress within and around the main trough of Jakobshavn Isbræ. Outside of that area, we set the basal shear stress equal to the local driving stress. In general, this means that

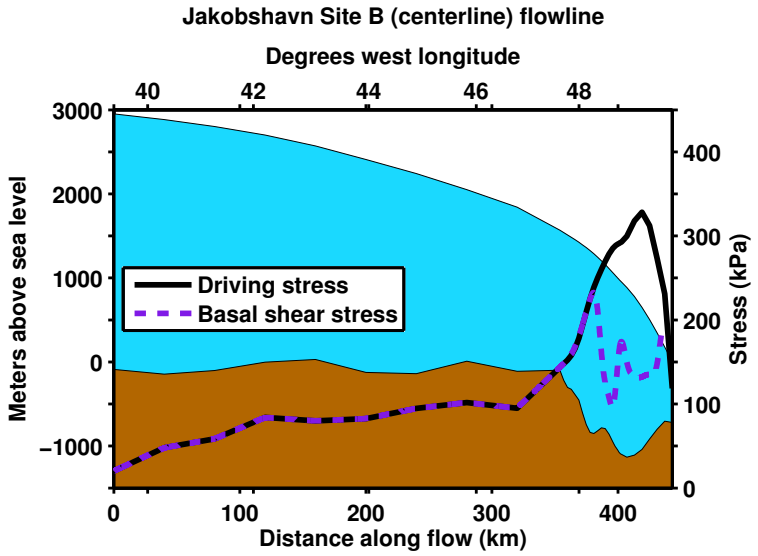

Figure 2.2: Geometry of the Jakobshavn Isbræ centerline, which runs through the Site B borehole. Computed driving stress and the basal shear stress calculated by Shapero et al. (2015) are shown. Outside the extent of the calculated Shapero et al. (2015) basal shear stress field, we assume that the basal shear stress is equal to the driving stress.

we do not "conserve" the observed 2D field of driving stress as we distribute it over our series of curvilinear flowlines.

The bed under the main channel of Jakobshavn is soft and cannot support the full driving stress ($\tau_b << \tau_d$). The basal shear stress field (Shapero et al., 2015) indicates that much of the driving stress that pushes ice quickly through the weak-bedded outlet glacier is bridged to strong-bedded areas underlying the shear margins. In our flowline model, we do not account for this lateral bridging, which would occur between flowlines and would thus be difficult to implement within a model run. That is to say, we neglect entirely any lateral stress transfer between flowlines. We also do not require that stress is balanced along flowlines, as the basal shear stress field indicates that the driving stress is primarily bridged *across* flow rather than *along* flow. We use computed basal shear stress

fields for areas under the fast-flowing regions of major outlet glaciers (Shapero et al., 2015). Upstream of these areas, and for most of the length of most flowlines, we assume $\tau_b = \tau_d$, and the driving stress is supported locally rather than bridged to other areas.

In summary, our model underestimates the deformational heat produced by ice flow (Eqn. 2.8) within major, fast-moving outlet glaciers where the basal shear stress is locally less than the driving stress. A potential area for improvement is to estimate the magnitude of the shear heating from observed strain rates at the ice-sheet surface, while still giving them the depth dependence predicted by Equation 2.8.

2.2.4 Flow law parameter, including water content

We use the flow law parameter $A(T)$ for cold ice from the standard Paterson formulation (Cuffey and Paterson, 2010):

$$\begin{aligned} A(T) = \quad & A_0 \exp\left(-\tfrac{Q_c}{R}\left[\tfrac{1}{263} - \tfrac{1}{T}\right]\right), \\ \text{with} \quad & A_0 = 3.5 \times 10^{-25}\,\mathrm{Pa}^{-3}\mathrm{s}^{-1} \\ & Q_c = \begin{cases} 6 \times 10^4 & \mathrm{J/mol} \quad \text{if } T < 263\,\mathrm{K} \\ 11.5 \times 10^4 & \mathrm{J/mol} \quad \text{if } T > 263\,\mathrm{K} \end{cases} \\ & R = 8.314\,\mathrm{J/mol/K} \end{aligned} \tag{2.9}$$

This parameterization is applicable for ice at the pressure-melting point, but it does not take into account the liquid water at grain boundaries that increases the ability of the ice to flow. To represent this enhanced softness in temperate ice, we used a secondary parameterization based on observations of radio wave speed through the temperate ice layer in Storglaciären (Gusmeroli et al., 2010). That study converted wave speed to intergranular water content and fitted a linear function to relate the ice softness to the fractional water content, μ. We apply their results to supplement our flow law:

$$A_0 = \max\left[362.43\mu,\ 1\right] \cdot 3.5 \times 10^{-25}\,\mathrm{Pa}^{-3}\mathrm{s}^{-1} \tag{2.10}$$

We assume, as is standard, that $\mu \leq 0.01$. This amounts to softening of a factor of $\sim$3.6 for ice that is saturated ($\mu = 0.01$) with intergranular water. This parameterization is in rough agreement with other field and laboratory studies of the flow law parameter for temperate ice (Cuffey and Paterson, 2010).

2.2.5 Polythermal mode

In locations where the shear heating source term is large, the ice may warm to its local pressure-dependent melting point. At these locations, the model sets ice temperature to the local melting point and uses any additional heat generated toward melting ice internally. This gives rise to distinct zones of sub-temperate or cold ice (ice below its melting point) and temperate ice (ice at its melting point, with microscopic pockets of liquid water present between grains). Because most of the shear heating occurs near the bed, the temperate ice layer, when present, usually occupies the bottom portion of the ice sheet. We follow MacAyeal (1997) for implementing the physics to govern the evolution of the polythermal glacier.

Basal temperate ice and upper-ice-column cold ice

Greenland outlet glaciers concentrate most of their ice deformation in the bottom few tens or hundreds of meters of ice. Thus, it is the basal ice that is likely to become temperate. This contrasts with polythermal glaciers in other areas of the world; e.g., Svalbard glaciers, which are likely to host thin layers of temperate ice in some places, due to the refreezing of liquid meltwater in their percolation zones (Hutter et al., 1988). Interestingly, new evidence suggests that this may be the case in some parts of Southeast Greenland as well (Forster et al., 2013; Munneke et al., 2014). However, here we focus on typical conditions in western Greenland, where the thickest layers of temperate ice are likely to form at the bed.

Ice in the basal temperate ice layer is at the melting point, which is pressure-dependent:

at higher pressures, liquid water can exist at lower temperatures. This is opposite to most substances, whose solid phase has a higher density and thus is the preferred phase at high pressures. The Clausius-Clapeyron relation gives the pressure melting point, T_{pmp}, as a function of pressure p:

$$T_{pmp} = 273.15 - \Phi p \tag{2.11}$$

The Clausius-Clapeyron constant Φ controls the pressure melting point. It differs slightly among pure ice ($\Phi = 0.074$ K MPa^{-1}) and glacier ice ($\Phi = 0.079$ K MPa^{-1}); we use the glacier-ice value, which was measured at Jakobshavn Isbræ (Lüthi et al., 2002).

The fraction of liquid water added to the temperate layer at a given timestep is directly proportional to the magnitude of the shear heating within the temperate layer:

$$\mu(t) = \mu(t - \Delta t) + \frac{\Delta t}{\rho_w L_f} \int_b^{CTS} W(z) dz \tag{2.12}$$

We assign a constant, vertically averaged μ to the entire temperate ice column. This follows general assumptions that liquid water can flow relatively freely through the highly porous ice matrix (Aschwanden et al., 2012).

The cold layer in the upper ice column and the basal temperate ice layer are demarcated by the ***cold-temperate ice surface***, or **CTS**. (It is also sometimes called the cold-temperate transition surface.) This surface is nearly horizontal and may spread over length scales of hundreds of kilometers (Aschwanden et al., 2012).

Conservation of energy during phase changes

Note: This section follows MacAyeal (1997) closely.

When ice crosses the cold-temperate ice surface (CTS), a phase change may occur. However, the scenarios differ depending on whether it is cold ice or temperate ice crossing the CTS.

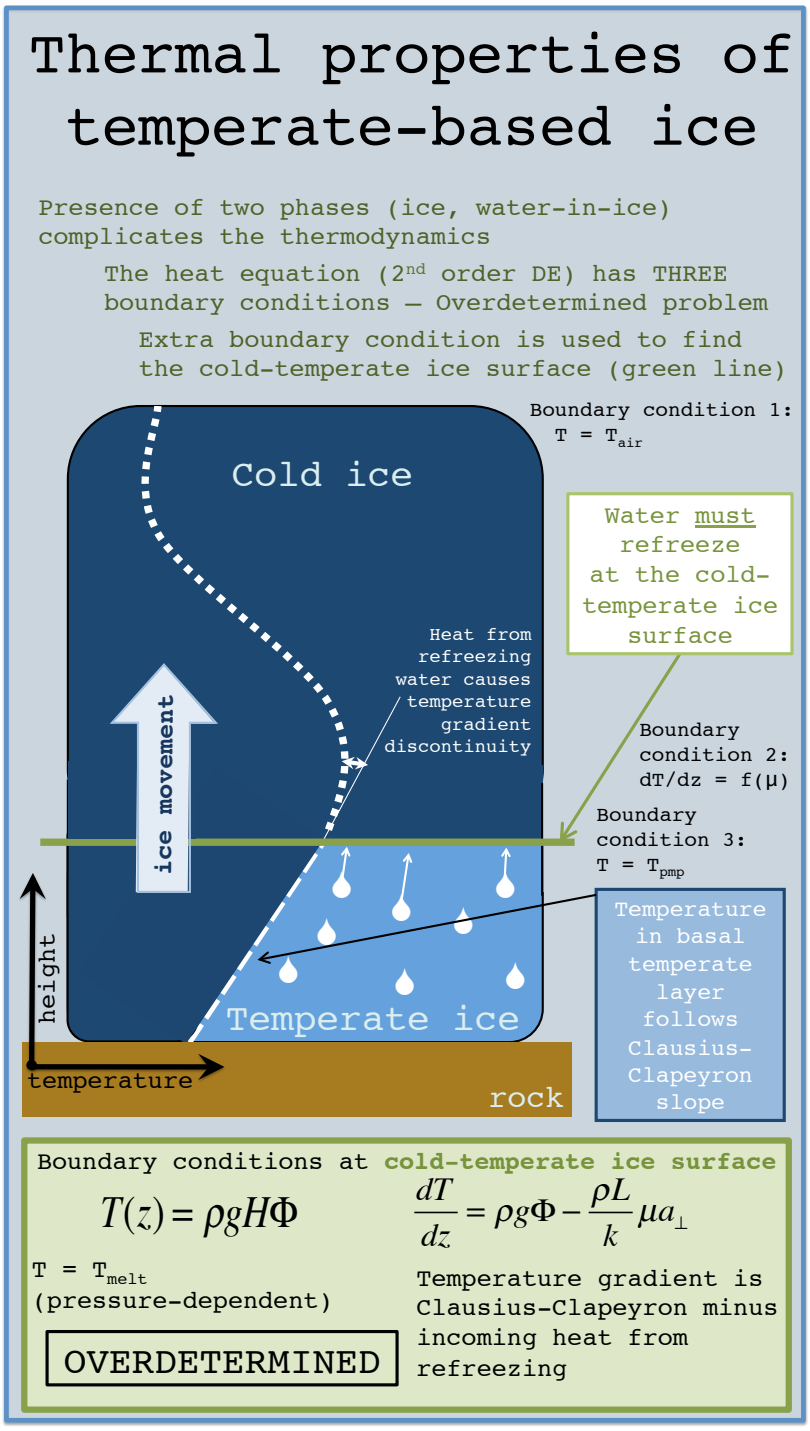

Figure 2.3: A summary of the phase changes and boundary conditions described in this section. The CTS is the green line in the middle of the figure that separates temperate ice (light blue) from cold ice (dark blue). Two complementary boundary conditions must be enforced at the CTS.

When cold ice travels through the CTS, it must warm to the melting point. Thus, the vertical temperature gradient $^{dT}/_{dz}$ also approaches the Clausius-Clapeyron gradient, $\rho g \Phi$. Once the ice crosses the CTS, a fraction of the ice *may* melt and reside englacially between ice grains. This is not required, however, and the timescale on which it may occur is unconstrained. This situation generally occurs in the accumulation zone, where net ice motion is downward.

When temperate ice travels upward through the CTS into the cold-ice region, however, a phase change *is* required. The liquid water pockets in the temperate ice *must* refreeze before the rest of the ice can cool to the temperature of the cold ice around it. This generates a latent heat of freezing, which the cold ice layer above conducts off of the CTS, absorbing this heat into the colder ice above it. Figure 2.2.5 illustrates this setup.

The rate of conduction thus limits the flux of liquid water that can travel across the CTS. More specifically, the heat flux across the boundary must be balanced by the difference in temperature gradients across the boundary:

$$Q = \left[k \frac{dT}{dz'} \bigg|_{cold} - k \rho g \Phi \right] \tag{2.13}$$

Here we use z' to represent the direction perpendicular to the CTS. This is nearly vertical and is discussed further in the next section.

The heat flux Q is a function of the water content of the temperate ice μ, where μ is a fraction for which $0 \leq \mu \leq 0.01$, and the velocity perpendicular to the interface, $a_\perp$.

$$Q = \rho L_f \mu a_\perp \tag{2.14}$$

In "normal" conditions where only a single phase is involved, the temperature gradient across any point, including the CTS, would be continuous (as it is when cold ice crosses the CTS). In this case, though, the temperature gradient is discontinuous, and the magnitude of the discontinuity is equal to the amount of heat being conducted across the

interface:

$$-k\frac{dT}{dz'}\bigg|_{cold} - k\frac{dT}{dz}\bigg|_{temperate} = \rho L_f \mu a_\perp \tag{2.15}$$

Here, the left-hand side gives the calculated temperature-gradient discontinuity, and the right-hand side gives the rate of heat conduction.

Equations 2.13 and 2.15 are permutations of each other and are included to illustrate different aspects of the same concept.

Spatial variation of CTS location

In Eqn. 2.13, we introduced the "near-vertical" direction z'. This axis is relevant only at the CTS and is meant to reflect that while the CTS is nearly horizontal, it is not: its vertical coordinate can vary with x. This variation tends to be largest near basal hills and valleys, which are common under outlet glaciers and cause the temperate ice thickness to vary spatially. The axis z' points in the direction of $\hat{n}$, the unit vector normal to the CTS at the point in question.

The orientation of the CTS is important in the calculation of $a_\perp$:

$$a_\perp = \overrightarrow{V} \cdot \hat{n} \tag{2.16}$$

where $\hat{n}$ is the unit normal vector to the CTS and $\overrightarrow{V}$ is the velocity vector (x and z) at the CTS. When the horizontal component of $\hat{n}$ is greater than approximately 10^{-4}, the large horizontal velocity u is a larger contributor than the vertical velocity to $a_\perp$. Thus, while the CTS is nearly horizontal and $a_\perp$ primarily arises from vertical ice motion, we calculate the full two-dimensional form. This constitutes an improvement over an earlier polythermal ice-sheet model (Greve, 1997) that approximated the CTS at each horizontal grid point as a separate horizontal plane.

Polythermal ice boundary conditions

Polythermal ice in the heat equation can be represented as two separate systems (cold ice and temperate ice) connected by a common boundary condition at their interface.

For basal temperate ice, the boundary conditions are simple:

$$\begin{aligned} &\text{(Temperate BC 1)} \quad T(CTS) = T_{pmp}(CTS) \\ &\text{(Temperate BC 2)} \quad T(b) = T_{pmp}(b) \end{aligned} \tag{2.17}$$

In fact, the temperatures are prescribed through the entire temperate ice zone (T=T_{pmp}), so no solution is required in this zone. The only necessary computation is the additional amount of ice melted by strain heating, μ (Equation 2.12).

For cold ice, the boundary conditions are more complicated: there are three of them, two at the CTS and one at the ice-sheet surface.

$$\begin{aligned} &\text{(Cold BC 1)} \quad T(CTS) = T_{pmp}(CTS) \\ &\text{(Cold BC 2)} \quad \left.\frac{dT}{dz'}\right|_{CTS} = k\rho g\Phi + \rho L_f \mu a_\perp \\ &\text{(Cold BC 3)} \quad T(s) = T_{air} \end{aligned} \tag{2.18}$$

This sets up an overdetermined problem: the heat equation (Eqn. 2.1) is a second-order differential equation and thus requires only two boundary conditions.

The extra boundary condition is used to set the position of the CTS within the vertical coordinate z. Given the surface boundary condition (Cold BC 3), there is only one z that will satisfy both the remaining boundary conditions, Cold BCs 1–2. Thus, the problem is not actually overdetermined.

Bisection scheme for locating the CTS

The model locates the CTS through the bisection method.There is a range of possible values for the height of the CTS above the bed; initially, this range is $Z_{CTS} \in [b, s]$; that is, anywhere between the bed b and the surface s. In each step of the iteration, the CTS is set to the midpoint of the interval and the heat equation in the cold ice is solved with the two

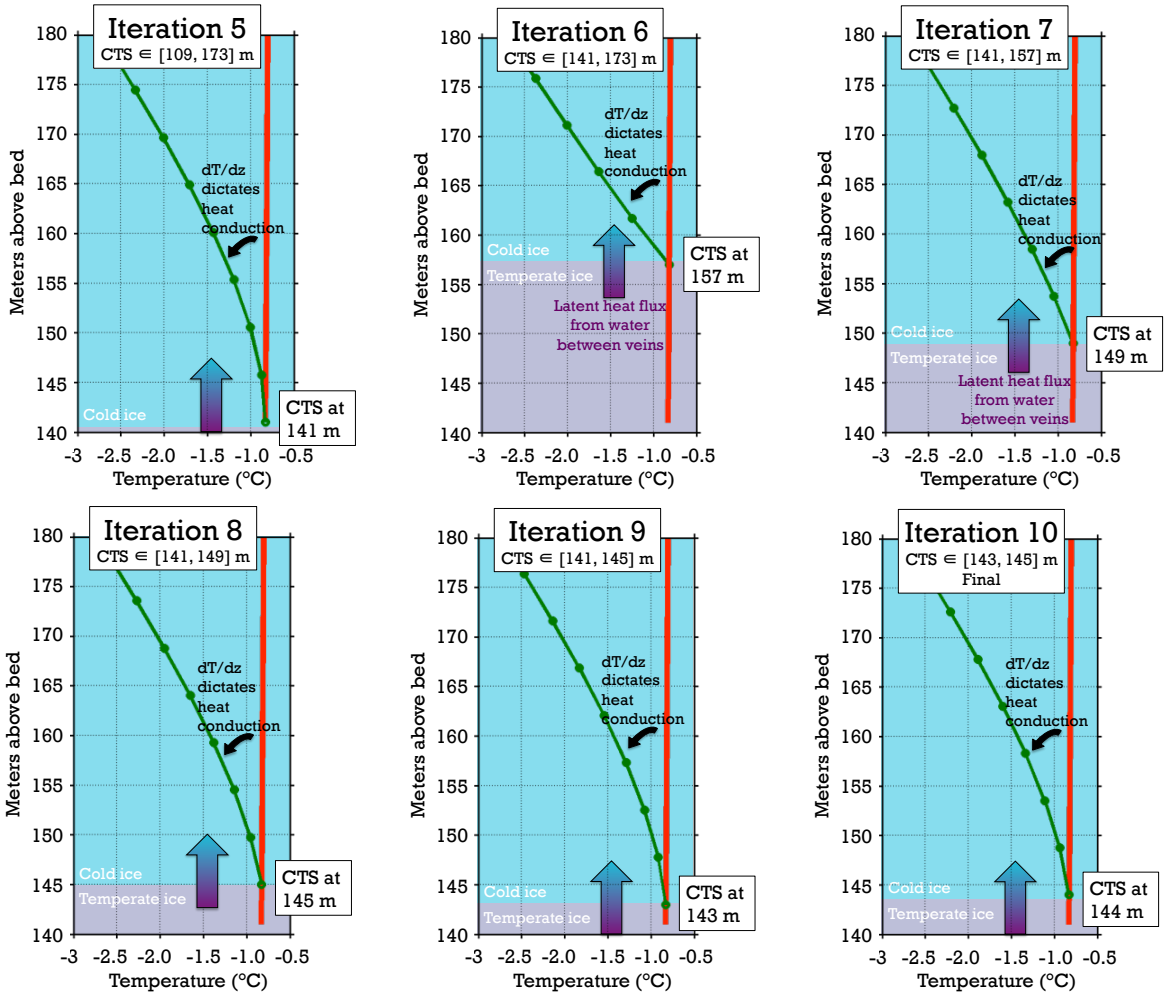

Figure 2.4: Bisection scheme used to locate the CTS. At each step of the iteration, the CTS (the boundary between cold ice (blue) and temperate ice (lavender)) is raised or lowered depending on whether the calculated temperature gradient (black arrow) at the previous iteration was too shallow or too steep, respectively. The CTS in the next timestep is set at the midpoint of an ever-decreasing interval until the width of that interval reaches the tolerance δz, shown here as 1 meter. In the model, a tolerance of $\delta z = 10^{-3}$ m is used. This figure also illustrates the effect of the CTS position on the temperature gradient above the CTS (green lines): a higher CTS causes a steeper (more negative) gradient.

Dirichlet boundary conditions (Cold BCs 1 and 3). The resultant temperature gradient at the CTS is calculated and compared to the remaining boundary condition (Cold BC 2).

If the calculated temperature gradient is steeper than the desired boundary condition, the tested position becomes the upper limit of the new range, so that the CTS will be lowered in the next timestep. If the temperature gradient is too shallow, the CTS must be raised in the next timestep, so the position tested in this timestep becomes the lower limit of the new range.

The range continues to narrow by a factor of two as new CTS heights are tested. Iterations continue until the span of the range is less than the error tolerance δz, which was usually 10^{-3} meters. This is illustrated in Figure 2.2.5. For an initial range of [0, 1500] meters, $\log_2 \left({}^{1500}/_{10^{-3}}\right) \sim 20$ iterations are expected before the method converges. Because the heat equation is solved in each iteration, this method is rather computationally expensive.

In Jakobshavn Isbræ, the high flow speeds advect cold ice ($\sim$-30°C) from near the divide downstream more rapidly than this ice can diffusively cool. Thus, the minimum temperature ($\sim$-25°C) occurs near the middle of the ice column, which is usually a few hundred meters above the CTS. Thus, raising the CTS brings the prescribed melting-point temperature at that boundary closer to this mid-column minimum, steepening the temperature gradient (left-hand side of Cold BC 2, Eqn. 2.18 or, equivalently, Eqn. 2.15). The temperature gradient at the CTS is nonlinear in z, as suggested in Figure 2.2.5 – the steepness of the temperature gradient increases faster-than-linearly with z.

In the ablation zone, relative ice motion is upward (Fig. 2.2.2) and, when the bed is melted, increases linearly with z (Eqn. 2.5). Thus, raising the CTS also raises the velocity of the ice across it, $a_\perp$, although the small horizontal component of the motion u across the CTS also contributes slightly. However, the heat flux across the CTS is also a function of the liquid water content μ, which temporarily *decreases* in a given timestep when the CTS rises. This is because μ is the water content averaged over the entire temperate ice thickness (Eqn. 2.12), so that as the temperate ice thickens, the average μ declines, until

the heat generated in the next timestep can melt more ice.

These effects of μ and the z-component of $a_\perp$ are both linear with changes in the CTS and act in opposite directions. Thus, as the CTS rises, the heat flux across it (right-hand side of Cold BC 2, Eqn. 2.18 or Eqn. 2.15) stays roughly constant. The different behavior of each side of Eqn. 2.15 allows a solution for z_{CTS} to be found.

Temperature versus enthalpy approaches

Simple ice-sheet models treat only cold ice. These models cap the temperature at the melting point and discard any additional energy that was generated in ice at the melting point. Thus, they do not conserve energy. Furthermore, these "cold-ice" models generally overestimate the amount of temperate ice present. This is because when the solution to the heat equation at a given timestep indicates $T > T_{pmp}$, these models reset the temperature at these points to the melting point. However, the advection and diffusion of the extra warmth above the melting point generally pulls additional grid points over the melting point (MacAyeal, 1997).

My temperature-based polythermal model represents an improvement over these cold-ice models in that it (1) conserves energy, and (2) allows the formation of temperate ice layers that contain liquid water. However, temperature-based polythermal models are "somewhat cumbersome to implement" (Aschwanden et al., 2012), and iterative approaches to locating the CTS require increased computing time. Specifically, the bisection method implemented in my model is well-known to be slow.

A recent development in ice-sheet modeling is the enthalpy formulation for polythermal ice sheets (Aschwanden et al., 2012). This approach also conserves energy and allows a two-phase system to develop, but features relative ease of implementation and reduced computing time. These are attractive characteristics. However, given the same constitutive relations and input parameters, the results of enthalpy-based and temperature-based polythermal ice-sheet models should be identical.

2.3 Model Evaluation and Tuning

The model operates on basic physical principles: conservation of energy (the heat equation) and conservation of mass (incompressibility and the velocity field)[1]. Yet uncertainties in the flow law of ice as well as the unknown past conditions of the ice sheet limit the extent to which models can be applied "off the shelf" to real-world ice sheets.

Here we use previous field observations to constrain these uncertain components of our model: the enhancement factor E in the flow law, and the specific shape and magnitude of the vertical velocity proflie $w(z)$.

2.3.1 Vertical velocity

The vertical velocity term (Eqns. 2.5–2.7) is the largest in the heat equation. It is largest by a factor of two or more at many places in the ice column, including near the bed, where the next-largest term, the horizontal velocity, reaches its minimum. The vertical-velocity profile also largely determines the age of ice at various depths within the ice column (Dansgaard and Johnsen, 1969). Yet the vertical-velocity profile within a glacier is often relatively unconstrained because of uncertainties in the flow law and difficulties in measuring it in situ. We thus use existing measurements of ice age at depth to constrain the vertical velocity field we use in our model.

We use isochrones traced in radar data from the Pâkitsoq region of western Greenland (Wang et al., 2002) to evaluate the velocity field within our model. To produce isochrones within our model, we run the model with tracers (extremely cold temperatures and low thermal diffusivity) alongside a "true" model run with normal temperatures and thermal diffusivity. The velocity field is calculated from these "true" model temperatures, not the artificially cold "tracer" temperatures. The present-day locations of the tracers indicate the isochrones.

[1]Unlike full thermo-mechanical ice-sheet models, which calculate the shape and deformation of the ice sheet such that the stresses balance, my model does not address the third fundamental conservation law, conservation of momentum.

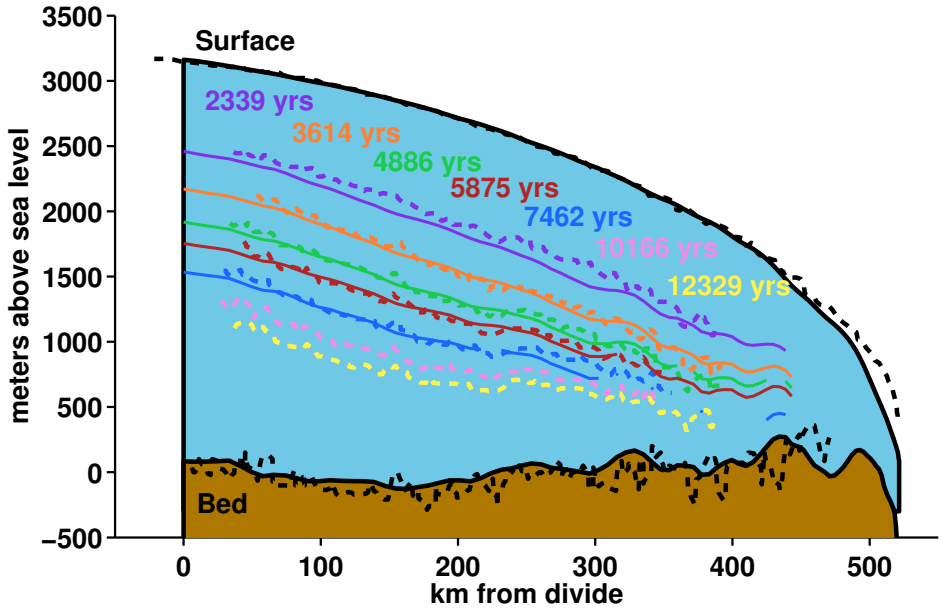

Figure 2.5: Modeled (solid) and observed (dashed) isochrones in the Pâkitsoq catchment. Observations from Wang et al. (2002).

We track layers from only the past 9,000 years (the Holocene); prior to this, the ice sheet was rapidly adjusting to the new, warmer climate after the last glacial period (Fahnestock, 2001). Over the past 9,000 years, accumulation rates at Summit, and thus likely the rest of Greenland, were relatively constant (Cuffey and Clow, 1997). Ice in the lower $\sim$40% of the ice column predates the Holocene (Wang et al., 2002), however, so we include Last Glacial Maximum (LGM) climate history in our model.

Although we do not track LGM isochrones, we run our model beginning at 25,000 years before present, through the LGM and deglaciation, during which the ice sheet thinned dramatically. To simulate this dynamic thinning, we increase the downward velocity at every point in the domain by a fixed percentage during the past 15,000 years, following (Lüthi et al., 2002), who enhanced Holocene accumulation rates to simulate thinning and to match borehole observations. We tune such a thinning factor, a', as well as the kink height h in the vertical velocity (Eqns. 2.6–2.7), to best match the isochrones of Wang et al. (2002).

We trace isochrones in our model in runs with various Dansgaard-Johnsen kink heights $h \in [0, 0.25H]$ and various thinning factors that simulate Holocene deglaciation by enhancing downward velocity by a factor of $a' \in [1.0, 1.3]$. The isochrones traced with the best-fit parameters $h = 0.15$ and $a' = 1.2$ are shown in Figure 2.5. These values compare well to the commonly used kink height for flow away from ice divides ($h = 0.2$) (Fudge et al., 2014) and to the thinning factor ($a' = 1.3$) used by Lüthi et al. (2002). We use these values in all further model runs.

2.3.2 Deformational heating

The amount of deformation that occurs in the ice of Jakobshavn Isbræ is not well known. It was once thought that the bed supported hundreds of meters of deformational ice motion per year (Echelmeyer and Harrison, 1990), but more recent geophysical (Block and Bell, 2011) and model-based (Joughin et al., 2012; Shapero et al., 2015) evidence for a weak

bed suggests that deformation may play substantially less of a role in the motion of the glacier.

Ice from the Last Glacial Maximum (LGM), due to its high impurity content, is softer than Holocene ice (Lüthi et al., 2002). E represents the additional softness of LGM ice, which occupies only the lower $\sim$40% of the ice column. However, for simplicity, we apply E through the entire ice column. This has a minimal effect on ice temperature because the shear stress is so highly concentrated in the basal (LGM) ice, and very little is accommodated in the Holocene ice in the upper parts of the ice column. Results from our model indicate that applying E to the entire ice column, rather than just the LGM ice, warms the Holocene ice artificially by $<0.2^{\circ}$C. This is in agreement with Schøtt et al. (1992). To avoid the extra step of locating the Holocene-LGM boundary along each flowline, we simply apply E to the entire ice column.

The degree of softening E seems to vary from place to place and from model to model (Wang et al., 2002). We tune the enhancement factor E in our model based on measured englacial temperatures at borehole sites within the region of study. We allow E to vary spatially to the extent constrained by the available boreholes. On Jakobshavn Isbræ, Iken et al. (1993) and Lüthi et al. (2002) provide temperature measurements in four deep boreholes, which we explore in the next section.

In the Pâkitsoq region, Thomsen et al. (1991) and Ryser et al. (2014) provide temperature measurements in seven boreholes. These results are presented in Section 2.4 and Chapter 3.

2.4 Application to Jakobshavn Isbræ

We applied our model to flowlines that pass through three boreholes drilled within the main trunk of Jakobshavn Isbræ in 1988–1989 (Iken et al., 1993) and one borehole drilled 4 km outboard of the center of the trunk in 1995 (Lüthi et al., 2002). The solid orange curves in Figure 2.7 show the results of the model.

The quantity of heat produced by the ice as it shears under stress (Eqn. 2.8) depends

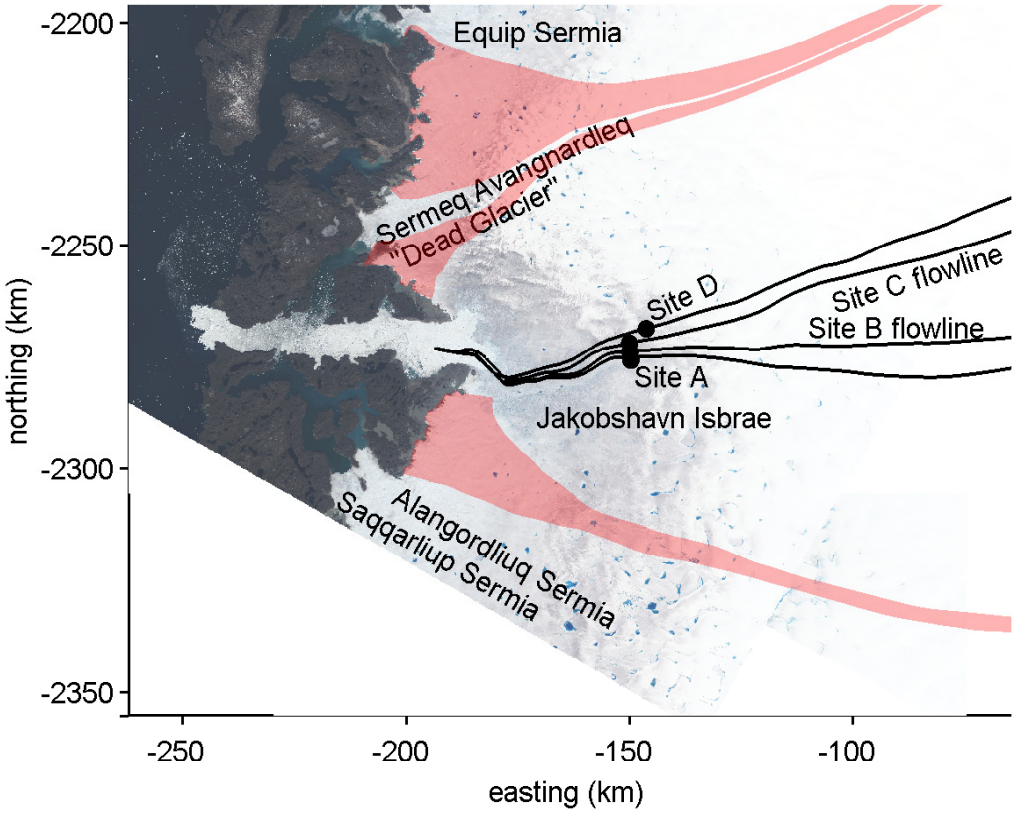

Figure 2.6: Illustration of converging and diverging flow in western Greenland. Glacier catchments with diverging ice flow are colored pink; catchments with converging ice flow are uncolored. Background image was taken by Landsat on 3 July 2014. Locations of Jakobshavn Isbræ boreholes A–D (Iken et al., 1993; Lüthi et al., 2002) are shown with dots. The flowlines through them used in the model are drawn as black lines.

on both the basal shear stress, which we take from Shapero et al. (2015), and the rheology of the ice (Eqns. 2.9–2.10). Our model represents ice rheology through a temperature-dependent component $A(T, \mu)$, which evolves with the model, and a temperature-independent enhancement factor E, which is a free parameter. E is usually near 3 in western Greenland (Schøtt et al., 1992).

We used ice temperatures measured in the Jakobshavn Isbræ boreholes to constrain the enhancement factor E in our model. Because E directly affects the magnitude of shear heating, which is concentrated at the bed, the influence of E is greatest at the bed. We ran our model along each flowline independently and adjusted the enhancement factor E to best match the measured temperatures near the bottom of each borehole. The measurements best constrain the model at Site D, where a temperate ice layer 31 meters thick underlies the ice (Lüthi et al., 2002); at Site A, where the temperate ice layer is between 0 and 90 meters thick; and at Site B, where Iken et al. (1993) estimated a temperate ice layer approximately 300 meters thick. The temperate ice thickness at Site C is not well constrained because difficulties in the field prevented observations of temperatures in the bottom $\sim$600 meters of the ice sheet there.

We evaluated the fit of the model, focusing on the lower half of the ice column, with various enhancement factors. We found $E = 1.5$ at Sites A and B and $E = 4.6$ at Site D. For simplicity and spatial continuity, we assigned $E = 1.5$ at Site C.

With these enhancement factors, we find temperate ice thicknesses of 19, 230, 0, and 34 meters at Jakobshavn drill sites A, B, C, and D, respectively. These match the measured or inferred temperate ice thicknesses ($<$90, 200–300, $<$700, and 31 meters) to within approximately 10%.

The estimate of a 300-meter-thick temperate ice layer (Funk et al., 1994) is a function of, among other things, the inferred basal topography. That study used seismic soundings (Clarke and Echelmeyer, 1996) that indicated a very deep trough that extended $\sim$1500 meters below sea level at the Site B drill site. Contemporary bed maps (Bamber et al., 2013; Morlighem et al., 2014) used in our model indicate a shallower trough, $\sim$1050 meters

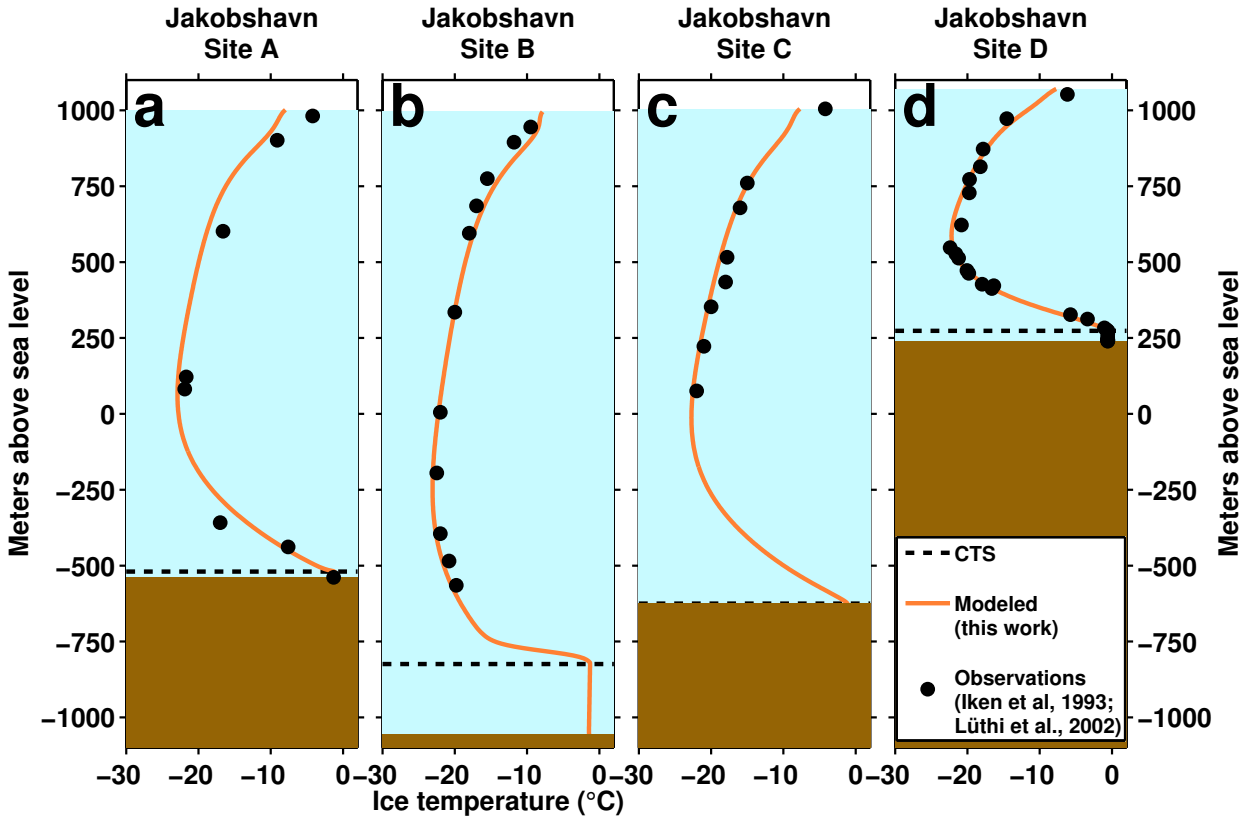

Figure 2.7: Measured (black dots) and modeled (orange lines) temperature profiles at the four Jakobshavn boreholes shown in Figure 2.6. The regions below the dashed black lines (cold-temperate transition surfaces, or CTS) contain temperate ice.

below sea level. The ∼450-meter difference in ice thickness between our work and Funk et al. (1994) likely explains much of the ∼100-meter difference in temperate ice thickness.

2.5 Conclusion

The primary importance of this model is in setting up my thesis work. Specifically, I use the basal temperature this model predicts to constrain the location of the frozen-bed – wet-bed transition point in western Greenland (Chapter 5). I also use this model as a base model on which I build features to study the upper portion of the ice column (Chapter 3).

The reliability of the base model for the thermal conditions in the bottom portion of the ice column allows me to dismiss this area as "understood" and focus on less well-understood features in the upper few hundred meters of the ice sheet.

I contributed full-column temperature profiles from this model to a study of the basal shear stress of three large outlet glaciers in Greenland (Shapero et al., 2015). As demonstrated in this chapter, this model accurately captures the temperatures observed in Jakobshavn Isbræ. Although no englacial measurements exist for the Kangerdlugssuaq and Helheim Glaciers of East Greenland, their flow characteristics are similar to those of Jakobshavn. This work (Shapero et al., 2015) was the first study to rigorously incorporate the effects of ice viscosity into the inverse problem to solve for basal shear stress. The flowline model presented here, run along $\sim$20 closely spaced flowlines that span the width of each glacier, provided the temperature, water content, and softness inputs for the inverse problem.

Chapter 3

THE CONTRIBUTION OF ENGLACIAL LATENT HEAT TRANSFER TO SEAWARD ICE FLUX IN WESTERN GREENLAND

Note: This chapter is being prepared for submission to a longer-format journal such as the *Journal of Glaciology*.

Englacial latent heat transfer, or cryo-hydrologic warming, is a process whose near-term effect on Greenland Ice Sheet mass balance is currently unknown (IPCC, 2014). Using the temperature model described in Chapter 2, with the few additions described here, I investigated the importance of this process in Greenland.

I developed and applied the model, interpreted the output, synthesized the ideas, and wrote the paper. Ian Joughin aided and advised me with all of these tasks. Michiel van den Broeke, Jan Lenaerts, and Jan van Angelen (University of Utrecht, Netherlands) provided the RACMO2 data for air and firn temperatures and surface mass balance. For these contributions, van den Broeke, Lenaerts, and van Angelen will likely appear as coauthors on the manuscript I submit for publication.

The contribution of englacial latent heat transfer to seaward ice flux in western Greenland

Kristin Poinar and Ian Joughin

Abstract. Surface melt water can refreeze within firn layers and crevasses to warm ice through latent-heat transfer on decadal to millennial timescales. Earlier work posited that the consequent softening of the ice would accelerate ice flow, potentially increasing ice-sheet mass loss. Here, we calculate the effect of meltwater refreezing on ice temperature and softness in the Pâkitsoq (near Swiss Camp) and Jakobshavn Isbræ regions of western Greenland using a numeric model and existing borehole measurements. We show that in the Jakobshavn catchment, meltwater percolation within the firn warms the ice at depth by at most a few degrees Celsius. By contrast, meltwater refreezing in crevasses (cryo-hydrologic warming) at depths of $\sim$300–350 meters warms the ice in Pâkitsoq by up to 10°C, but with minimal increase in ice motion ($<$10 m/yr). This area is representative of land-terminating ice in western Greenland, where the ablation zone is wide and substantial cryo-hydrologic warming is likely to occur. We find that only $\sim$37% of the western Greenland ice flux, however, travels through slow-moving areas where significant cryo-hydrologic warming can occur. Our findings suggest that the cryo-hydrologic warming process likely has only a limited effect on the dynamic evolution of the Greenland Ice Sheet.

3.1 Introduction

The Greenland Ice Sheet sheds mass in two ways: through surface ablation and through dynamic loss into the ocean. The former includes the sublimation and melt runoff components of surface mass balance (SMB), while the latter encompasses all direct ice discharge to the ocean (e.g., iceberg calving). Both of these processes have contributed to increased mass loss from Greenland since the 1990s, with SMB-related losses now contributing ap-

proximately twice as much mass loss as ice discharge does (van den Broeke et al., 2009). Understanding these sources of mass loss is necessary if we are to quantify and forecast the mass balance of the Greenland Ice Sheet, which is an important contributor to global sea level (Vaughan et al., 2013). Interactions between increased SMB-related mass loss and ice discharge have received particular attention recently due to their potential importance to ice-sheet mass balance (Phillips et al., 2010).

Surface melt is the major source of ablation (90% versus 10% from sublimation) (Ettema et al., 2009). Not all melt is lost as runoff, however, since $\sim$45% of the annual surface melt refreezes within the ice sheet or overlying firn layers. Although that fraction of melt does not contribute directly to sea level rise, it may affect ice discharge indirectly through latent heat transfer: the ice sheet absorbs the latent heat of the refrozen meltwater and consequently becomes warmer and softer. This process in turn affects ice dynamics since under a given driving stress, softer ice will flow more quickly downslope, enhancing dynamic mass loss (Cuffey and Paterson, 2010). It is most likely to have a significant effect only when it warms ice quickly, since the ice sheet will have evolved to a shape consistent with its rheology over long periods (centuries to millennia).

Refreezing can occur both in firn (Mock and Weeks, 1965) and in glacial ice (Jarvis and Clarke, 1974). It has been argued that the latter, sometimes called cryo-hydrologic warming, can quickly and substantially enhance the seaward velocity of the ice sheet in certain areas (Phillips et al., 2013, 2010). The effect of cryo-hydrologic warming over larger areas of the Greenland Ice Sheet, however, has not yet been evaluated (Vaughan et al., 2013). In this paper, we assess the influence on englacial temperature of refreezing in the firn and deeper within the ice sheet. We then assess the influence of cryo-hydrologic warming over a large section of central western Greenland to estimate its effect on ice-sheet-wide dynamic mass loss.

Above the equilibrium line altitude (ELA), in the percolation and wet snow zones, most of the meltwater percolates downward into the firn, where it refreezes (Benson, 1962; Greuell and Konzelmann, 1994; Mock and Weeks, 1965). Recently, Humphrey et al.

(2012) observed that this process warms the top 10 meters of firn in western Greenland as much as 12°C above the mean annual air temperature. Over many hundreds of years, this warmth in the firn heats the underlying ice column through thermal diffusion and downward advection as new snow accumulates above it. Such warmth sourced from the surface of the ice sheet can, in some places, have a greater effect on ice temperature at depth than the basal geothermal flux (Meierbachtol et al., 2015). In Svalbard, this heat source may even be responsible for sustained fast ice flow in outlet glaciers by melting the bed, which is hundreds of meters below the firn (Schäfer et al., 2014).

Below the ELA, where bare ice is exposed by the end of the summer, meltwater collects in crevasses and supraglacial lakes. Lakes can hydrofracture to the bottom of the ice sheet and deliver the meltwater to the bed, through vertical shafts known as moulins, over a period of hours (Das et al., 2008). Moulins can remain active for multiple years, but ultimately creep closed as they advect away from their water sources (Catania and Neumann, 2010). This limited lifetime, along with the small size ($<\sim$10 m diameter) and density ($<\sim 10/\text{km}^2$) (Phillips et al., 2011) of moulins, suggests that they should have only a limited thermal effect. Indeed, results from a numeric model that incorporates moulins confirms this (Vorkauf, 2014).

Some surface lakes, however, do not form moulins; instead, water in these lakes can refreeze in place (Darnell et al., 2013). This transfers latent heat onto the ice-sheet surface and diffusively warms the upper portion of the ice column. The influence of such lakes, however, is limited by the time it takes the ice beneath them to advect through the lake basin. For typical flow speeds of 100 m/yr and typical lake widths of 1–3 km, this amounts to a few decades, limiting the diffusion depth to tens of meters. Furthermore, this downward diffusion of heat competes with ice ablation rates near the equilibrium line (up to $\sim$1 m/yr). Thus, the thermal influence of supraglacial lakes generally is limited to the top $\sim$10 meters of the ice sheet. Overall, moulins and supraglacial lakes alter the temperatures near the ice-sheet surface considerably but influence englacial temperatures only marginally. We thus exclude supraglacial lakes from this analysis.

Meltwater that enters crevasses can accumulate and may reach depths of hundreds of meters over a period of weeks (van der Veen, 2007). The meltwater can refreeze onto the walls of crevasses at rates approaching millimeters per day (Alley et al., 2005), thus contributing a substantial amount of latent heat to the ice over even a relatively short time period. Therefore, latent heat transfer through crevasses in the ablation zone (cryo-hydrologic warming) can have a considerable effect on the column-averaged temperature, particularly with recent increases in surface melt (Phillips et al., 2013). Model analysis suggests that this englacial refreezing process, under certain conditions, could warm the ice at 500 meters depth by 10°C in fewer than ten years (Phillips et al., 2010). Temperature observations in Greenland boreholes suggest that the ice has warmed englacially via latent heat transfer in crevasses (Meierbachtol et al., 2015; Thomsen, 1988; Thomsen and Olesen, 1990), though such field evidence does not constrain the timescale over which such warming has occurred.

In this study, we investigate the current magnitude of the effect of englacial refreezing of meltwater on ice dynamics in western Greenland. We study both the accumulation zone, which warms primarily through refreezing in firn, and the ablation zone, where crevasse-based cryo-hydrologic warming dominates. We choose central western Greenland because its ablation zone is comparatively extensive, stretching up to 100 km into the interior, compared to 0–10 km in southeastern Greenland (Ettema et al., 2009). The ice divide is also relatively far inland in central western Greenland, making the accumulation zone up to 400 km wide, compared to approximately 200 km elsewhere. The breadth of the ablation zone in central western Greenland allows the ice ample transit time to warm through latent heat transfer, and the wide accumulation zone allows extensive refreezing within the firn. In other areas of Greenland or on smaller Arctic ice caps, the melt area is smaller, so the warming should be less pronounced there, although it may still be substantial (e.g., Zdanowicz et al., 2012). Thus, studying central western Greenland allows an upper bound on the potential for englacial refreezing to affect ice dynamics.

3.2 Study Area in Western Greenland

Our study area extends from 64.5–72.0°N in western Greenland. Because englacial temperature data are sparse across this area, we focus our modeling effort on areas where observations of englacial temperatures are most plentiful. We then extend our conclusions over the larger study area using climatological and remote-sensing-derived observations of travel time and ice balance fluxes.

Boreholes were drilled in the Jakobshavn Isbræ catchment in 1988–1989 (Iken et al., 1993) and in 1995 (Lüthi et al., 2002) and instrumented with thermistors that, after overwintering and data processing (Humphrey, 1991), gave near-equilibrium englacial temperatures at various depths. We also use temperature data from boreholes drilled in the Pâkitsoq area, a slow-moving region of divergent ice flow 20 km north of Jakobshavn Isbræ, downstream of Swiss Camp Camp (69.57°N, 49.28°W). Temperature measurements in Pâkitsoq were made in the late 1980s (Thomsen, 1988; Thomsen and Olesen, 1990) and in 2011 (Ryser et al., 2014).

Surface mass balance estimates (Ettema et al., 2009) and velocity data (Howat et al., 2011) indicate that the Jakobshavn Isbræ catchment collects approximately one twentieth ($\sim$5%) of the steady-state discharge of the ice sheet. In comparison, the Pâkitsoq area and its adjacent outlet glacier Sermeq Avangnardleq account for $\sim$0.03% of Greenland's steady state ice flux.

Ice flow differs substantially between the Jakobshavn and Pâkitsoq areas. The 110,000-km^2 Jakobshavn Isbræ catchment (the size of Pennsylvania) funnels ice from a $\sim$300-km-wide section of the divide into a 5-km-wide outlet glacier. This convergence of ice manifests in a deeply incised bedrock trough (Clarke and Echelmeyer, 1996) and flow velocities up to 17 km/yr (Joughin et al., 2014). Meanwhile, ice in the neighboring Pâkitsoq area originates at a point on the flank of the ice sheet where its neighboring catchments begin to converge (Figure 1). This ice gradually spreads out to form a 20-km wide catchment, with flow speeds of less than $\sim$100 m/yr, which generally slow along flow (Joughin

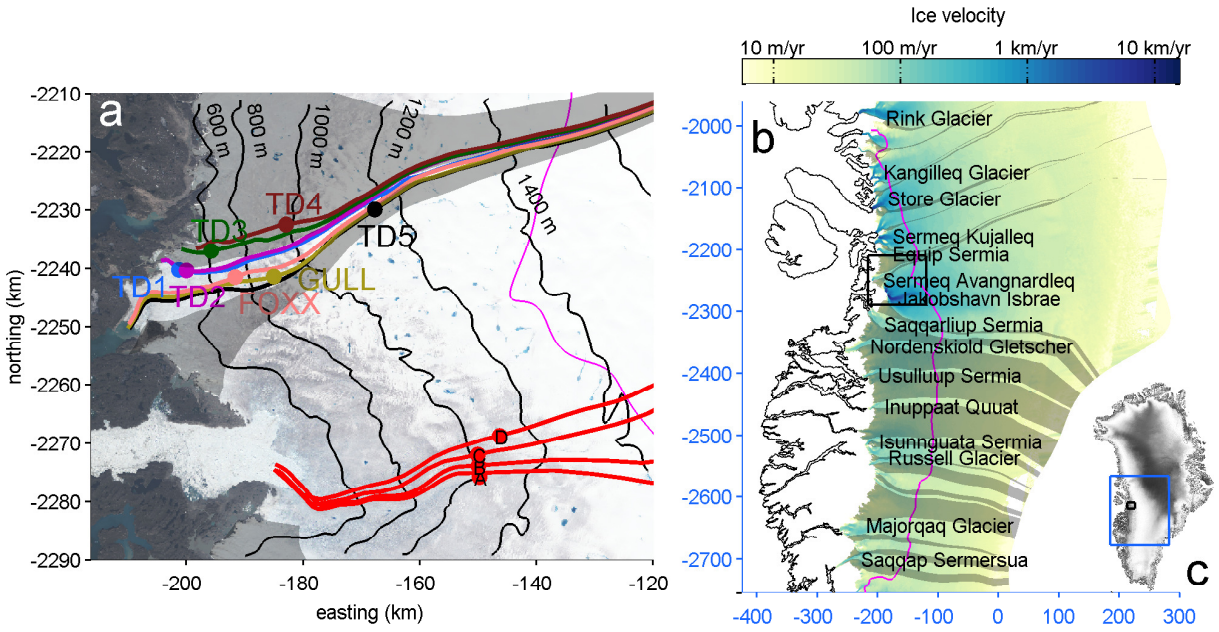

Figure 3.1: (a) Modeled flowlines (colored lines) and borehole sites (colored dots) in the Jakobshavn and Pâkitsoq catchments. Red flowlines travel through boreholes on Jakobshavn while other colors show flowlines in Pâkitsoq. Surface elevations from Howat et al. (2014) and the ELA from RACMO2 (pink) are shown atop a Landsat image from 3 July 2014. Regions of divergent flow are shaded gray. (b) Study area in western Greenland, with surface velocity from Joughin et al. (2010) shown west of the divide, and major outlet glaciers labeled. Regions of divergent flow are shaded gray. (c) Locations of panels a (black box) and b (blue box).

et al., 2010). The flowlines plotted in Figure 1a illustrate these contrasting regional velocity patterns. In addition, the ice in the Jakobshavn catchment is much thicker (Clarke and Echelmeyer, 1996) than in the Pâkitsoq catchment (Howat et al., 2014).

Both the Jakobshavn and Pâkitsoq regions host crevasse fields. The fast flow of Jakobshavn produces extensive local crevassing. In Pâkitsoq, although the speeds are much slower, the surface is also heavily crevassed because bedrock bumps cause the relatively thin ice to crack as it stretches to flow over them. The ELA is relatively constant across these two regions, at approximately 1500–1600 m (averaged over 1960–2011), as indicated by RACMO2 surface mass balance output (van Angelen et al., 2013). It is important to note that although the ELA is the elevation at which snowfall balances snowmelt on average, snowmelt does occur in most years above the ELA.

3.3 Methods

We assess the effect that surface melt has on ice temperature and viscosity through its refreezing within the firn in the accumulation zone and within glacial ice in the ablation zone. To quantify the effect of latent heat transfer, we represent refreezing processes in a numeric model for ice temperature and compare the model output to existing measurements of englacial temperatures in the ablation zone of western Greenland. This allows us to delineate and characterize regions where englacial refreezing significantly affects ice flow. Based on these results, we evaluate the overall importance of these two refreezing processes on the flow of the western Greenland Ice Sheet. Here we briefly describe the model used in this study.

3.3.1 Temperature model without englacial latent heat transfer

We use an existing thermal model (Chapter 2) to determine englacial temperature within vertical columns linked to form flowlines. The model is polythermal: it includes physics for sub-temperate ice (ice colder than its melting point), temperate ice (ice at its melting

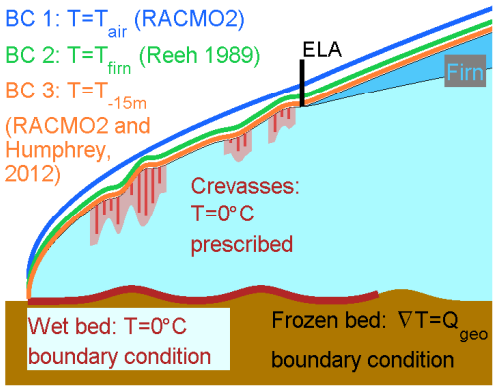

Figure 3.2: Illustration of surface and basal boundary conditions used in the model (blue, green, orange) and englacial temperature prescriptions (0°C; red) applied to the idealized crevasse fields.

point), and liquid water within the temperate ice (located between ice grains and produced by shear heating). The phase transitions that occur as the ice flows and shears are described by (MacAyeal, 1997), Funk et al. (1994), and Greve (1997), which form the basis for the inclusion of polythermal ice in our model. The model assumes the modern-day geometry of the ice sheet (surface and basal topography, geothermal flux, and surface velocities) but also incorporates paleoclimate information (temperature and surface mass balance) from the last glacial period, extending back to 50 ka (Cuffey and Clow, 1997). To simulate dynamic thinning since the last glacial maximum, we enhance accumulation rates by 30% during the Holocene, following Lüthi et al. (2002).

The model calculates along-flow vertical shear heating as a function of the basal shear stress, which we take from Shapero et al. (2015), and the rheology of the ice. Ice rheology is represented by a standard temperature-dependent rate factor, $A(T)$, which evolves with the model (Cuffey and Paterson, 2010), and a temperature-independent flow-enhancement factor E, which is a free parameter. We used ice temperatures measured in the Jakobshavn

Isbræ boreholes to constrain E. Because E controls the magnitude of shear heating, which is concentrated at the bed, its influence is greatest at the bed. This is convenient for our study since tuning E to capture temperatures near the bed has little influence on refreezing processes, which have greater effects higher in the ice column.

We adjusted the enhancement factor E along each Jakobshavn flowline to best match the measured temperatures near the bottom of each borehole. We found that E = 1.5 at Sites A and B and E = 4.6 at Site D produced the best match. Field measurements at Site C did not access the deeper ice, precluding tuning there, so we also use E = 1.5 at Site C. Varying E from 1 to 5 at these four borehole sites affected temperatures in the bottom 500 meters of the ice column by up to 5°C but changed temperatures in the upper ice column by less than 0.4°C. With these tuned enhancement factors, we find temperate ice layers with thicknesses of 19, 230, 0, and 34 meters at Jakobshavn drill sites A, B, C, and D, respectively. In part due to our tuning process, these values are in good agreement with direct and indirect borehole measurements of temperate ice thickness, of $<$90 meters, $\sim$230–300 meters, and 31 meters at Sites A, B, and D, respectively. In Pâkitsoq, we used E=3 (**?**).

This base model provides a platform from which to investigate the effects of added latent heat on ice temperatures. In the next two subsections, we describe how we adapt the model to include latent heat from refreezing in the firn and crevasse fields.

Model representation of near-surface latent heat transfer in firn

Most large-scale ice-sheet models do not incorporate the thermal effects of latent heat from refreezing in firn. Here, we explore the sensitivity of temperature at depth to thermal conditions within the firn by applying three distinct sets of surface ($\leq$15 m depth) boundary conditions (BCs) to our model:

- **BC 1:** Two-meter air temperature from the RACMO2 regional climate model,

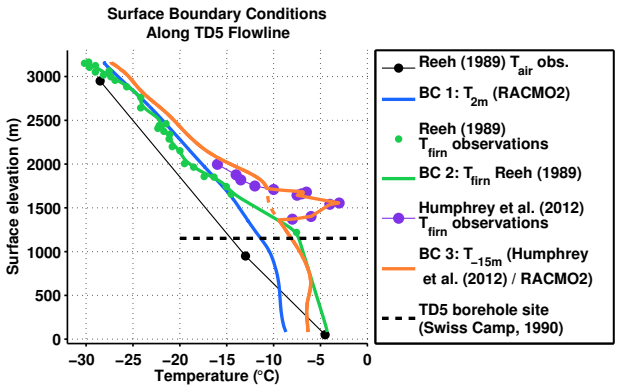

Figure 3.3: Surface boundary conditions used in the model, versus surface elevation along the TD5 (Swiss Camp) flowline within the Pâkitsoq catchment. Location of the borehole is indicated by the black horizontal line at 1150 meters. Dots indicate observations (other studies) and lines indicate the boundary conditions applied in our model. The green line is a smoothed fit through the Reeh (1989) measurements. The dashed orange line at ∼1400–1700 meters elevation indicates the RACMO2 output that we replace with field observations (purple) from Humphrey et al. (2012) at those elevations.

- **BC 2:** Near-surface temperature measurements from 1955–1980s, collated by Reeh (1989), that reflect the refreezing of meltwater within the firn,

- **BC 3:** Temperatures at 15-m depth calculated from the SMB routine (Bougamont et al., 2005) of the RACMO2 regional climate model (van Angelen et al., 2013) and supplemented by field measurements (Humphrey et al., 2012), as described below.

Figure 3 shows the spatial variation of each of these boundary conditions along a flowline within the Jakobshavn catchment. We use the air temperature (BC 1) as a control case and BC 3 as an end-member case. Although BCs 2–3 represent subsurface temperatures, we apply them directly to the surface of the modeled ice sheet.

The first two boundary conditions are unmodified from their original sources (Reeh, 1989; van Angelen et al., 2013). We found some substantial differences, however, when we compared the RACMO2 firn temperature estimates to field measurements acquired along an elevation transect directly upstream of our Pâkitsoq study region. These data indicate that surface meltwater warms the firn to temperatures as much as 14°C above the mean-annual air temperature (Humphrey et al., 2012). To account for the model-data differences, we used a combination of the observations and the model results. Specifically, where the two near-surface modeled and observed temperatures disagree, we take the warmer of the two (solid orange curve in Fig. 3).

Model representation of englacial latent heat transfer in crevasses

In the ablation zone, meltwater collects in crevasse fields and supraglacial lakes. We focus on meltwater in crevasses, which can refreeze at tens to hundreds of meters depth within the ice sheet and contribute latent heat toward warming the surrounding ice. We simplify this latent heat transfer problem by assigning englacial temperatures of 0°C to areas we identify as crevasse fields. In these areas, we prescribe 0°C temperatures from the surface to some assigned depth that varies across crevasse fields.

Our model has a horizontal resolution of 3 km, which is comparable in scale to a typical crevasse field (Joughin et al., 2013), but much coarser than the width of a single crevasse. Thus, within the area represented by one grid element, we would expect hundreds of crevasses that might extend to many different depths, yet we can only specify one such depth per grid element. To represent the variety of depths that meltwater likely reaches within a single crevasse field, we run multiple realizations of our model and allow the crevasse depths to vary among realizations. This has a similar smoothing effect as horizontal diffusive processes have on true englacial temperatures within crevasse fields (Phillips et al., 2010).

We also generalize the nature of the ice-sheet surface by randomizing the locations of modeled crevasse fields along our flowlines. We give each grid point below 1700 m elevation a 50% chance of being assigned as a crevasse field (0°C temperature prescribed from the surface to some controlled random depth of tens to hundreds of meters) and a 50% chance of being bare ice (BC 3 assigned at the surface). We tested multiple such crevassed-area parameters, ranging from 20% to 90% crevassed, and found little influence on the overall results. The highest-elevation borehole (TD5) was an exception, where a 20% crevassed-area parameter provided a markedly better fit, which may be indicative of sparser crevassing at this elevation. In general, though, we found a lack of sensitivity to crevasse density, which likely reflects the fact that once crevasses warm the ice at depth, the upper ice column advects downstream faster than it can diffusively cool. Thus, for the other six flowlines, we use a 50% area parameter to reflect the observations of Colgan et al. (2011), who identified ∼50% of the Pâkitsoq area as crevasse fields.

We assign crevasse depths in a controlled random fashion. At each crevasse field model grid point, we enforce a 0°C englacial temperature from the surface to some depth Z, where $Z \in [0\ Z_{max}]$ and is chosen from a uniform random distribution. Thus, the expected average crevasse depth in each run is $Z_{max}/2$. There is no prescribed pattern of crevasse depth along the flowline. We perform eleven sets of model runs, where each run within a set has the same Z_{max} but randomized depths Z at each randomly located

crevasse field. We vary Z_{max} across sets, from 20 to 500 meters.

We choose this approach for its ease of implementation and ad hoc simplicity in investigating sensitivity to melt, rather than as a model that incorporates the full physics of the problem. In general, one would expect crevasses to deepen with downstream distance because strain rates increase, meltwater production rates increase, and accumulated meltwater volumes increase downstream. Quantitatively representing these factors, however, remains difficult, and observations that could constrain a more complex model are limited; hence our simple approach.

Comparison of model with englacial heat transfer to observations

For each Z_{max}, we perform 10 model runs in which we vary the locations and depths of crevasse fields. We represent the ice temperature at each borehole by the mean output temperature among these runs. We perform separate sets of runs along each flowline through the seven borehole sites studied: TD1, TD2, TD3, TD4, and TD5 (Thomsen, 1988; Thomsen and Olesen, 1990), and FOXX and GULL (Lüthi et al., 2015). Figure 1 shows these flowlines. We compare the results for each Z_{max} to measured borehole temperatures and choose the Z_{max} with the best match (lowest RMS error) as representative of the typical crevasse depth in the areas near each borehole.

3.4 Results

We ran our model varying the surface boundary condition and the englacial meltwater penetration depth to find the values that produce the best fit to the temperatures observed in boreholes in the Jakobshavn and Pâkitsoq areas of western Greenland.

3.4.1 Model results from Jakobshavn Isbræ

We modeled flowlines that pass through the three boreholes drilled within the main trunk of Jakobshavn Isbræ in 1988–1989 (Iken et al., 1993) and the one borehole drilled 4 km

Table 3.1: Model parameters and outputs for the eleven borehole sites modeled.
*Thomsen and Olesen (1990), †Ryser et al. (2014), ‡Iken et al. (1993), §Lüthi et al. (2002)

Borehole site / **Parameters**	TD5* (Swiss Camp)	TD4*	GULL†	FOXX†	TD3*	TD2*	TD1*	Jak. Site A‡	Jak. Site B‡	Jak. Site C‡	Jak. Site D§
Surface elev. (m)	1150	960	880	710	600	490	490	980	970	930	1020
Enhancement E	3.0	3.0	3.0	3.0	3.0	3.0	3.0	1.5	1.5	1.5	4.6
Results: Temperature and velocity											
Change in defm. vel. due to in-firn refreezing (m/yr)	+0.2 (4%)	+0.1 (3%)	+0.4 (4%)	+0.6 (4%)	+0.03 (2%)	+0.01 (0.4%)	+0.05 (2%)	+7 (2%)	+6 (2%)	+12 (8%)	+0.4 (4%)
Total change in defm. vel. (m/yr) (% of defm. vel.) (% of surf. vel.)	+0.2 (4%) (0.2%)	+5.1 (131%) (12%)	+4.9 (14%) (2%)	+9.6 (63%) (10%)	+2.2 (123%) (7%)	+1.6 (66%) (5%)	+2.6 (122%) (7%)	-	-	-	-
Final modeled defm. vel. (m/yr)	6.5	7.3	14.5	16.0	4.3	4.4	4.6	513	555	184	10.0
Surface vel. (m/yr)	110	42	75	93	29	35	35	1260	1410	1240	713
RMS difference from observations (°C):											
In-firn refreezing	3.5	10.1	9.6	9.6	4.8	3.9	3.0	2.4	1.0	1.5	0.8
Final	2.1	1.8	4.5	2.3	0.9	0.5	1.0	2.4	1.0	1.5	0.8
Crevasse depth Z_{max} giving best fit (m)	300	350	300	350	350	250	300	-	-	-	-
Results: Latent heat transfer											
Time spent in ablation zone τ_{ELA} (yrs)	280	530	490	560	840	840	820	20	20	20	20
Thickness of ice ablated since ELA (m)	200	400	400	600	1000	1200	1200	7	6	10	5
Energy input from melt, E_{frz} (MJ/m^3)	5.7	19	28	21	7.9	8.7	3.9	-	-	-	-
Refreezing rate since ELA, R_{frz} (cm/yr)	4.0	5.7	13	7.5	1.1	0.6	0.4	-	-	-	-

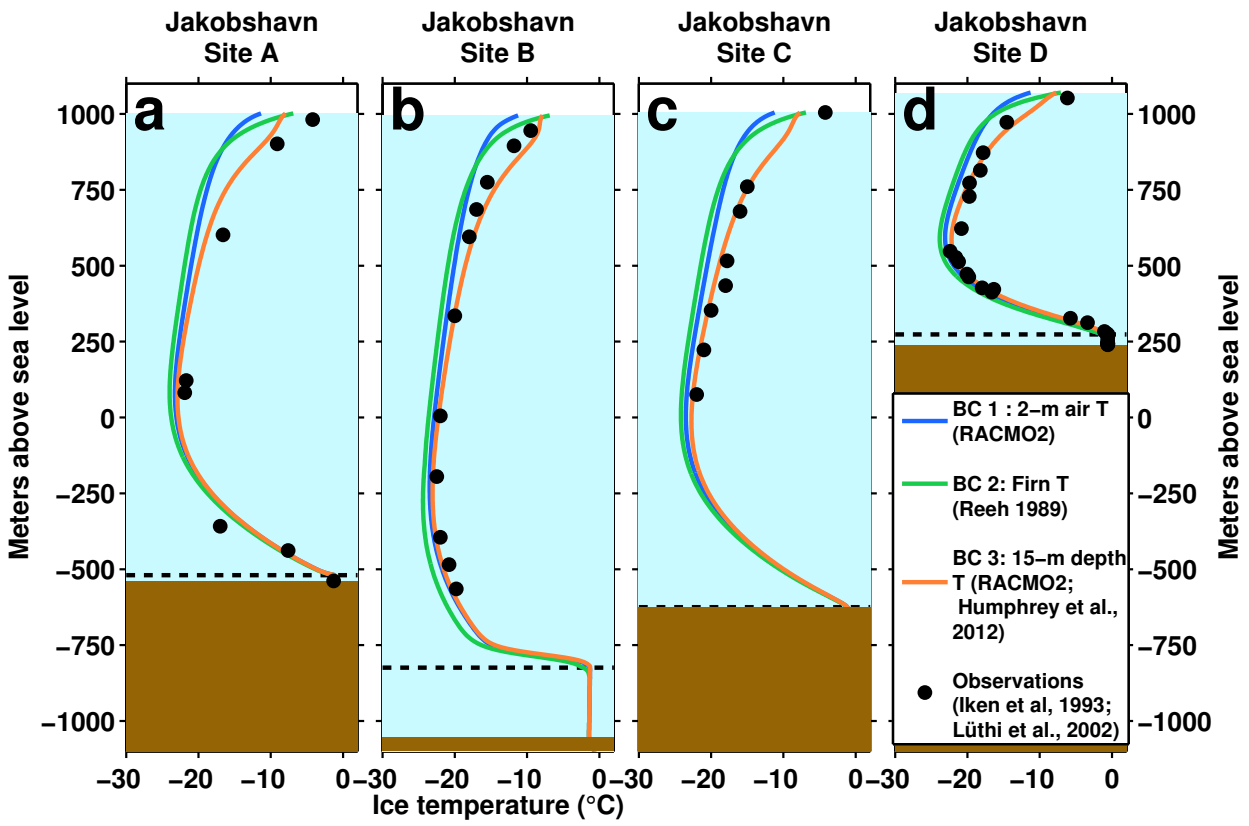

Figure 3.4: Model results at the four Jakobshavn boreholes (by panel) for the three surface boundary conditions tested (colored lines), plotted alongside measured englacial temperatures (black dots). (a–c) Sites A–C (Iken et al., 1993); (d) Site D (Lüthi et al., 2002). Modeled temperate ice thicknesses with the 15-m depth boundary condition (BC 3, orange) are (a) 19 m, (b) 230 m, (c) 0 m, and (d) 34 m. The dashed black lines show these temperate ice thicknesses at each borehole site.

outboard of the center of the trunk in 1995 (Lüthi et al., 2002). Using the two-meter air temperatures from RACMO2 as the surface boundary condition (BC 1), the modeled temperature profiles shown in Figure 4 (blue curves) are all colder than the observations. This difference is greatest within approximately 200 meters of the surface, where modeled temperatures are as much as 7°C cooler than observations (e.g., Site A). More typically, modeled temperatures are 3–5°C cooler than observations.

Using the near-surface temperature measurements compiled by Reeh (1989) (BC 2; green curve in Figure 4) also yields englacial temperature profiles that are substantially cooler than the borehole measurements and, at some depths, even cooler than the control run. The temperature profiles computed using 15-m depth temperatures from RACMO2 and Humphrey et al. (2012) (BC 3) fit the borehole measurements to within a root mean square (RMS) difference of 2°C. All of the surface boundary conditions produce similar fits to the deepest temperatures due to our adjustment of the enhancement factor. The overall fit is best at Site D (RMS difference 0.8°C) and poorest at Site A (RMS difference 2°C). We consider 2°C an acceptable margin consistent with anticipated uncertainties in the model and observations. Furthermore, the differences show no systematic variation with depth. Thus, for the Jakobshavn drill sites, we accept the results of the model using BC 3 and do not add crevasse-based latent heat transfer in the Jakobshavn catchment.

3.4.2 Model results from Pâkitsoq

In the Pâkitsoq area, we modeled flowlines that pass through five boreholes drilled between 1988–1990 (Thomsen and Olesen, 1990) and two boreholes drilled in 2011 (Ryser et al., 2014). We tested all three boundary conditions as well as a suite of model runs incorporating englacial latent heat transfer, with crevasses carrying meltwater to a variety of depths.

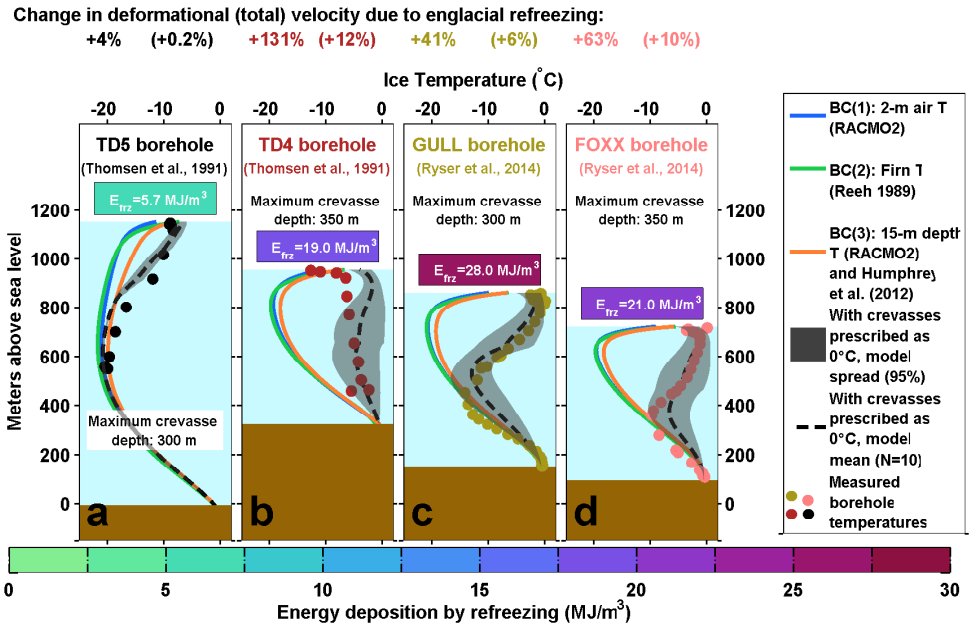

Figure 3.5: Model results at four of the Pâkitsoq boreholes (TD5, TD4, FOXX, and GULL), which are located nearest the ELA. Shown are model results using the three surface boundary conditions tested (blue, green, and orange lines), model results incorporating both BC 3 and the thermal effects of crevasses (black dashed lines and shading), and measured englacial temperatures (colored dots; references shown on each panel). The maximum crevasse depths Z_{max} used in the model are listed on each panel. The percentage change in deformational velocity allowed by the crevasse-induced warming compared to using only BC 3 are shown above each panel, with numbers in parentheses indicating the percentage change in total (surface) velocity. The colored boxes show E_{frz}, the apparent energy input from refrozen meltwater at each site (Equation 1), corresponding to the color bar below.

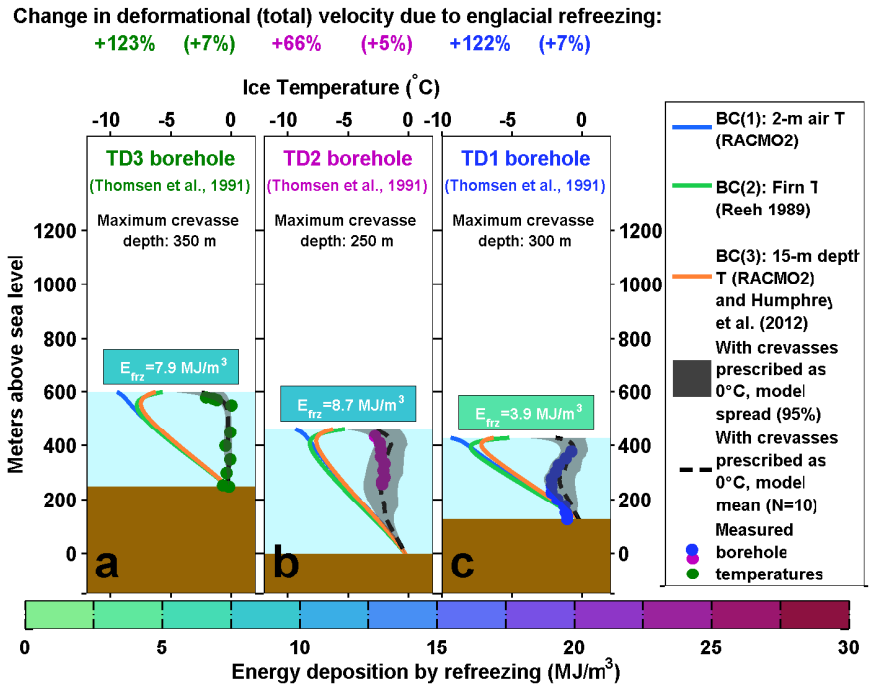

Figure 3.6: Model results at three of the Pâkitsoq boreholes (TD3, TD2, and TD1), which are at lower elevations than the borehole sites in Figure 5. Shown are model results using the three surface boundary conditions tested (blue, green, and orange lines), model results incorporating both BC 3 and the thermal effects of crevasses (black dashed lines and shading), and measured englacial temperatures (colored dots; references shown on each panel). The maximum crevasse depths Z_{max} used in the model are listed on each panel. The percentage change in deformational velocity allowed by the crevasse-induced warming compared to using only BC 3 are shown above each panel, with numbers in parentheses indicating the percentage change in total (surface) velocity. The colored boxes show E_{frz}, the apparent energy input from refrozen meltwater at each site (Equation 1), corresponding to the color bar below. This figure has the same vertical scale as Figure 3.5 but a narrower and warmer temperature range.

Firn refreezing boundary condition

The results of the model at the seven Pâkitsoq borehole sites are shown in Figures 5 and 6. Colored solid lines indicate model output using the three surface boundary conditions. As in the Jakobshavn catchment, all seven boreholes are warmer than the model predicts using our control run with 2-m air temperatures (BC 1). The RMS differences at Pâkitsoq, however, are larger than at Jakobshavn, reaching as high as 19°C at the GULL borehole and at least 5°C at all other Pâkitsoq boreholes. Furthermore, the firn heating boundary conditions (BCs 2–3), which we successfully used to model the Jakobshavn temperatures, add only ∼3°C at most to the englacial temperatures and thus are unable to explain the warm observed temperatures.

Using BC 3, the overall discrepancy between measured and modeled temperatures is largest (RMS difference 10°C) at the TD4 borehole site. This site is located well within the ablation zone (surface elevation s = 960 m; ELA at 1500 m). The discrepancy is also large at the FOXX and GULL boreholes farther downstream (observations 9.6°C warmer than the model). The fit generally improves from here with distance downstream, through the lower-elevation boreholes TD3, TD2, and TD1. The ice in these boreholes is, on average, 4°C warmer than modeled. The fit is better at the lower-elevation boreholes largely because most of the cold ice in the upper column has melted away, leaving only the warmer layers below. The relatively narrow range between the surface temperatures and the melting point here (∼7°C) effectively limits the possible RMS difference. The model still does a poor job, however, of capturing the overall shape of the temperature distribution: the modeled temperature profiles are too cold. This suggests that englacial latent heat sources (meltwater refreezing within crevasses) play a significant role in warming the ice.

Effect of englacial refreezing

Next we assess the role of englacial latent heat transfer through crevasses at the Pâkitsoq borehole sites. To examine sensitivity of the temperature response to crevasse depth, we

tested eleven different upper bounds on crevasse depth, Z_{max}, spanning 20 to 500 meters. We selected a best-fit crevasse depth for each borehole from this relatively wide range for crevasse depth. At each best-fit crevasse depth, our model was able to produce temperature profiles that approximately match the observations at all seven Pâkitsoq boreholes. The model-observation RMS difference is $\sim$2°C at upper-elevation sites (TD5, TD4, FOXX, and GULL, $s > 700$ meters) and < 1°C at lower-elevation sites (TD1–3, $s < 600$ meters).

Relative crevasse depth

Table 1 shows the best-fit crevasse depths Z_{max} identified for each Pâkitsoq borehole site. The best-fit crevasse depth (Z_{max}) averages $\sim$300 meters and spans a relatively narrow range (250–350 meters), despite the wide range tested. There is no apparent relationship between elevation on the ice sheet and Z_{max}. The relative penetration depth of the crevasses into the ice sheet does, however, increase downstream, as the thickness of the ice columns generally decreases. For instance, at TD1 and TD3, the best-fit crevasse depths Z_{max} represent the full ice thickness at the borehole sites. (Keep in mind that Z_{max} is the maximum crevasse depth over a uniform distribution; the average depth of crevasses is half of this value.) Thus, crevasses penetrate, on average, through half of the ice thickness there. At the high-elevation site TD5, however, Z_{max} (300 meters) penetrates only the top 10% of the ice sheet. Crevasses penetrate through 50–60% of the ice thickness at the remaining four borehole sites.

While our model is relatively simple, the match to the data suggests that penetration of the water-filled crevasses that allow englacial refreezing is generally limited to 300–350 meters.

Spatial distribution of englacial refreezing rates

Crevasse fields warm the ice sheet by giving meltwater access to the cold ice at depth, where it refreezes. Lüthi et al. (2015) calculated that such refreezing had deposited approximately 25 MJ/m^3 of energy into the ice at the FOXX and GULL borehole sites. To compare the results of our model to their value, we calculate an apparent energy deposition density E_{frz} for each borehole:

$$E_{frz} = \frac{\rho\, C_p}{s-b} \int_b^s (T_{obs} - T_{BC3})\, dz \tag{3.1}$$

This quantity takes the difference between the column-averaged difference between the observations (T_{obs}) and our profiles modeled without englacial, crevasse-type refreezing, but with the near-surface boundary condition (BC 3) adapted to represent in-firn refreezing (T_{BC3}) and scales it to an energy density. We use E_{frz} to interpret the amount of water that evidently refroze englacially.

The results of this calculation are shown in Table 1. Some sites (TD4, FOXX, GULL) have apparent energy inputs in excess of $\sim$20 MJ/m^3, in agreement with Lüthi et al. (2015), while values for the other sites are a factor of two less. Interestingly, these high-energy-input sites tend to consist of cooler ice. The ice columns there are also thicker and the modeled crevasse depths are greater (Z_{max} $\sim$350 m), though, so that although these sites collect larger volumes of meltwater, they also distribute the heat over a larger depth range.

Next we average E_{frz} over the amount of time the ice has spent in the ablation zone to calculate an apparent refreezing rate, R_{frz}:

$$R_{frz} = \frac{C_p}{L_f\, \tau_{ELA}} \int_b^s (T_{obs} - T_{BC3})\, dz \tag{3.2}$$

Here, τ_{ELA} is the amount of time elapsed since the ice at the borehole site crossed the equilibrium line. We take this as an approximation to the amount of time during which

melt was refreezing englacially. We note, however, that this time likely is an underestimate because melt that could fill crevasses does occur above the ELA.

The thicker, cooler, higher-elevation profiles have apparent refreezing rates of tens of centimeters per year (Table 1). More latent heat has been supplied to the ice that reaches GULL than to any other borehole, a quantity that represents 15% of the available meltwater since it crossed the ELA. By contrast, the low-elevation, warm-ice sites (TD1–TD3) have relatively low E_{frz} energy inputs and refreezing rates R_{frz}. These rates ($\sim$1 cm/yr or less) represent less than one percent of the total meltwater available to the ice over its journey through the ablation zone. Yet observations indicate near-melting temperatures throughout the entire ice column. Presumably, this is due to a combination of shear heating, the ablation of cold ice, and these modest refreezing rates.

Effect on ice velocity

An anticipated consequence of the cryo-hydrologic warming seen in the Pâkitsoq boreholes is an increase in ice velocity, as the warmed and rheologically softened ice should flow faster in response to a given driving stress. We calculate the expected speedup from a base case (BC 3; no englacial refreezing) based on the temperature change at the site of each borehole. We assume no change in driving stress. The results are shown in Figure 5 and Table 1. The velocity increases range from 0.2 m/yr at TD5 to 10 m/yr at FOXX. These increases represent 4% and 60% of the deformational velocity at these respective sites. The observed motion at these sites, however, is much greater than the computed deformational velocity, due to basal sliding (Joughin et al., 2010). Thus, the actual increase due to enhanced deformation relative the observed speed is 0.2% and 10%, respectively.

Overall, while englacial warming may substantially affect ice rheology and thus increase the deformational velocity at a site, it appears that it increases the total ice velocity considerably less. The maximum effect that englacial warming has on the total velocity at the sites we studied is 10%. This is because of the prevalence of basal slip, and because

the rheology of the upper ice column, where our work shows that latent heat transfer is occurring, is less important to ice flow than the rheology of the lower ice column. Furthermore, the shape of the ice sheet has been in steady state over at least approximately the past 12,000 years (Wang et al., 2002), which suggests that the present-day amount of englacial warming has likely been occurring in the lower ablation zone for millennia. millennia.

3.5 Scaling over western Greenland

Next we next investigate the importance of deep englacial refreezing, of the type observed in Pâkitsoq, on scales broader than individual catchments. We use the central western sector of the Greenland Ice Sheet, from 64.5–72.0°N latitude, as our study area. Although this area contains a number of major outlet glaciers, including Jakobshavn Isbræ, Store Glacier, and Rink Isbræ, this area also has high surface melt rates and a comparatively large fraction of land-terminating ice. These attributes make it the region of the ice sheet most broadly similar to the Pâkitsoq catchment.

3.5.1 Time spent in the ablation zone

To identify areas within this region that are likely to host significant englacial refreezing, we first identify the characteristics that distinguish the ice in Pâkitsoq from the ice in the Jakobshavn catchment. Figure 1a shows the catchment boundaries for these and other regions. In Pâkitsoq, the ice flow diverges, implying decreasing speed along a flowline and thus a long travel time for the ice flowing along it. By contrast, in the lower Jakobshavn catchment, flow is convergent, which implies increasing speed and short travel times. Figure 1a suggests that these flow characteristics largely manifest slightly downstream of the ELA. Thus, the travel time of ice through the ablation zone is much greater in Pâkitsoq ($\sim$300–800 years) than it is in Jakobshavn (20 years), as detailed in Table 1.

We use the time spent in the ablation zone (or, equivalently, the time elapsed since

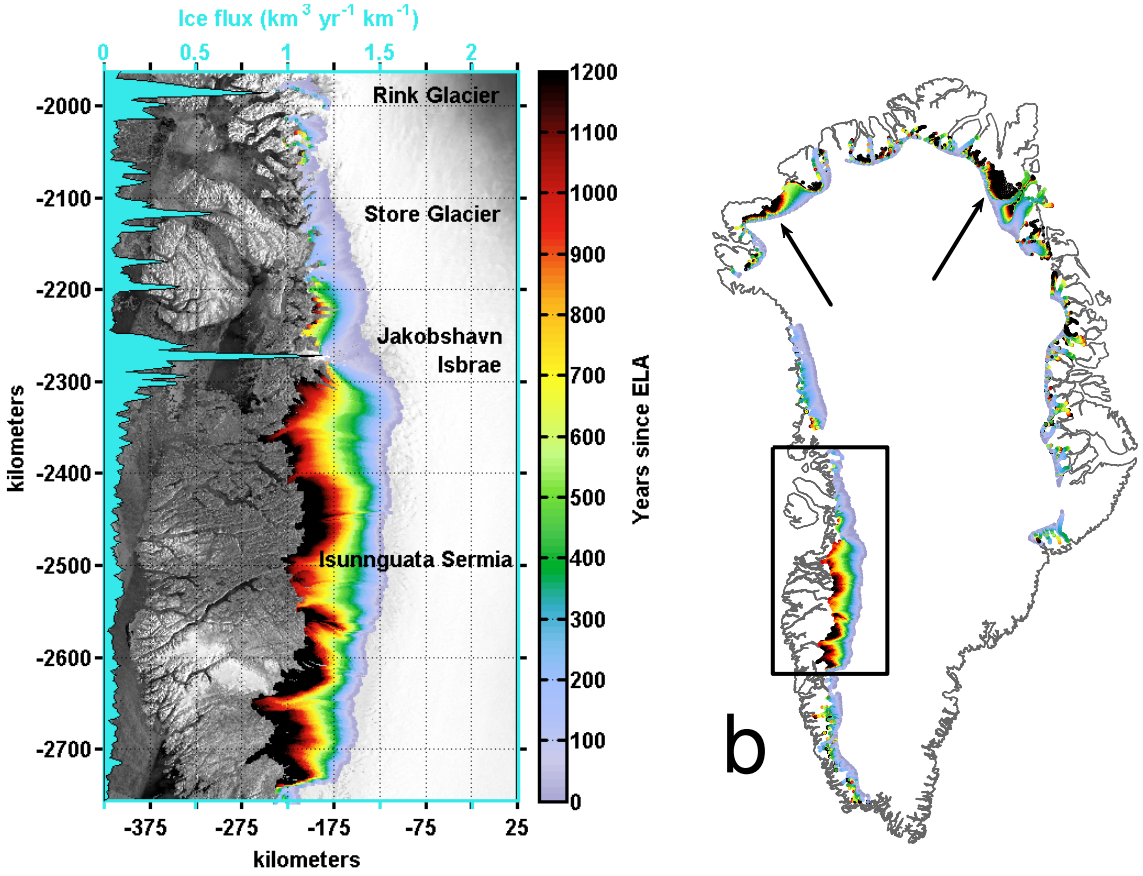

Figure 3.7: (a) Time elapsed since crossing the equilibrium line for all points within the 61.5–72.5°N study area. Blue data on the leftmost axis show the total ice flux across 2-km gates along the ELA. These fluxes were computed by summing the SMB (from RACMO2) within the catchment upstream of each gate, which we traced using observed surface velocities (Joughin et al., 2010). (b) Time elapsed since crossing the equilibrium line for the entire ablation zone of the Greenland Ice Sheet. The box indicates area of focus in panel (a). Arrows in Northwest and Northeast Greenland point to the largest areas where ice spends >1000 years in the ablation zone.

crossing the ELA) to distinguish between fast-moving, convergent, Jakobshavn-like ice and slow-moving, divergent, Pâkitsoq-like ice. We compare this to our model setup, which simulates deep englacial refreezing only at locations with surface elevations $\leq$1700 meters. This contour is approximately 20 km upstream of the ELA in the Jakobshavn and Pâkitsoq areas, where the ELA is at $\sim$1500 meters elevation (Figure 1a). We chose the 1700-meter contour for our model because satellite images indicate that some englacial fractures exist above the ELA, although they are relatively sparse.

Although some water may access sparse crevasses at higher elevations, for simplicity, we use the ELA to approximate where significant englacial refreezing can begin. Ice with a longer tenure in the ablation zone will collect and refreeze more water. In addition, where there is ample melt water to fill crevasses, they can hydrofracture deeper (Alley et al., 2005) Finally, additional time spent in the ablation zone increases the magnitude of cryo-hydrologic warming, as the latent heat deposited in crevasses can diffuse more broadly within the ice sheet (Phillips et al., 2010). Thus, the time spent in the ablation zone should be a reliable proxy for the amount of warming ice will experience from englacial latent heat transfer.

Table 1 shows the time elapsed since the ice at each borehole site crossed the ELA. The ice in all seven Pâkitsoq boreholes had spent multiple centuries (280–840 years) in the ablation zone. Of the seven Pâkitsoq sites, the TD5 borehole (τ_{ELA} = 280 years) shows the least evidence of englacial latent heat transfer and represents a natural midpoint between cold, Jakobshavn-like englacial temperatures and cryo-hydrologically warmed, Pâkitsoq-like temperatures. Thus, we take 250 years as a representative minimum amount of time that ice must spend in the ablation zone in order to show appreciable cryo-hydrologic warming.

We calculate the amount of time spent in the ablation zone for each point on the surface of the ice sheet within the central western Greenland region shown in Figure 1b. We do this simply by integrating the inverse of the measured surface velocity (Joughin et al., 2010) from each point on the ice sheet surface along its flow path upstream to the ELA.

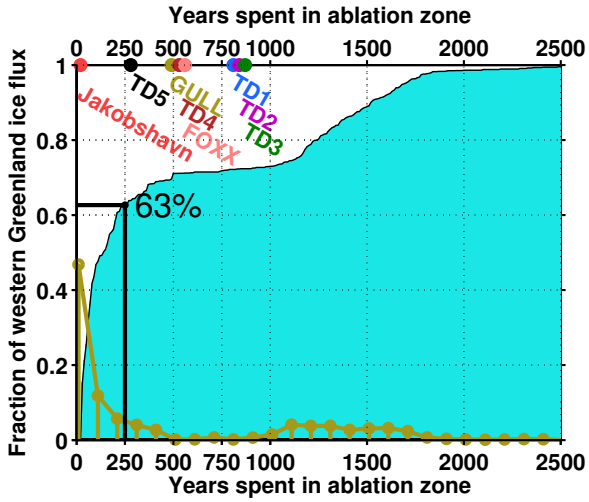

Figure 3.8: *Cumulative histogram of ice flux through the central western Greenland study area, binned by the total amount of time ice that crosses each ELA flux gate will spend in the ablation zone before reaching the terminus. The gold stems outline a histogram of the normalized discharge, binned in 100-year intervals of time spent in the ablation zone. Also shown are the elapsed time in the ablation zone for ice at the seven Pâkitsoq boreholes and the Jakobshavn boreholes collectively.*

Because we are looking at warming in the top part of the ice column and because sliding accounts for much of the speed, we do not correct for speed as function of depth. Residence times in the ablation zone for all points in our central western Greenland study area are shown in Figure 7a.

3.5.2 Weighting for ice flux

Figure 7a shows that ice in a large swath of the ice sheet with low ice flux and divergent flow has relatively long ablation-zone residence times ($>\sim$1000 years). By contrast, convergent, fast-flowing, high-flux glaciers cover relatively little area; Jakobshavn Isbræ, which outputs more ice than any other western Greenland glacier, has a disproportionately small footprint in Figure 7a. This suggests that one should interpret ablation-

zone residence times not through their size on a map, but through their relative ice flux.

We calculate balance ice fluxes by integrating the SMB, which we average over 1960–2011 from RACMO2, within the catchments of multiple 2-km-wide gates along the ELA. We sum the residence-time data and weight them by the balance flux to produce cumulative distributions of ice flux versus time spent in the ablation zone (Figure 8). These results show that ∼63% of the ice flux across the equilibrium line in central western Greenland occurs in regions where the ice spends less than 250 years in the ablation zone. This illustrates the significant contribution of large outlet glaciers to the seaward ice flux. As shown in Table 1, the fastest-moving ice in Jakobshavn Isbræ spends only 20 years in the ablation zone; Figure 8 shows that such ice ($\tau_{ELA} \leq$20 yrs) accounts for a full 15% of the ice flux through central western Greenland.

The ice at the seven Pâkitsoq borehole sites spends 280–840 years in the ablation zone before arriving at each drill site. For the faster-moving ice in Jakobshavn Isbræ and in many glaciers north of it, ice moves through the ablation zone generally in less than a century. To the south of Jakobshavn Isbræ, residence times typically are greater than 1000 years. As the Pâkitsoq boreholes suggest, this timescale allows substantial cryo-hydrologic warming (∼10°C or greater).

3.6 Discussion

Here we discuss our results in the context of the boundary conditions used in ice sheet models as well as the implications of cryo-hydrologic warming on sea-level rise predictions.

3.6.1 Latent heat transfer in firn

Our model results for Jakobshavn Isbræ (Figure 4) clearly show that it is necessary to include the latent heat of refreezing in firn to model englacial temperatures. Ice temperatures modeled using RACMO2 two-meter air temperature (BC 1) are as much as ∼7°C

cooler than observations in the top few hundred meters of the ice column, although the difference dwindles with depth and is $<1^{\circ}$C by depths of $\sim$1000 meters. We note that although we tuned the enhancement factor E in the Jakobshavn catchment, in Pâkitsoq, the good match at depth is not especially sensitive to the value of the enhancement factor.

Variations among boundary condition cases

The results using the Reeh (1989) boundary condition (BC 2) are also substantially cooler than observed ice temperatures, even though this surface temperature parameterization was developed to reflect the refreezing of meltwater within firn. Reeh (1989) used temperatures measured at depths of 3 meters (in snow pits) and 7–20 meters (in shallow ice cores) at various elevations in western Greenland from 1955 through the 1980s. These field measurements may underrepresent refreezing due to the nature of local site selection: high, dry locations are often chosen over lower-lying areas, where slush and surface water tend to inhibit operations. Thus, the poorer agreement of Jakobshavn boreholes with the simulations using BC 2 could suggest that the Reeh (1989) parameterization is colder than the true firn temperatures due to sparse sites that undersampled the true influence of percolating meltwater.

The firn temperatures also may have changed substantially since 1955, when the earliest of the (Reeh, 1989) measurements were collected. Polashenski et al. (2014), for instance, observed considerable increases in modern firn temperatures since that time. The RACMO2 model output supports this idea, as temperatures at 15-meter depth (BC 3) are almost everywhere warmer than the Reeh (1989) parameterization (Figure 3). In fact, even the two-meter air temperatures (BC 1) exceed the Reeh (1989) parameterization at elevations above $\sim$1800 meters.

Inferred near-surface temperature history

The Jakobshavn temperature profiles modeled using the near-surface RACMO2 boundary condition (BC 3) show warm inflections at approximately 60–130 meters depth (Figure 4). There, the ice is approximately 3°C warmer than expected from the otherwise smooth curve. A simple analysis of SMB and surface velocities shows that the ice at ∼100 meters depth originated at the surface approximately at the onset of increased firn temperatures (Figure 3). It is unclear, however, whether this specific output of our model is actually observable in the Jakobshavn ice because the near-surface temperature measurements there are too sparse (∼100-meter vertical spacing) to indicate this level of detail.

Near-surface observations in the TD5 borehole show a similar pattern to the near-surface warmth we modeled in the Jakobshavn boreholes: temperatures in the top 200 meters are ∼7°C warmer than expected with BC 3. Our model with englacial latent heat transfer occurring at 50% of the ice sheet area, however, finds ice temperatures another ∼8°C warmer than observed (not shown). With a sparser distribution of crevasses (20% of the ice sheet surface), the model produces a more satisfactory fit to the data (Figure 5a). Lüthi et al. (2015), however, excluded englacial latent heat transfer at this site and instead identified a past warm period to explain this near-surface warmth. Yet satellite images show crevasses and meltwater are present at elevations near TD5, so one would expect to see their thermal influence. Thus, while we do not rule out a past warm period, we consider that crevasse-based englacial warming is a viable and simpler alternative for explaining near-surface warmth at the TD5 drill site.

3.6.2 Englacial temperatures in Pâkitsoq

In Pâkitsoq, our results suggest that at elevations below ∼1700 m, crevasses carry water to an average of ∼150 meters depth ($Z_{max} \sim 300$ m) within the ice sheet, where it has a substantial (∼2–10°C) influence on englacial temperatures. We find no variation between apparent crevasse depth and elevation. However, the relatively constant crevasse depth

along flow (Z_{max} 250–350 meters) represents a greater fraction of the ice column as the ice moves downstream and thins. At the lowest-elevation borehole (TD1), we found a Z_{max} of 300 m, equivalent to the full thickness of the ice there.

Our results agree well with those of Lüthi et al. (2015), who used a similar approach but different techniques to model a subset of the Pâkitsoq boreholes. They assumed a spatially constant crevasse depth of 400 meters and allowed each crevasse to persist for 50 years before returning its ice to a standard surface boundary condition. For comparison, with our model grid spacing of 3 km, surface velocities of approximately 100 m/yr, and 50% of grid points hosting crevasses, our model has an effective crevasse lifetime of 45 years. Along the TD5 flowline, this decreases to 36 years because of the sparser crevasse distribution there (20% of grid points).

Lüthi et al. (2015) assigned a substantially greater penetration depth (400 m) than we found ($\sim$150 m). We note that their zone of crevassing begins at Swiss Camp (s=1150 m), whereas ours begins at s=1700 meters, a horizontal difference of 50 km. We speculate that our expanded area of crevassing compensates for our shallower and slightly shorter-lived crevasses compared to Lüthi et al. (2015).

Lüthi et al. (2015) excluded the TD4 borehole from their analysis. Indeed, our work suggests that this site is anomalous: it requires the deepest crevasses (Z_{max}=350 m) but has a temperature profile that our model could not recreate and whose shape is different from the other sites (Figure 5). Field reports suggest drilling difficulties here (Thomsen and Olesen, 1990), so it is possible that the reported temperatures at TD4 are inaccurate. It is also possible that the drill site was close to a relict moulin or deep crevasse.

The warm ice observed in the Pâkitsoq catchment has analogues elsewhere in Greenland. For example, Harrington et al. (2015) found ice substantially warmer than mean-annual air temperature in Isunnguata Sermia, southwestern Greenland. Their five drill sites spanned a similar range of elevations and showed comparable, though slightly warmer, englacial temperatures to the Pâkitsoq sites we studied. The Isunnguata sites, however, have all spent substantially longer in the ablation zone (850–1200 years) than the Pâkitsoq

ice has. These tenures represent roughly the 75th percentile of the ice in western Greenland (Figure 8). The warmth in those boreholes is not surprising given the long timescale over which the ice has had to collect meltwater. The rate of warming is evidently slower in the Isunnguata catchment, though, perhaps due to differences in the surface hydrology (e.g., a greater presence of moulins).

3.6.3 Context for field measurements of cryo-hydrologic warming

Given the continuum of warmth observed in boreholes in Pâkitsoq and on other land-terminating ice (Harrington et al., 2015), it seems unlikely that englacial latent heat transfer through surface crevasses has begun recently or that a sudden transition has occurred. Our results suggest that englacial temperatures are in equilibrium with a surface meltwater supply that has regularly reached up to ∼300–350 meters depth and has been operating continuously over the past few thousands of years. Even to the extent that the process of englacial latent heat transfer may migrate to higher elevations over time, our results at the TD5 borehole suggest that the effect largely will be limited to the upper ice column, where warming has little influence on flow.

Our conclusion of near-equilibrium englacial temperatures contrasts with Phillips et al. (2013), who identified a recent rapid increase in englacial latent heat transfer as evidenced by the apparent acceleration of ice motion in western Greenland. Unfortunately, their conclusion was reached through interpreting artifacts in velocity measurements, which have since been corrected (`http://nsidc.org/data/docs/measures/nsidc0478_joughin/`). The updated measurements suggest no such acceleration. This lack of acceleration supports our hypothesis that any recent cryo-hydrologic warming has had little effect on flow.

The influence of cryo-hydrologic warming largely is limited to slow-flowing regions of divergent flow, which mostly lose mass in situ via surface melting rather than by iceberg calving. As it is likely that latent heat from melt water has been warming this ice over

much of the Holocene, the ice sheet should have evolved to have a lower surface slope that would produce balance velocities consistent with this warmer, softer ice. Higher on the ice sheet where the ice is cold, however, inland migration of the ELA could newly warm and soften the ice, increasing flow speed modestly. Our results suggest that such warming, however, will not have a sudden, catastrophic effect on ice flow, as has sometimes been suggested (Phillips et al., 2010). Rather, the upper ice column will warm but will have a moderate and gradual effect on ice flow. It will take additional decades to centuries to warm the full ice column, and over these timescales, other influences on ice flow are likely to have a larger effect (e.g., ice-sheet thinning directly due to surface melt).

3.6.4 Ice-sheet-wide interpretation

Central western Greenland hosts a considerable amount of land-terminating ice that spends hundreds of years in the ablation zone: roughly 50% by area, as shown in Figure 7a. Ablation, as opposed to ice dynamics, is the primary control on mass balance in these areas. To substantiate our claim that this region is the largest in Greenland where ablation of land-terminating ice controls mass balance, we compare it to the ablation zone in other regions of the ice sheet. Figure 7b shows the time elapsed since crossing the ELA for the entire Greenland Ice Sheet. Like Figure 7a, this map highlights areas where significant cryo-hydrologic warming likely occurs viz. a long tenure in the ablation zone. The largest such area occurs in central western Greenland (20,000 km^2), but ice in certain pockets of northern and Northeast Greenland ($\sim$5000 km^2 each) spends thousands of years in the ablation zone before ultimately ablating. These pockets, located near Humboldt Glacier (τ_{ELA} $\sim$2000 years) and Nioghalvfjerdsfjorden (τ_{ELA} $\sim$8000 years), are particular examples where surface melt is the dominant mode of ice loss. Elsewhere in Greenland, especially along its east and west coasts, dynamic mass loss, characterized by short τ_{ELA} ($<\sim$250 years), is the primary ice loss mechanism, so that cryo-hydrologic warming likely has little influence.

Figure 7b does not give a complete picture of the effects of melt – for example, southeast Greenland experiences similar annual melt rates as central western Greenland, although the high snowfall rates there make the net SMB positive (Ettema et al., 2009; van Angelen et al., 2013), excluding this area from the map.

3.7 Conclusion

Our ice-sheet model uses a computationally inexpensive parameterization of firn thermal processes in its surface boundary condition. Our results suggest that this greatly improves estimates of englacial temperatures, particularly in areas of fast-moving ice.

Our model also shows that in certain areas, englacial refreezing of surface meltwater can substantially increase ice temperatures at depth, which can translate to a substantial increase in softness. Our results in the Pâkitsoq area show that although considerable englacial refreezing is occurring, increasing ice temperatures by as much as $\sim$10°C, the effect on overall flow is small ($<$10%) because of the predominance of basal sliding there.

Furthermore, our study of ice flux through central western Greenland suggests that divergent, slow-flowing areas, where warming is likely to occur, are only modest contributors to dynamic mass loss over central western Greenland. This is because most of the ice flux across the ELA ($\sim$63%) moves too quickly through the ablation zone to experience appreciable cryo-hydrologic warming. This region represents the area of Greenland with greatest vulnerability to cryo-hydrologic warming due to its large extent of land-terminating ice that spends many hundreds of years in the ablation zone. Thus, we conclude that cryo-hydrologic warming does not likely pose a significant threat to the stability of the Greenland Ice Sheet.

Chapter 4

CONSTRAINTS ON THE STORAGE OF SURFACE MELTWATER IN GREENLAND CREVASSES

Note: This chapter is being prepared for submission to a short-format journal such as *Geophysical Research Letters*.

This chapter complements the previous chapter. The two pieces of work are nearly independent of each other, yet reach very similar conclusions: most water-filled crevasses in western Greenland penetrate the top few hundred meters of the ice sheet, where they leave a warming signature.

The model I developed for this work is the first of its kind: it is a physically based fracture mechanics model that also incorporates the phase changes and latent heat transfer associated with refreezing water englacially. The model incorporates elastic deformation and refreezing, which are processes that most influence the crevasse depth. Future work will be to incorporate creep (viscous) deformation into the model. Sensitivity tests I designed to estimate the effects of creep suggest that creep has a relatively small effect on crevasse depth. Thus, I do not expect the future addition of creep closure to substantially change the conclusions of this chapter.

I developed and applied the model, interpreted the output, synthesized the ideas, and wrote the paper. Ian Joughin aided and advised me throughout these processes.

Constraints on the storage of water in Greenland crevasses

Kristin Poinar and Ian Joughin

Abstract. Crevasses fed by lakes or supraglacial streams can create hydrofractures that form moulins, which are important conduits for transferring surface meltwater to the bed. The fate of crevasses that receive lower volumes of meltwater, however, has been less explored. To study the depth, water balance, and effect on ice temperature of a typical meltwater-fed crevasse in western Greenland, we combined an elastic model for crevasse propagation with a thermal model for englacial refreezing rates. We constrained this model with inferred englacial refreezing rates in the Swiss Camp region and observations of the supraglacial hydrological network. We find that typical crevasses persist, water-filled, at ∼200–300 meters depth for years to decades without refreezing or draining to the bed; the slow refreezing of the meltwater warms the ice by ∼10°C. This depth holds across a relatively wide range of water input values representative of the Swiss Camp region, suggesting that crevasse depth likely will be insensitive to future increases in surface melt rates.

4.1 Introduction

Recent decades have seen increased surface melt and crevassing in western Greenland (Colgan et al., 2011; van de Wal et al., 2012). Hydrofracturing of water-filled crevasses can create moulins (Alley et al., 2005; Clason et al., 2015; Das et al., 2008; Krawczynski et al., 2009; Stevens et al., 2015; van de Wal et al., 2012), which transport the meltwater to the bottom of the ice sheet (Das et al., 2008), where it alters the basal hydrologic system and affects the motion of the ice sheet (Das et al., 2008; Doyle et al., 2013; Hoffman et al., 2011; Joughin et al., 2013; van de Wal et al., 2012). However, not all crevasses fed by meltwater form full-ice-thickness hydrofractures. Many of those that do not reach the bed can store meltwater englacially for long periods of time (Jarvis and Clarke, 1974; Lüthi et al., 2015).

This leads to cryo-hydrologic warming, which can also affect ice motion (Phillips et al., 2010). Given the recent increases in melt and crevassed extent, an increase of meltwater delivery to the englacial cryo-hydrologic system is expected (Phillips et al., 2013) and may have already been observed in some places (Rennermalm et al., 2013).

Rapid hydrofracture and longer-term englacial storage are two possible fates of surface meltwater that encounters surface crevasses. Work in the 2000s greatly enhanced our understanding of hydrofracture (Alley et al., 2005; Das et al., 2008; Krawczynski et al., 2009; Stevens et al., 2015), but the behavior of englacial of meltwater on longer (seasonal or multi-year) timescales is not yet well constrained. Understanding englacial meltwater is important because it is unclear how much surface melt reaches the ocean in a given melt year (Smith et al., 2015). It is currently unknown what fraction of the surface melt that does not run off is stored englacially and how much is stored subglacially (Rennermalm et al., 2013; Smith et al., 2015).

Here we study crevasse fields in the western Greenland ablation zone to bound the volumes of water that are likely to reside englacially, the time scales over which liquid water is likely to persist there, its contribution to cryo-hydrologic warming, and the depths that typical water-filled crevasses reach. We use field and satellite evidence and a numerical model for crevasse propagation to investigate the englacial characteristics of a field of meltwater-filled crevasses.

4.2 Methods

To study the propagation of typical closely spaced crevasses in western Greenland, we developed a two-dimensional half-space model that incorporates the deformational and thermal aspects of crevassing. We constrained the meltwater influx into the crevasses in our model using observations of satellite imagery and results from a previous study of englacial refreezing. We describe these methods briefly here and point the reader to the Supplement for more detail, where appropriate.

4.2.1 Characteristics of the Swiss Camp study area

Crevasses tend to originate in regions of tension on topographic highs (Figure 4.1a), forming crevasse fields. Dry crevasses can only reach a few tens of meters depth (Nye, 1955), but water-filled crevasses can penetrate hundreds of meters deeper (Weertman, 1973). The amount of water that can enter each crevasse, however, is limited by the local relief: the position of crevasse fields on topographic highs means that only local meltwater is likely to enter most crevasses. We define local as the space spanning $[-R/2\ R/2]$ around a crevasse, where R is the distance separating neighboring crevasses.

As crevassed ice advects into compressive regions, the crevasses tend to close, leaving rumples on the ice-sheet surface (Figure 4.1b). Such regions generally occupy topographic lows (Joughin et al., 2013). Whereas regions in tension generally lack streams (Figure 4.1c) so that meltwater generally enters the nearest crevasse, compressive regions, such as the right half of Figure 4.1d, often host extensive stream networks that carry meltwater away from its point of origin.

Larger streams can incise into the ice-sheet surface, allowing them to flow out of basins and enter tensile regions, as shown in the left half of Figure 4.1d. Because of their relief, these streams likely collect additional meltwater from neighboring crevasses (Figures 4.1e and 4.1g). Crevasses farther from streams, however, may collect all or most of their local meltwater (Figure 4.1f).

We account for these characteristics of the surface hydrology by defining a spatial efficiency parameter, f, for use in our model. This parameter describes the fraction of local meltwater that flows into a crevasse: $f < 1$ represents crevasses in the vicinity of a surface stream (Figures 4.1e and 4.1g), while $f > 1$ indicates a crevasse that receives additional meltwater outside its local catchment (Figure 4.1e).

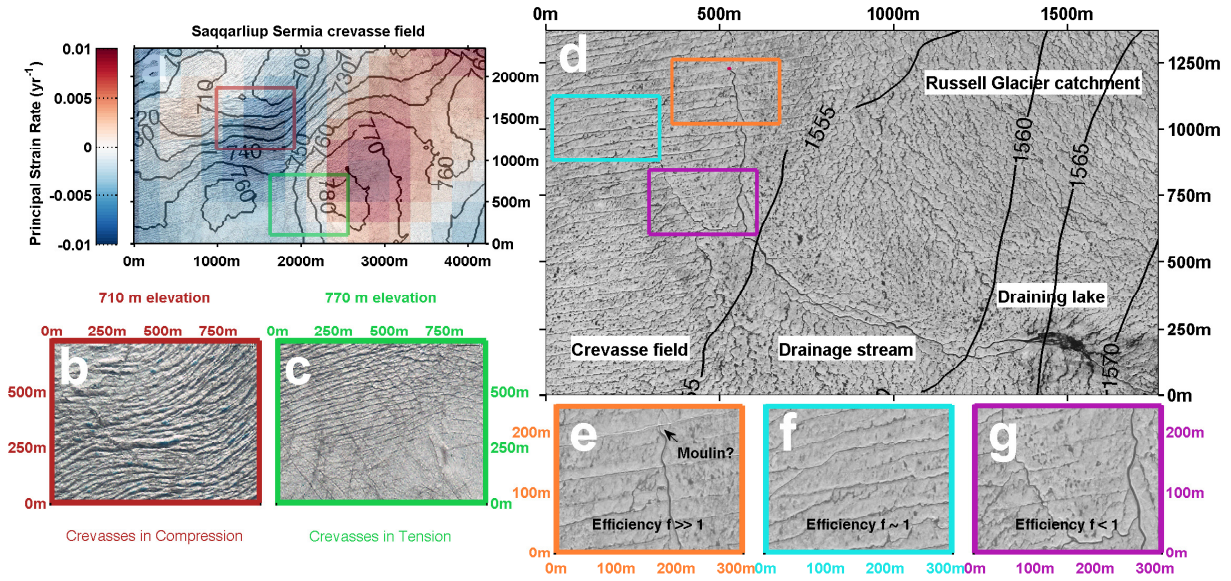

Figure 4.1: Examples of crevassed areas that our model represents. (a) A crevasse field on Saqqarliup Sermia, 20 km south of Jakobshavn Isbræ. Colors indicate surface strain rates; red is extensive and blue is compressional. Panel details (b) and (c) show the end and beginning of the crevasse field, respectively. Panel (d) shows a complex hydrological system upstream of Russell Glacier in Southwest Greenland. Detail (e) shows a supraglacial stream delivering meltwater into one crevasse ($f >> 1$), likely forming a moulin. Detail (f) shows a "typical" crevasse ($f \sim 1$), where streams are largely absent and drainage is primarily local. Detail (g) shows the faint crevasses the supraglacial stream flows across; they are likely shallow due to their relative lack of water ($f << 1$). Elevation contours, where shown, are from the GIMP DEM (Howat et al., 2014) and all WorldView images were provided by Paul Morin.

4.2.2 *Model for crevasse depth and shape*

Surface meltwater that flows into a crevasse will incite hydrofracture: it will elastically open and deepen the crevasse. Over a longer timescale, the crevasse walls will close elastically and through creep; this narrows the crevasse and makes it shallower. The meltwater inside will also steadily refreeze onto the crevasse walls, which diffusively warms the surrounding ice and contributes further to the closing and shoaling of the crevasse. Our model calculates the shape and depth of crevasses in the vicinity of Swiss Camp, central western Greenland, based on the elastic and refreezing processes. We are currently working on a module that will quantify the viscous (creep) deformation within the crevasse. We do not expect the addition of creep to change our results substantially, or to qualitatively change our conclusions. Our reasoning is explained in the Supplement (Section 4.6.2).

We ran the model through 50 years at 5-day timesteps. At each timestep, an influx of meltwater, V_{influx}, enters each crevasse. We allow crevasses to collect meltwater only when in regions of tension ($\sigma_{xx} > 0$):

$$V_{influx} = \begin{cases} f \cdot R \cdot b \cdot \Delta t, & \text{for } \sigma_{xx} > 0 \\ 0 \quad , & \text{for } \sigma_{xx} \leq 0 \end{cases} \tag{4.1}$$

Here, b is the ablation rate, R is the spacing between adjacent crevasses, and f is the spatial efficiency parameter. We assume $b = -2$ m/yr; we scale the total annual melt volume throughout the melt season based on daily melt rates from RACMO2 (van Angelen et al., 2013). We set R = 33 meters based on our field observations and in agreement with previously used values of ∼20–100 meters (Phillips et al., 2010).

The spatial efficiency parameter f, the fraction of the available local surface meltwater that enters each crevasse, can vary widely over short areas, as illustrated in Figure 4.1. We varied f among model runs across six orders of magnitude, from 0.001 to 300, in an effort to test the full span indicated by these observations. We set the upper limit

substantially above the volume threshold for full-thickness hydrofracture (Clason et al., 2015; Krawczynski et al., 2009) and the lower limit to a value which barely kept crevasses open through each summer.

The amount of water in a crevasse at any given time is the cumulative volume of the meltwater input (Equation 4.1) minus the volume of water refrozen onto the crevasse walls throughout the model run. To calculate the volume refrozen, we compute the temperatures surrounding each crevasse using the thermal model described in Section 4.2.3.

To model the elastic opening of a water-filled crevasse, we use the solution of Weertman (1996), later applied by Krawczynski et al. (2009), described in the Supplement (Section refElastic). The solution describes the shape of a crevasse that opened elastically to a given depth; that depth is primarily a function of the amount of water available to fill the crack. From the elastic term, we subtract a refreezing term to calculate the full crevasse geometry. We calculate the crevasse depth iteratively by matching the volume of available meltwater to the volume of a water-filled crevasse with a depth Z. We fill the crevasse with water to a depth w where the stress at the crack tip is equal to the fracture toughness of ice (van der Veen, 1998).

For each 5-day timestep, we add the amount of local ablation (Equation 4.1; a two-dimensional volume) to the volume of water in the crevasse. We repeat for a thirty-year period, which we chose to be representative of the time it takes the ice to advect across a 3-km crevasse field at 100 m/yr. After thirty years, we turn off the surface meltwater supply (Equation 4.1) but continue to let the crevasse shape and depth evolve for an additional twenty years.

4.2.3 Thermal model for englacial refreezing rates

Meltwater refreezes onto the crevasse walls at a rate dependent on the temperature of the ice. We calculate temperature within the ice blocks between the crevasses with a two-dimensional thermal model. This model prescribes a 0°C temperature to the ice in contact

with each crevasse, where the crevasse depths are taken from the elastic fracture model. The thermal model includes horizontal advection (100 m/yr), vertical advection (0–2.0 m/yr upward), horizontal and vertical diffusion, and latent heat transfer from refreezing. Boundary conditions are 0°C at the bed and the mean daily air temperature (averaged over 2006–2010) at the surface, also from RACMO2 (van Angelen et al., 2013). We use the ice temperature measured in boreholes at Swiss Camp in 1990 (Thomsen et al., 1991) as a lateral boundary condition at the upstream end of the domain.

The horizontal temperature gradient in the ice of the crevasse walls, $\frac{\Delta T}{\Delta x}$, determines the refreezing rate of meltwater, V_{frz}:

$$\frac{V_{frz}(z)}{\Delta t} = \frac{k}{L_f \rho}\left[\frac{\Delta T_L(x,z)}{\Delta x} + \frac{\Delta T_R(x,z)}{\Delta x}\right] \tag{4.2}$$

Here, k_i is the thermal conductivity of ice, L_f is the latent heat of freezing of ice, Δt is the thermal model timestep, and T_L and T_R denote temperatures at the left and right crevasse walls, respectively. The spatial step Δx is equal to the diffusion length over approximately one year (5 meters). This approximation is discussed in the Supplement (Section 4.6.3).

At each timestep, the model adds the surface meltwater to and subtracts the refrozen water from the total water volume within each crevasse. The influx of surface melt dominates in the spring and summer and makes the crevasse grow, while the loss of water due to englacial refreezing is relatively steady throughout the year. With no melt influx in the fall and winter, refreezing causes the crevasse to shrink. Figure 4.2 illustrates this evolution of a crevasse in the model.

4.2.4 Englacial refreezing rates informed by field observations

We use independent, indirect observations of englacial refreezing rates to constrain our model inputs. We calculate local refreezing rates within the region around Swiss Camp using previous results from a different numeric model for ice temperature (Poinar and Joughin, 2016) tuned to borehole observations near and downstream of Swiss Camp (Ryser

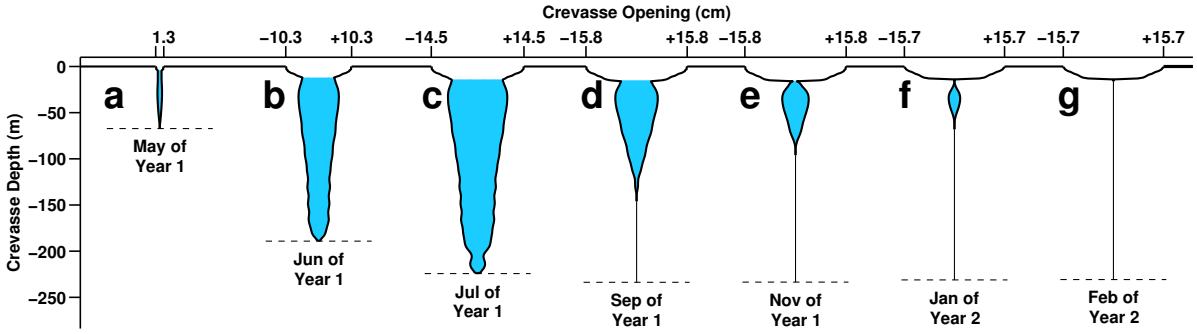

Figure 4.2: Evolution of a water-filled crevasse. A young crevasse fills with surface meltwater and deepens (a–c), but also slowly creeps closed even as it deepens. The elastic closure rate is greatest at the water line, where the inward cryostatic stress most exceeds the outward hydrostatic stress, which is zero there. At the end of the melt season (d), meltwater no longer deepens the crevasse, and refreezing is also seen to heal the crevasse at depth. Elastic closure will eventually pinch the crevasse closed (e–f), cutting it off from the surface water supply. After all water has refrozen, the surface expression of the crevasse (a "ditch") remains (g).

et al., 2014; Thomsen et al., 1991). This gives the temperature difference between non-crevassed ice and ice where latent heat within crevasses has refrozen and warmed the ice. From these values, we infer the rate at which water must have refrozen englacially. Details of this method can be found in the Supplement (Section 4.7).

We compare the inferred volumetric rate of refreezing to the refreezing rates in our model. We find that for a given ice temperature, freezing rates are primarily a function of crevasse depth, and that crevasse depth is primarily a function of the meltwater influx. Thus, we use the inferred rate of refreezing to constrain the free parameter V_{influx} for this region of the ice sheet.

4.3 Results

We ran the model for 50 years (5 km of motion) through a 3-km-wide region of tension representative of a crevasse field and a 2-km-wide region of compression in which $V_{influx} = 0$ (see Equation 4.1).

4.3.1 Sensitivity tests

Our model has several parameters: Poissons ratio, the background longitudinal shear stress, the shear modulus, the crevasse spacing, the fracture toughness, and the spatial efficiency parameter. We began by investigating the sensitivity of the modeled crevasse depth and the englacial temperature field to these parameters. The results are summarized in Table 4.1. We found low sensitivity to Poissons ratio ν the fracture toughness, and the background longitudinal stress σ_{xx}. Given the low sensitivity, we used the standard values for these parameters.

We tested the three values of the shear modulus μ identified by Krawczynski et al. (2009) based on the work of Vaughan (1995). This parameter had a greater effect on crevasse depth, with the maximum crevasse depth varying by >100 meters across these values of μ (Table 4.1). With this sensitivity in mind, we used the middle value of μ,

Table 4.1: Sensitivity of crevasse depth to various parameters

Parameter	Standard value	Perturbed value	Difference in crevasse depth after 30 years
Shear modulus μ	1.5 GPa	0.32 GPa 3.9 GPa	80 meters shallower 480 meters deeper
Poisson's ratio ν	0.3	0.35	0.1 meters deeper
Crevasse spacing R	33 meters	100 meters	110 meters deeper
Efficiency f	1	0.33 3	2 m shallower 580 m deeper
Background tensile stress σ_{xx}	100 kPa	200 kPa	5 m shallower
Fracture toughness	100 kPa $m^{\frac{1}{2}}$	150 kPa $m^{\frac{1}{2}}$	7 m shallower

1.5 GPa.

We explored sensitivity to different crevasse spacing R (33 and 100 meters) and found that on average, the wider-spaced crevasses penetrated $\sim$110 meters deeper. This is because more widely spaced crevasses have larger local catchments and thus collect higher water influxes (Equation 4.1). The larger blocks of cold ice between the more widely spaced crevasses compensated slightly for the additional water by allowing greater amounts of refreezing over time. We used R = 33 meters, which is consistent with our field and satellite observations, as our standard value.

Overall, we found f, through the meltwater input rate V_{influx}, to have the greatest influence on crevasse depth and ice temperature. The efficiency f can vary over a wide range due to the presence or absence of surface streams (Figure 4.1). Where these streams terminate into crevasses, $f >> 1$, and as a result, other crevasses in the stream catchment have $f < 1$.

4.3.2 *Annual freeze-up*

Figure 4.3 shows crevasse depth as a function of model time (0 to 50 years) and meltwater influx volume. Crevasses given low melt influxes ($V_{influx} < 3$ m^2/yr; f < 0.05) refreeze entirely each winter (blue line on Figure 4.3) for the entire 50-year Swiss Camp model run. This relatively low efficiency seems reasonable for regions where surface streams divert meltwater away from crevasses (Figure 4.1e).

We repeated this analysis for warmer, thinner ice (mean temperature -5°C, compared to -13°C at Swiss Camp; thickness 610 meters) represented by the FOXX borehole (Ryser et al., 2014) at 700 meters elevation. Crevasses in this warmer ice do not refreeze annually unless they receive slightly smaller influx volumes ($V_{influx} < 1.5$ m^2/yr; f <0.02). We also tested colder, thicker ice (mean temperature -17°) typical of the equilibrium line altitude (ELA; elevation 1500 meters). Here, the cold ice was able to annually freeze closed crevasses receiving slightly larger influx volumes ($V_{influx} < 7$ m^2/yr; $f < 0.1$). Plots of crevasse depth at these sites can be found in the Supplement (Section 4.8).

4.3.3 *Englacial water storage*

Crevasses that collect slightly more meltwater ($\sim 30 < V_{influx} < 80$ m^2/yr; $0.5 < f < 1.2$) also refreeze in the first winter at Swiss Camp, but this behavior changes before the end of the 50-year model run. Over time, the latent heat input warms the cold ice enough to lower the refreezing rates below the meltwater input rates. After this point, englacial water exists year-round. The ability of water to refreeze continues to decrease as the ice around the crevasse warms, but at the same time, the ongoing input of surface melt causes the crevasse to widen and deepen. Refreezing rates increase as each crevasse accesses deep, colder ice, and a near-equilibrium state is reached: the crevasses deepen only very slowly over model years ~2–30, as they reach a near-equilibrium depth of 200–350 meters, depending on f. A similar pattern is also observed in model runs for the warmer FOXX ice ($0.2 < f < 1.5$).

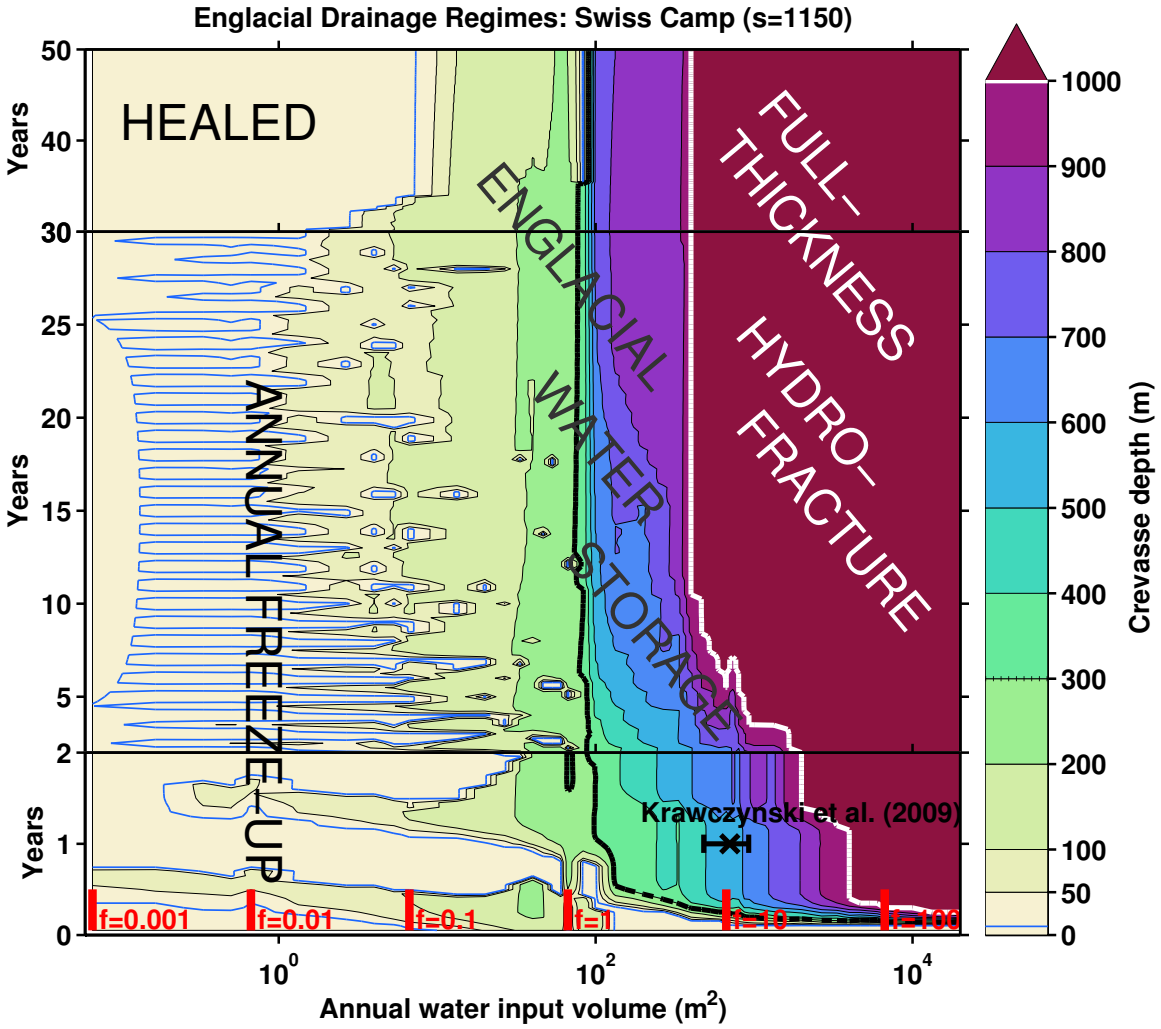

Figure 4.3: Englacial drainage regimes represented through the depth of a typical crevasse over time, as a function of meltwater influx (Eqn. 1), for ice near Swiss Camp. Blue line (10-meter crevasse depth) approximates a crevasse that will freeze closed each winter and reopen during the melt season ("annual freeze-up"). Heavy white line indicates the full ice thickness H=1000 meters; crevasses that extend this deep will drain to the bed ("full-thickness hydrofracture"). Between these two limits, water resides englacially year-round for decades without entirely refreezing. The expected melt volume required for moulin formation in less than one year (Krawczynski et al., 2009) is shown in the bottom right.

The crevasse annually deepens and shoals as the surface meltwater supply fluctuates. The degree of this vertical variation is the primary control on the annual variation in englacial freezing rates. In cases where the crevasse retains water through each winter ($f > 0.05$), the crevasse depth shows only a slight seasonal cycle.

We find that water can persist englacially for decades before it refreezes, even after being cut off from the surface water supply. Evidently, the width of the crevasse prevents quick refreezing by allowing only some of the water to contact the crevasse walls. That is, if a crevasse was wider at a given depth than the thickness of water it can refreeze within a timestep, the crevasse remained at least that deep. As the ice around the crevasse warmed cryo-hydrologically, however, its ability to conduct away the latent heat of freezing declined, so refreezing rates decreased. Thus, although each crevasse became shallower after losing access to surface meltwater, the rate at which it became shallower decreased over time.

In general, crevasses receiving the full local melt influx ($f \sim 1$) quickly reached depths of a few hundred meters. After this point, the meltwater influx and refreezing rates were in near-equilibrium for the duration of the 50-year model runs, and the crevasses maintained depths of a few hundred meters, while slowly refreezing.

4.3.4 Full-thickness penetration

We tested the ability of water-filled crevasses to form hydrofractures to the bed (crevasse depth of 1000 meters at Swiss Camp) by varying the filling rate through the efficiency parameter f. We find that crevasses require $V_{influx} > 400$ m^2/yr, or $f > 6$, to form through-ice hydrofractures, and that this can occur over as long as 10 years. Crevasses that receive less water than this can form very deep crevasses ($Z \sim 900$ meters for $f = 5$), but they fail to reach the bed before losing access to the surface water supply. Once they pinch off from the surface or advect out of the tensional crevasse field, they slowly refreeze and shoal, as discussed above.

At the warmer, thinner ice at the FOXX borehole, crevasses were able to hydrofracture to the bed with lower annual influx volumes ($V_{influx} > 400$ m^2/yr or $f > 1.5$) over similar timescales. In thicker, colder ice at the ELA, crevasses required more water ($V_{influx} > 700$ m^2/yr or $f > 10$) and more time ($\sim$16 years) to hydrofracture fully through the ice.

4.3.5 Depth of typical crevasses

The depth that a crevasse can penetrate to is highly sensitive to the water flux feeding it. For example, at Swiss Camp, doubling V_{influx} from 30 m^2/yr to 60 m^2/yr ($f \sim 0.5$–1) increased the near-equilibrium crevasse depth from 200 m to 280 m (Figure 4.3). We found similar sensitivities at the other sites (FOXX, ELA) we modeled. Near-equilibrium crevasse depth has an apparent threshold for higher water fluxes: redoubling V_{influx} ($f \sim 2$) at Swiss Camp increased the crevasse depth to 800 meters. This is because putting more water into a crevasse widens as well as deepens it, making the crevasse less able to pinch off from the surface by refreezing water or closing elastically at the water line.

To constrain the input water flux, we compare refreezing rates within our model to the inferred refreezing rates near Swiss Camp, calculated from previous independent modeling results (Poinar and Joughin, 2016). To calculate englacial refreezing rates within our crevasse model, we average the total volume of water refrozen within the crevasse over the 50-year model run time, for the values of f shown in Figure 4.4. We find the best match to inferred refreezing rates near the Swiss Camp borehole ($L_{frz} \sim 8.0$ cm/yr) with an efficiency parameter $f \sim 0.6$. In the warmer FOXX ice, where borehole observations indicate lower refreezing rates ($L_{frz} \sim 1.5$ cm/yr), we find $f \sim 0.2$. At the ELA, $L_{frz} \sim 3$ cm/yr, which we match with $f \sim 0.3$.

We use the input water volumes inferred above to constrain the typical crevasse depth in each region. We find that crevasses near Swiss Camp ($f \sim 0.6$) extend to 200–250 meters depth. Crevasses lower on the ice sheet (near the FOXX site) and higher on the ice sheet (near the ELA) each apparently reach $\sim$100–150 meters depth.

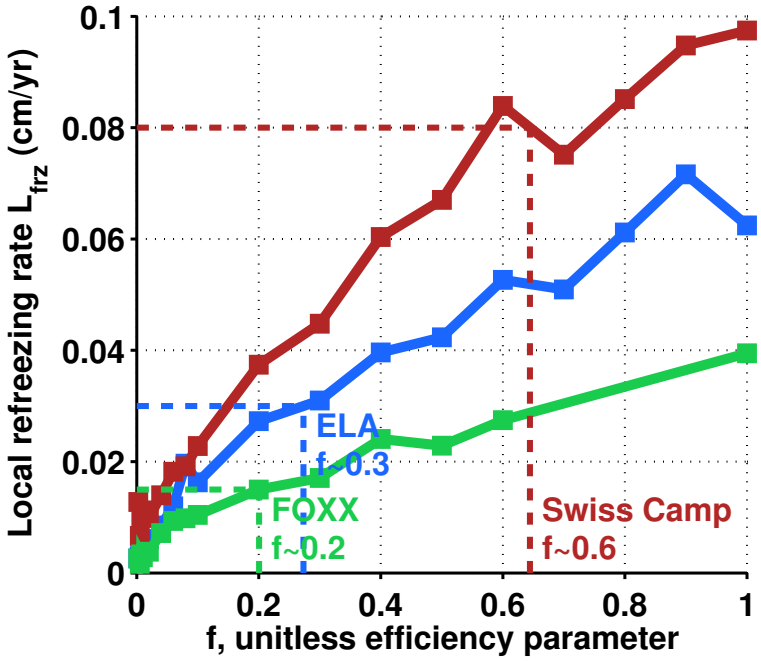

Figure 4.4: Use of the inferred local refreezing rate, L_{frz}, to constrain the volumetric influx efficiency parameter f at the three elevations on the ice sheet we tested. L_{frz} originates from temperature measurements in deep boreholes (Ryser et al., 2014; Thomsen et al., 1991), which show evidence of englacial latent heat transfer, compared to modeled temperature profiles that might be observed absent latent heat transfer (Chapter 3). In our model, L_{frz} is a strong function of f, as shown, and we use this dependence to constrain f. We find the greatest f at Swiss Camp (f ~0.6), where local refreezing rates are also highest.

4.3.6 Effect on ice temperature

Crevasses at Swiss Camp with f = 0.6 warmed the ice around them, through latent heat transfer and diffusion, by 2–15°C, depending on the depth examined. The latent heat also diffused vertically, but to a lesser extent: ice 100 meters below the deepest crevasse was 0.4°C warmer than the initial profile.

4.4 Discussion

Individual crevasses that receive large volumes of meltwater can hydrofracture to the bed on rapid timescales (Stevens et al., 2015), but these crevasses require water volumes that far exceed the local meltwater available in a single melt season (Fitzpatrick et al., 2014), as investigated by Krawczynski et al. (2009). Here, we investigate the possibility of full-thickness hydrofractures forming over longer timescales through the storage of meltwater within crevasses over multiple melt years. We found that crevasses that receive modestly less meltwater than required for single-season drainage to the bed can fracture through the full ice thickness, despite significant englacial refreezing (e.g., ∼30% of the influx over a three-year period). Crevasses that become full-thickness hydrofractures over a single melt season lose only ∼5% of their water volumes to refreezing.

Previous work combined temperature modeling with observations in boreholes to analyze the temperature field at crevassed sites near Swiss Camp (Poinar and Joughin, 2016). That study determined that crevasses reach depths of 150–200 meters on average (300 meter maximum) over a wide range of elevations downstream of Swiss Camp.

The persistence of englacial liquid water predicted by our model contrasts with the idea that crevasse fields constitute a slow, distributed drainage system that transfers water from the ice-sheet surface to the bed (Colgan et al., 2011). Our model shows that in most cases (f $< \sim$6), crevasses are not able to drain meltwater to the bed; instead, they reach a near-equilibrium, with englacial refreezing rates approximately balancing the surface melt influx. This near-equilibrium water balance persists until the crevasse closes and

loses access to the surface water supply.

Elastic closure at the water line tends to form a neck in most crevasses (excepting those that quickly hydrofracture through to the bed). We find that many of these crevasses pinch off at some point in their evolution, sealing a pod of englacial water off from the surface at tens or $\sim$100 meters depth (Figure 4.2). When this occurs, the model terminates melt influx into the crevasse, emulating the drifting of snow that would completely isolate the crevasse from the surface. Some of this snow may melt in the summer and accumulate, perhaps with other surface melt, in the depression as water. This would form wide, shallow, water-filled ditches of the type often seen in satellite or airborne imagery (Figure 4.1b), and often held up as evidence of water-filled crevasses. Our model results suggest that such near-surface ditches likely extend only a few tens of meters down and sometimes overlie a deep pod of englacial liquid water (Figure 4.2d–g). We find that this deep water can refreeze over periods of years to decades, depending on ice temperature and the volume and depth of the crevasse, so fully healed crevasses may also underlie these water-filled ditches.

While we find that, at most, f $\sim$ 0.6 of the local meltwater enters open crevasses, we note that in many cases, crevasses pinch off from the surface after a period of years to decades. Thus, crevasse fields actually collect and refreeze substantially less than 60% of the available surface meltwater. This is not surprising given a simple mass balance argument: crevasses that refroze $\sim$1 m/yr of surface melt would quickly widen and expand the ice sheet laterally.

Catania et al. (2008) observed vertically oriented shafts with high radar reflectivity in the ablation zone. Some of these shafts extended less than the full ice thickness, reaching depths of $\sim$400–600 meters at most, although due to the nature of their radar data, these depths are maxima. These observed features are consistent with our findings of englacial water pockets of depth $\sim$200–300 meters that can persist downstream of a crevasse field. The commonly observed "blue bands" in icebergs, drained lake basins, and throughout the ablation zones of glaciers and ice sheets (Alley et al., 2005) are consistent with the

results of our model. These bands tend to be centimeter-scale, consistent with the annual layers refrozen within shallow crevasses that refreeze annually (<10 cm for $f \sim 0.5$).

The nature of the surface hydrologic system may largely determine the types of crevasses formed. We find three fates for water-filled crevasses in the ablation zone: full-thickness penetration (f $>\sim$6; Figure 4.1e), englacial storage (Figure 4.2d–f), or blue bands and shallow ditches that overly healed crevasses (Figures 4.1b, 4.2g). Satellite imagery (Figure 4.1) and field observations suggest that only a very few crevasses receive enough water to hydrofracture to the bed, and that the efficiency parameter for these crevasses far exceeds the f=6 threshold we identified. Comparing our results to those of Krawczynski et al. (2009) (Figure 4.3), we find that these crevasses likely require $f > 10$ or more. Once the full-thickness hydrofracture has formed, meltwater from a wide catchment continues to flow into it, effectively setting f $>>$ 10 over many melt seasons.

Setting aside such crevasses, it is difficult to imagine a scenario where a crevasse receives a greater-than-local ($f > 1$) water input rate. This is because typical crevasses tend be located near topographic highs, and so tend to lose local meltwater rather than collect it. Mapping of supraglacial streams (Joughin et al., 2013) and tracing hydraulic gradients (Clason et al., 2015) indicate that surface meltwater tends to be carried away from crevasse fields, downhill into lake basins.

Penetration depths vary relatively little over the expected range of water influxes ($f \sim$ 0.2–1), but crevasse depth grows quickly with f for $f \sim 1.5$ and greater, reaching 800 meters at $f = 2$. To achieve this water influx, though, would require melt rates at Swiss Camp of approximately 6 m/yr, a value more than three times higher than the current average. While melt rates are expected to increase, the amount of melt that would be required to substantially deepen crevasses in this area is well outside of current projections for the next century.

4.5 Conclusion

We calculated the depth and thermal influence of meltwater-filled crevasses in the western Greenland ablation zone using a physically based model. Remote-sensing observations of supraglacial hydrology, and englacial refreezing rates inferred from field observations constrained the meltwater input parameter of the model. Within these constraints, we find that meltwater-filled crevasses quickly penetrate to 200–300 meters depth, and persist there for decades as the water slowly refreezes englacially, warming the ice in the top half of the ice column by $\sim$10°C. For such cryo-hydrologic warming to penetrate deeper into the ice sheet, where the stresses are higher and warmth would have a greater influence on ice flow, melt rates would have to increase by at least a factor of 3, which is beyond the expected climate response in the next century.

Our model also suggests that crevasse fields do not allow meltwater to reach the bed over wide spatial scales. Rather, crevasse fields refreeze small volumes of surface meltwater englacially. Water-filled crevasses tend to close elastically at or slightly below their water lines, forming a water-filled pocket that is isolated from the ice-sheet surface. These crevasses tend to retain surface expressions that, in our model, can be tens of centimeters wide. Such features can commonly be seen collecting shallow pools of meltwater on the ice-sheet surface. We suppose that these shallow pools signify narrower, pinched-off water-filled crevasses that extend to $\sim$200 meters below.

Supplemental Information

4.6 Model Details

4.6.1 Elastic component of the model

Crevasse opening is primarily an elastic mechanism. Weertman (1996) represented the elastic displacement of a crevasse wall as a sum of infinitesimal edge dislocations integrated upward from the crack tip. Weertman (1996) gives the analytic solution for the shape $W(z)$ of an elastically-opened crevasse as

$$\begin{aligned} \mathrm{W(z)} = {} & \frac{2(1-\nu)\sigma}{\mu}\sqrt{\mathrm{d^2\text{-}z^2}} + \frac{2(1-\nu)\rho_w \mathrm{g}}{\pi\mu}\mathrm{d}\sqrt{\mathrm{d^2\text{-}z^2}} - \frac{2(1-\nu)\rho_w \mathrm{g}}{\pi\mu}\sqrt{\mathrm{d^2\text{-}w^2}}\sqrt{\mathrm{d^2\text{-}z^2}} + \ldots \\ & - \frac{2(1-\nu)\rho_i \mathrm{g}}{2\pi\mu}\mathrm{z^2}\ \ln\left(\frac{\mathrm{d}+\sqrt{\mathrm{d^2\text{-}z^2}}}{\mathrm{d}-\sqrt{\mathrm{d^2\text{-}z^2}}}\right) + \frac{2(1-\nu)\rho_w \mathrm{g}}{2\pi\mu}\sqrt{\mathrm{z^2\text{-}w^2}}\ \ln\left|\frac{\sqrt{\mathrm{d^2\text{-}w^2}}+\sqrt{\mathrm{d^2\text{-}z^2}}}{\sqrt{\mathrm{d^2\text{-}w^2}}-\sqrt{\mathrm{d^2\text{-}z^2}}}\right| + \ldots \\ & - \frac{2(1-\nu)\rho_w \mathrm{g}}{\pi\mu}\mathrm{w\ z}\ln\left|\frac{\mathrm{w}\sqrt{\mathrm{d^2\text{-}z^2}}+\mathrm{z}\sqrt{\mathrm{d^2\text{-}w^2}}}{\mathrm{w}\sqrt{\mathrm{d^2\text{-}z^2}}-\mathrm{z}\sqrt{\mathrm{d^2\text{-}w^2}}}\right| + \frac{2(1-\nu)\rho_w \mathrm{g}}{\pi\mu}\mathrm{w^2}\ln\left|\frac{\sqrt{\mathrm{d^2\text{-}z^2}}+\sqrt{\mathrm{d^2\text{-}w^2}}}{\sqrt{\mathrm{d^2\text{-}z^2}}-\sqrt{\mathrm{d^2\text{-}w^2}}}\right| \end{aligned} \tag{4.3}$$

Here, W is the half-width of the crevasse (assumed symmetric), z is the depth coordinate, w is the depth to the water level, ν is Poissons ratio for ice, μ is the shear modulus for ice, g is the gravitational constant, and ρ_i and ρ_w are the densities of ice and water, respectively. The crevasse depth is identified as the point where its width $W(z) = 0$. The quantity σ (in the first term) is the stress

$$\sigma = \sigma_y^{'} - \frac{2\rho_{\mathrm{i}}\mathrm{gd}}{\pi} + \rho_{\mathrm{i}}\mathrm{gd}\left(\frac{2}{\pi}\ \mathrm{Sin}^{-1}\left(\tfrac{\mathrm{w}}{\mathrm{d}}\right)\text{-}1\right) + \frac{2\rho_{\mathrm{w}}\mathrm{g}}{\pi}\sqrt{\mathrm{d^2\text{-}w^2}} \tag{4.4}$$

where σ_y' is the deviatoric stress in the crevasse opening direction y. We assign the water depth d as that which creates a stress at the crack tip equal to the fracture toughness of ice, which we take as $K_{IC} = 0.1$ MPa $\mathrm{m}^{\frac{1}{2}}$ (van der Veen, 1998, 2007).

The crevasse depth Z, where $W(Z)$=0 in Eqn. 4.3, is primarily a function of the amount of water available to fill the crack and, to a lesser extent, the longitudinal deviatoric stress σ'_y (van der Veen, 2007; Weertman, 1996). We assume that the longitudinal deviatoric stress is independent of depth and has a sinusoidal along-flow shape, with a wavelength of 6 km (Joughin et al., 2013; Sergienko et al., 2014). This prescribed stress field is zero at the onset of the model at Swiss Camp, but becomes increasingly tensile for the first 1.5 km along flow.

4.6.2 Effect of creep closure on crevasse depth

Our multi-decadal timescale is long enough that creep (viscous deformation) will affect crevasse shape and depth. Although we do not currently have creep implemented in the model, we explore the sensitivity of our results to the inclusion of creep by running our model with a coarse approximation of creep deformation. We vary the magnitude of this deformation over a wide range (four orders of magnitude) for completeness.

In our test, we represent the depth dependence of creep deformation based on the hydrostatic stress field around the crevasse. The hydrostatic stress σ_{zz} is a function of the pressure from the ice sheet and the water filling the crevasse. To find σ_{zz}, we integrate the ice and water overburden pressures, which respectively act to close and open the crevasses:

$$\sigma_{zz}(z) = \begin{cases} \rho_i g z, & \text{for } z < w \\ \left(\rho_i - \rho_w\right) g z - \rho_w g w, & \text{for } z > w \end{cases} \tag{4.5}$$

This function reaches its maximum at the water line ($z = w$) and decays to zero at the surface ($z = 0$) and the crack tip ($z = Z$). Thus, we prescribe that the deformation reach a maximum at the water line and decay to zero at the top and bottom of the crevasse.

We find that including creep deformation changes the maximum depth of typical crevasses by as much as 50 meters ($\sim$20%). This change is due to the compounded and

opposing effects of pinch-off, which occurs earlier and more often with high creep rates, and narrowing. Pinch-off tends to shoal crevasses, as they are cut off from the surface meltwater supply sooner, and thus receive less water overall. Narrowing, on the other hand, tends to deepen crevasses, as the small amount of creep closure in each timestep requires the crevasse to deepen to hold the given water volume.

These competing effects suggest that the effects of creep cannot be reliably parameterized. This underscores the importance of accurately representing creep in the model. We plan to use a full-Stokes ice-sheet model (Elmer/ICE) to calculate the stresses and strain rates in the blocks of ice separating crevasses in a crevasse field.

4.6.3 Thermal component of the model

The thermal model then solves for the temperature of the ice columns between adjacent crevasses using a two-dimensional semi-implicit finite-difference scheme. The model uses the staggered leapfrog method for vertical advection and a fully upwinded scheme for horizontal advection. It includes a latent heat source term

$$\left.\frac{dT}{dt}\right|_{LH} = \frac{k}{\rho C}\frac{d^2T}{dx^2} \tag{4.6}$$

which we calculate across $2dx$ = 10 meters.

We use a uniform horizontal velocity of 100 m/yr, which we base on observations at Swiss Camp, and assume this is entirely due to sliding. Vertical advection is scaled linearly from zero at the bed to 2.0 m/yr upward at the surface, which we base on the RACMO2 surface mass balance at Swiss Camp. We set the basal boundary condition to the pressure melting point. The upstream boundary condition is set to temperatures measured in boreholes at Swiss Camp in 1990 (Thomsen et al., 1991), which we take as an approximately typical ice column in the absence of warming from meltwater refreezing in crevasses (Phillips et al., 2013; Poinar and Joughin, 2016). Because horizontal advection through the system dwarfs horizontal diffusion, the outflow boundary condition has only

a negligible effect on ice temperatures in the rest of the domain. We therefore set the outflow boundary condition equal to the temperature of the ice upstream of it by the diffusion length scale , where Δt is the time step of the thermal model, for simplicity. Our domain extends 500 meters beyond the farthest-downstream crevasse to minimize the diffusive effects of the downstream lateral boundary condition.

The annual thickness of the frozen-on layer varies with depth, but is everywhere less than one meter and is typically only a few centimeters. This means that the diffusion time for the frozen-on layer to equilibrate with the ambient temperature gradient is a week or less, which is suitably short so that the thickness of the frozen-on layer can be ignored in the thermal model. We calculate the temperature gradient at each point in the vertical domain within each crevasse, as temperatures vary considerably with depth, and for both walls of each crevasse to allow for along-flow variations in temperature.

4.7 Inferred englacial refreezing rates in the Swiss Camp region

To constrain the meltwater influx (V_{influx}, which is closely tied to the efficiency parameter f) in our model, we compare englacial refreezing rates inferred in the Swiss Camp region to the refreezing rates our model calculates, for a broad range of f. We compute the inferred local refreezing rate, L_{frz}, from a model (Poinar and Joughin, 2016) tuned to replicate borehole observations downstream of Swiss Camp (Ryser et al., 2014; Thomsen et al., 1991). From that flowline model, we compute the temperature difference ΔT between ice that has warmed cryo-hydrologically and ice that has not. By integrating this temperature change over a short spatial scale $\Delta x \sim 10$ km and over the full ice column z, we calculate the inferred local refreezing rate:

$$L_{frz}(x) = \frac{C_p}{L_f}\frac{u_s}{\Delta x}\int_b^s (\Delta T)\,dz \tag{4.7}$$

In this equation, C_p is the specific heat capacity of ice, L_f is the latent heat of freezing, and u_s is the surface velocity at each point along the flowline x.

We compare the inferred volumetric rate of refreezing, $L_{frz} \cdot R$, to the refreezing flux V_{frz} in our model. For a given ice temperature, the freezing is primarily a function of crevasse depth, which is controlled by the meltwater influx. Thus, we use the inferred rate of refreezing to constrain the free parameter V_{influx} for the Pâkitsoq region of the ice sheet.

4.8 Crevasse depths at higher and lower elevations

We studied the sensitivity of crevasse depth to the meltwater input f and the elapsed time at various elevations on the ice sheet. Figure 4.3 shows this sensitivity at the Swiss Camp site (surface elevation $s \sim 1150$ meters). Here we present similar figures for a higher elevation s=1500 meters, near the ELA (Figure 4.5), and at a lower elevation $s \sim 610$ meters, at the FOXX borehole site of Ryser et al. (2014) (Figure 4.6).

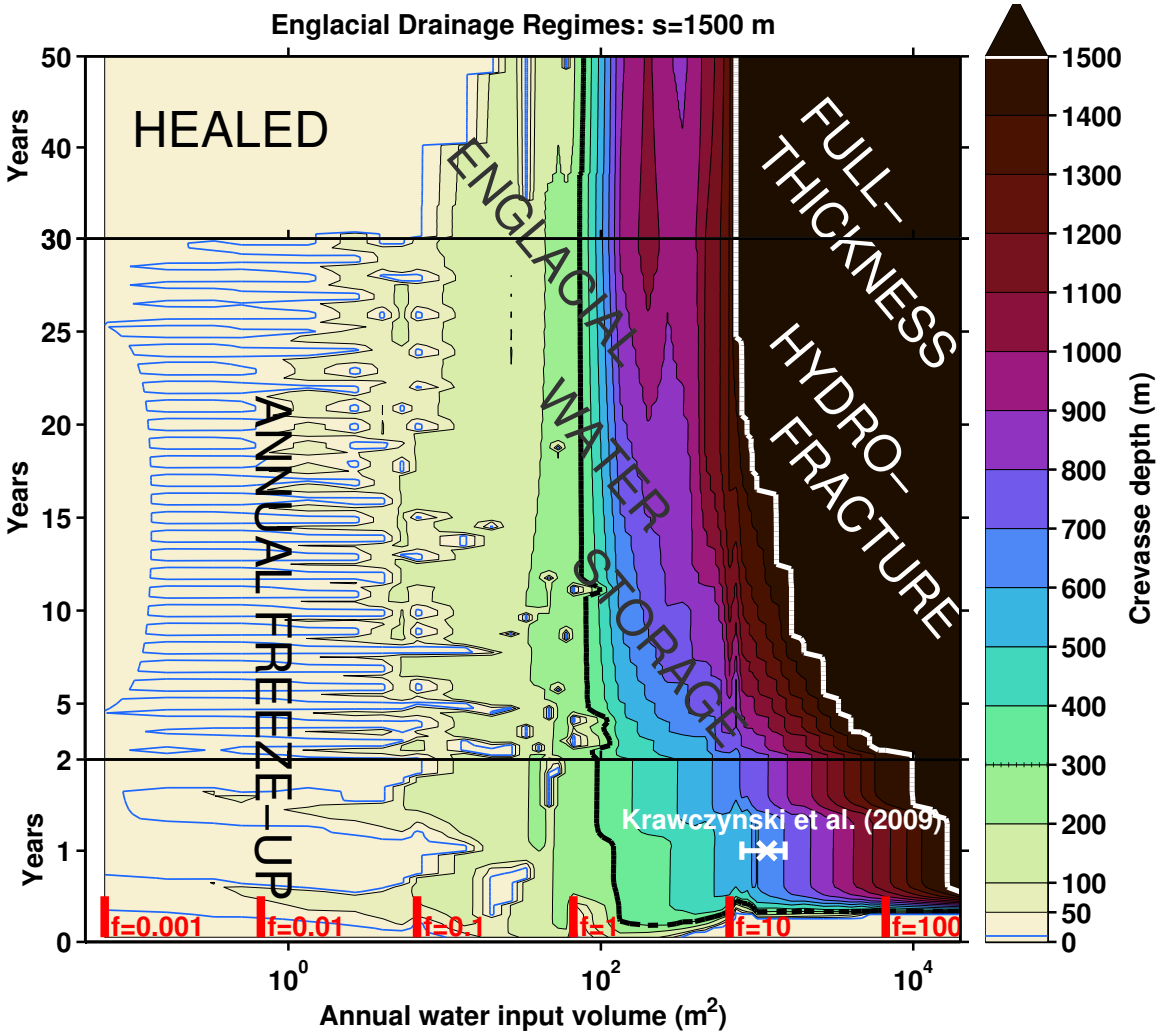

Figure 4.5: Englacial drainage regimes represented through the depth of a typical crevasse over time, as a function of meltwater influx (Equation 4.1), near the ELA at $s \sim$1500 meters. Blue line (10-meter crevasse depth) approximates a crevasse that will freeze closed each winter and reopen during the melt season ("annual freeze-up"). Heavy white line indicates the full ice thickness H=1500 meters; crevasses that extend this deep will drain to the bed ("full-thickness hydrofracture"). Between these two limits, water resides englacially year-round for decades without entirely refreezing.

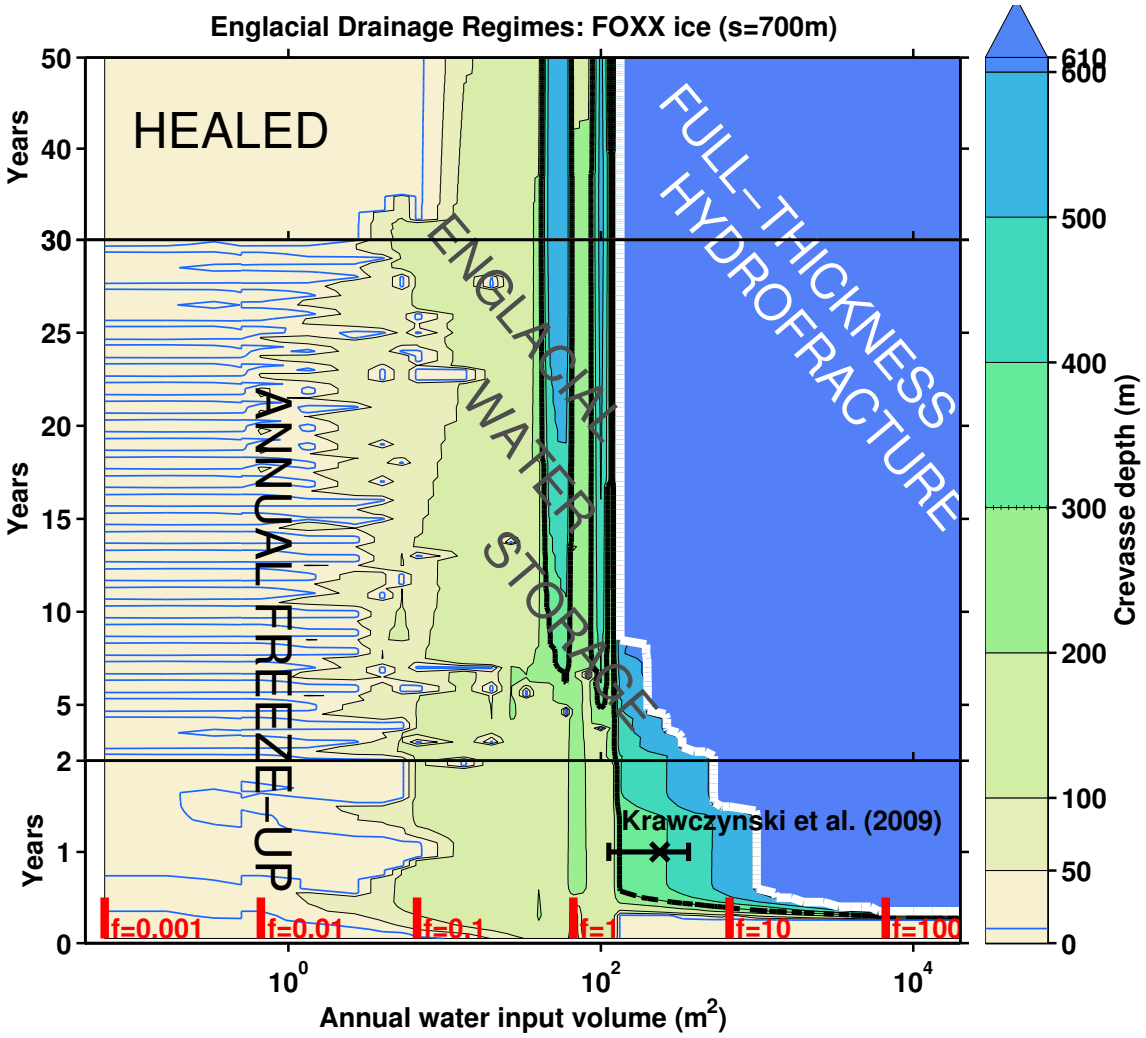

Figure 4.6: Englacial drainage regimes represented through the depth of a typical crevasse over time, as a function of meltwater influx (Equation 4.1), at the FOXX borehole site at s ∼700 meters (Lüthi et al., 2015; Ryser et al., 2014). Blue line (10-meter crevasse depth) approximates a crevasse that will freeze closed each winter and reopen during the melt season ("annual freeze-up"). Heavy white line indicates the full ice thickness H=610 meters; crevasses that extend this deep will drain to the bed ("full-thickness hydrofracture"). Between these two limits, water resides englacially year-round for decades without entirely refreezing. The expected melt volume required for moulin formation in less than one year (Krawczynski et al., 2009) at this location is shown in the bottom right.

Chapter 5

LIMITS TO FUTURE EXPANSION OF SURFACE-MELT-ENHANCED ICE FLOW INTO THE INTERIOR OF WESTERN GREENLAND

Note: This chapter was originally published in *Geophysical Research Letters*.

A popular topic in the Greenland Ice Sheet scientific literature (circa 2008–2015) has been the expansion of supraglacial lakes to higher elevations, toward the interior of the ice sheet. Such lakes form where surface meltwater collects in local elevation lows, or lake basins, on the surface of the ice sheet; hence *supra*glacial. We currently observe that such lakes, at lower elevations, drain their water to the base of the ice sheet, but their future behavior at higher elevations has been merely speculative. In this work, I used my thermal model to investigate the nature of the bed of the ice sheet under such lakes. I also analyzed multiple remote sensing (visual and radar-band imagery, ice-sheet surface velocity data) and climate-model-based datasets to investigate the behavior of the ice-sheet surface in the vicinity of these high-elevation lakes.

I found that high-elevation lakes, though prevalent, have low potential to drain through to the ice-sheet bed locally. Thus, these new and expanding supraglacial lakes will have only a minimal effect on basal hydrology, and thus also should only minimally influence ice flow and ice-sheet stability.

I wrote the manuscript and performed the modeling (using the thermal model described in Chapter 2), remote sensing, and analysis. Ian Joughin conceived the project along with Sarah Das and Mark Behn, and further conversations with them in the field (2008, 2010) helped me develop the ideas. Jan Lenaerts and Michiel van den Broeke provided the climate model (RACMO2) data, which I analyzed. Nick Selmes contributed a peer review that improved the presentation of the ideas.

AGU PUBLICATIONS

97

Geophysical Research Letters

RESEARCH LETTER
10.1002/2015GL063192

Key Points:
- Greenland Ice Sheet meltwater volumes are increasing notably at high elevations
- Low strain rates limit the likelihood of moulin formation at high elevations
- High-elevation meltwater will reach an already wet bed at lower elevations

Supporting Information:
- Text S1 and Figures S1 and S2

Correspondence to:
K. Poinar,
kpoinar@apl.washington.edu

Citation:
Poinar, K., I. Joughin, S. B. Das, M. D. Behn, J. T. M. Lenaerts, and M. R. van den Broeke (2015), Limits to future expansion of surface-melt-enhanced ice flow into the interior of western Greenland, *Geophys. Res. Lett.*, *42*, doi:10.1002/2015GL063192.

Received 23 JAN 2015
Accepted 20 FEB 2015
Accepted article online 24 FEB 2015

Limits to future expansion of surface-melt-enhanced ice flow into the interior of western Greenland

Kristin Poinar[1], Ian Joughin[1], Sarah B. Das[2], Mark D. Behn[2], Jan T. M. Lenaerts[3], and Michiel R. van den Broeke[3]

[1]Polar Science Center, Applied Physics Laboratory, University of Washington, Seattle, Washington, USA, [2]Department of Marine Geology and Geophysics, Woods Hole Oceanographic Institution, Woods Hole, Massachusetts, USA, [3]Institute for Marine and Atmospheric Research, Utrecht University, Utrecht, Netherlands

Abstract Moulins are important conduits for surface meltwater to reach the bed of the Greenland Ice Sheet. It has been proposed that in a warming climate, newly formed moulins associated with the inland migration of supraglacial lakes could introduce surface melt to new regions of the bed, introducing or enhancing sliding there. By examining surface strain rates, we found that the upper limit to where crevasses, and therefore moulins, are likely to form is ~1600 m. This is also roughly the elevation above which lakes do not drain completely. Thus, meltwater above this elevation will largely flow tens of kilometers through surface streams into existing moulins downstream. Furthermore, results from a thermal ice sheet model indicate that the ~1600 m crevassing limit is well below the wet-frozen basal transition (~2000 m). Together, these data sets suggest that new supraglacial lakes will have a limited effect on the inland expansion of melt-induced seasonal acceleration.

1. Introduction

A major concern at the time of the fourth Intergovernmental Panel on Climate Change report [*Lemke et al.*, 2007] was that surface meltwater could lubricate the base of the Greenland Ice Sheet, enhancing sliding and increasing the seaward flux of ice. Initial observations indicated that surface-melt-induced basal lubrication could accelerate ice sheet flow seasonally by a factor of 2 or more in slow-moving regions (<100 m/yr) [*Zwally et al.*, 2002]. Since then, it has been shown that the modulation of ice flow by basal lubrication is a time-evolving, nonlinear process, whereby the subglacial drainage system adapts to sustained periods of melt so that its sensitivity to melt declines over the melt season [*Schoof*, 2010; *Bartholomew et al.*, 2011a]. Thus, while the input of water initially leads to an ice-flow speedup, increasing the volume of water also increases drainage efficiency, stabilizing ice motion, and giving rise to the observed seasonal cycle in ice motion [*Sundal et al.*, 2009; *Palmer et al.*, 2011; *Bartholomew et al.*, 2011b]. As a result, the time-averaged velocity may be independent of [*van de Wal et al.*, 2008] or even negatively correlated to [*Sundal et al.*, 2011] surface melt volume. Surface melt also appears to have little effect on the acceleration of fast-moving outlet glaciers [*Joughin et al.*, 2008].

As the climate warms, melting is increasing at higher elevations (farther inland) on the ice sheet surface [*van de Wal et al.*, 2008; *Hoffman et al.*, 2011; *Howat et al.*, 2013; *Fitzpatrick et al.*, 2014]. An outstanding question is whether this surface meltwater can access the bed through moulins, and if so, whether the seasonal melt-induced speedup that presently occurs at lower elevations will be observed at new inland locations [*Sundal et al.*, 2009; *Palmer et al.*, 2011; *Bartholomew et al.*, 2011b; *Howat et al.*, 2013]. In particular, if surface melt reaches the bed in areas where the bed is frozen, its latent heat could warm the basal ice to the melting point and more permanently increase its seaward velocity [*Parizek and Alley*, 2004; *Bamber et al.*, 2007; *Sundal et al.*, 2009; *Howat et al.*, 2013].

Moulins often form from hydrofracture under or near supraglacial lakes. Hydrofracture occurs when the driving stress associated with the differential pressure between water in a crevasse and the surrounding lower density ice exceeds the fracture toughness of ice, forcing the crevasse tip downward; this can continue to the bed if the water supply (e.g., supraglacial lakes) is sufficient [*Alley et al.*, 2005; *Krawczynski et al.*, 2009]. Hydrofracture can occur directly beneath a lake or where an overflow stream from a lake reaches a crevasse [*Das et al.*, 2008; *Tedesco et al.*, 2013]. At lower elevations, moulins tend to form near the lakes they drain [*Joughin et al.*, 2013]. We refer to drainage that occurs beneath a lake or through a moulin a few kilometers away as "local" drainage. By contrast, "nonlocal" drainage occurs when melt travels >~10 km downstream before entering a moulin.

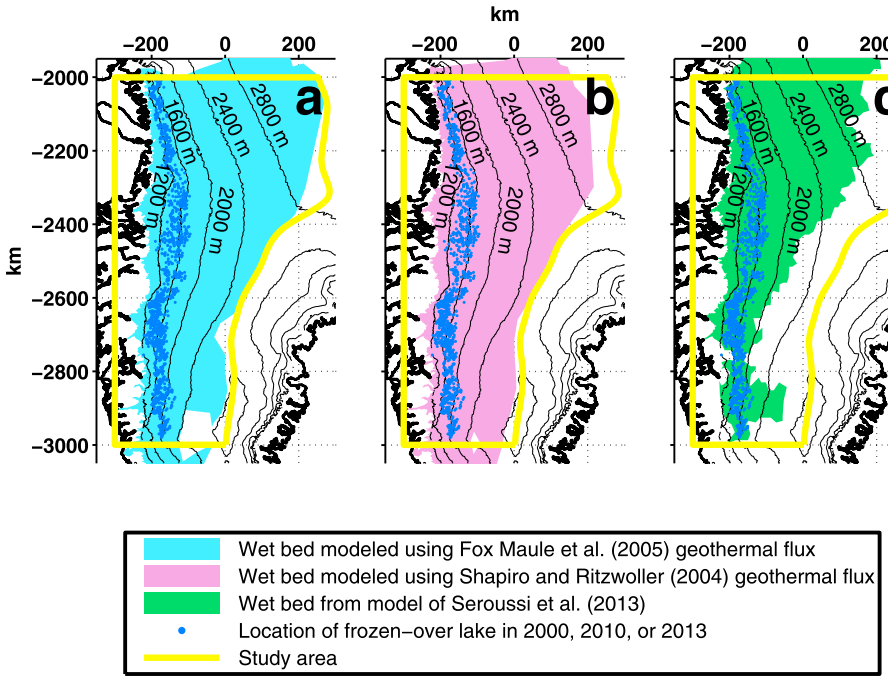

Figure 1. Locations of frozen-over lakes identified using satellite data from 2000, 2010, and 2013 (blue dots) overlain on wet-bedded areas (shaded) modeled using geothermal flux from (a) *Fox Maule et al.* [2005] and (b) *Shapiro and Ritzwoller* [2004]. (c) Wet-bedded areas modeled by *Seroussi et al.* [2013]. The yellow box shows the study area, which extends east to the divide. Our model (Figures 1a and 1b) was not run east of the divide; the white areas west of the divide indicate frozen beds. The black lines indicate the surface elevation contours from the Greenland Ice Mapping Project (GIMP) digital elevation model (DEM) [*Howat et al.*, 2014].

An ongoing concern is the extent to which high-elevation surface melt can drain locally [e.g., *Selmes et al.*, 2013]. This has important implications for ice dynamics because it determines where surface melt lubricates the bed. In this study, we apply numerical models and remote sensing to investigate the extent to which the inland propagation of surface melt is likely to form new moulins that could influence the flow and stability of the Greenland Ice Sheet.

2. Extent of Wet Bed

We first assess the vulnerability of the thermal state of the ice sheet bed to future incursions of surface meltwater. The basal velocity of an ice sheet is influenced by (1) the extent to which the bed is melted or frozen, and (2) the efficiency of the basal drainage system. To assess the former, we performed a series of thermal model calculations (see the supporting information) to identify those areas of the bed that are frozen and those that are melted within a 420,000 km^2 study area from the coast to the divide in western Greenland (Figure 1). Due to the uncertainty in geothermal flux, we varied this parameter in our models. Figures 1a and 1b show the results of our model forced with geothermal flux data sets from *Fox Maule et al.* [2005] and *Shapiro and Ritzwoller* [2004], respectively. Figure 1c shows the results of a model by *Seroussi et al.* [2013], which uses a modified version of *Shapiro and Ritzwoller*'s [2004] geothermal flux. The three panels are similar and also broadly agree with other modeling results (see the supporting information). A key result of these calculations is that little area below 2000 m elevation within our study area has a frozen bed. Thus, we use the 2000 m contour as a conservative estimate of the melted-frozen basal boundary; i.e., the true boundary is likely somewhat farther inland.

3. Expansion of Surface Melt

Next, we analyze the ongoing inland migration of surface melt. Figure 2a shows the annual snow and ice melt versus elevation within our study area. Melt at all elevations has increased from the climatological average

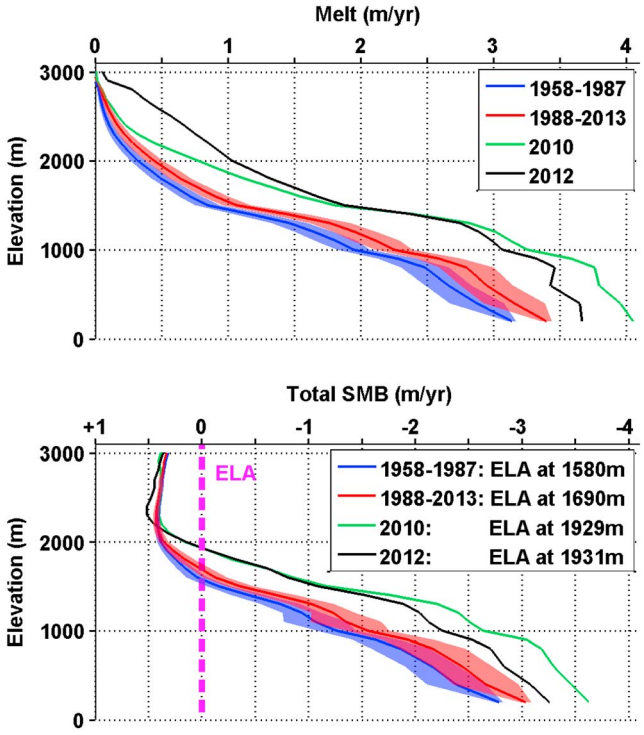

Figure 2. Average annual (a) surface melt and (b) surface mass balance from RACMO2.3 within the study region as a function of elevation. The blue lines show the climatological average over 1958–1987 with the 95% confidence interval for the mean over this period (shaded). The red shows the same over the 26 year period from 1988 to 2013. See the supporting information for details. The exceptional melt years 2010 and 2012 are shown in green and black, respectively.

(defined as 1958–1987) in the period of 1988–2013. The difference between the means of the two periods is positive at 95% confidence at all elevations from 400–2600 m (see the supporting information).

The increase in surface melt has raised the equilibrium line altitude (ELA) substantially within our study area (Figure 2b); the ELA now (1988–2013) averages 1690 m elevation, which is 110 m higher and 12 km farther inland than in 1958–1987 (1580 m). In the extreme melt years of 2010 and 2012, the ELA temporarily rose an additional 240 m (31 km farther inland). These results corroborate shorter-term regional observations [e.g., *van de Wal et al.*, 2012]. As the ELA rises, so too does the elevation of the bare ice zone, where supraglacial lakes are able to coalesce and potentially form moulins [*Howat et al.*, 2013].

4. Variations in Supraglacial Lakes and Streams With Elevation

The site of origin of a parcel of surface meltwater is often not coincident with the site where it enters the basal hydrologic system. Thus, although some surface melt reaches the bed locally, some does not, with the relative amounts and transport distances determined by its specific routing through the surface hydrological network of surface lakes and streams. To examine these characteristics, we used Landsat images (pixel size of 30 m) and satellite-based radar images (pixel size of 20 m) to study supraglacial lakes, moulins, and streams in our study area (see the supporting information). In particular, we identified all lakes with "lake ice," still visible on their surfaces in the summers of 2000, 2010, and 2013, which had the greatest number of cloud-free Landsat images available. A frozen ice cover indicates that a lake contained water that overwintered [*Darnell et al.*, 2013]; i.e., it did not drain completely in the previous summer. Figure 1 shows the locations of these "frozen-over" lakes. Their distribution generally spans 1100–1800 m elevation and typically ends just above the ELA.

Unlike more comprehensive mappings [e.g., *Lampkin*, 2011; *Selmes et al.*, 2011, 2013], we did not attempt a thorough analysis of lake size, depth, or other characteristics. Instead, we qualitatively studied how the size and drainage nature of supraglacial lakes varie with elevation. To illustrate the results of this analysis, in Figure 3, we show representative 10×10 km regions at four elevations spanning 1000–1900 m within our study area. At 1000 m elevation, summertime images (Figure 3a) show lakes that are deep blue in color and generally hundreds to thousands of meters in diameter. Wintertime images (Figure 3b) show moulins in or near most drained lake basins, fed by local streams. At 1300 m elevation (Figure 3c), the lakes are slightly larger [*Sundal et al.*, 2009; *Fitzpatrick et al.*, 2014], and some have ice covers that are visible in the wintertime radar data (Figure 3d) as bright or dark patches, depending on whether the ice cover is floating or frozen through, respectively [*Jeffries et al.*, 1994; *Surdu et al.*, 2014]. Evidence from ice-penetrating radar further suggests that these lakes overwinter under snow and lake ice [*Koenig et al.*, 2014]. At 1600 m elevation (Figure 3e), most lakes are ice covered and can exceed 5 km^2 in size. Wintertime images (Figure 3f) also show the presence of floating and frozen-through lake ice here. At 1900 m and above (Figures 3g and 3h), ice cover

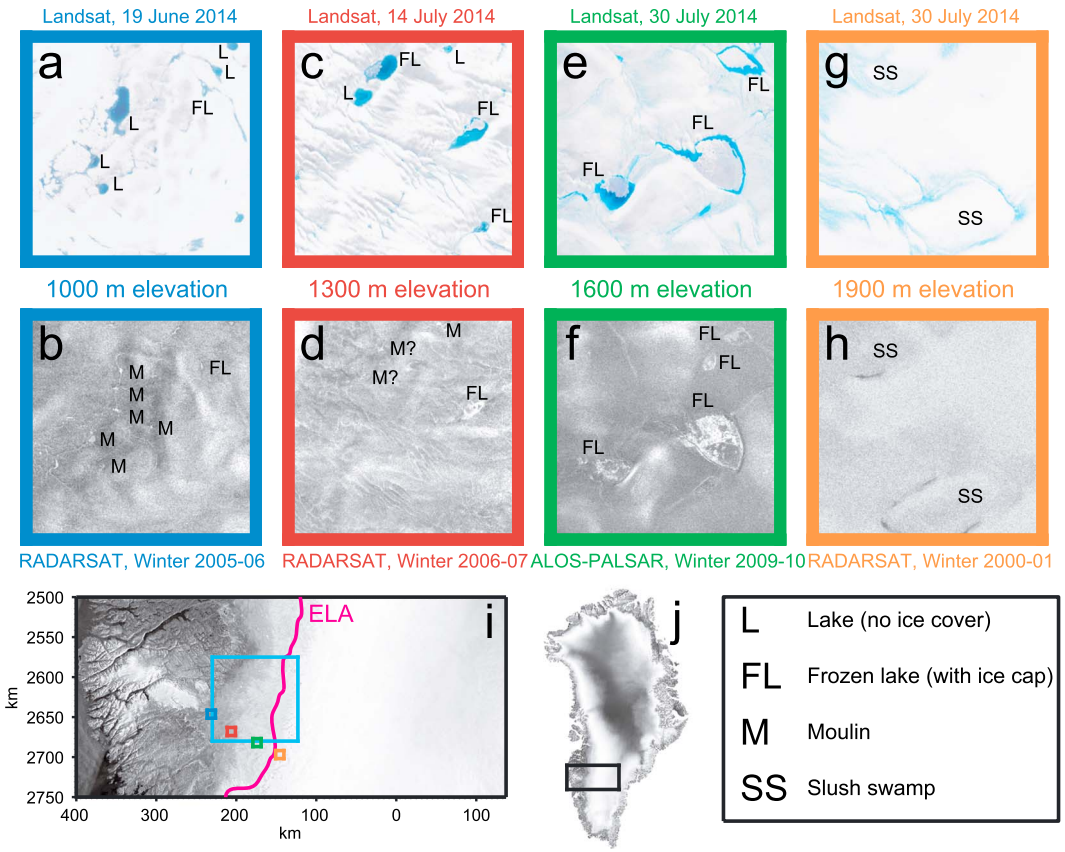

Figure 3. The nature of surface hydrologic features at multiple elevations in southwestern Greenland. (top) Summertime visible-spectrum Landsat images. (bottom) Wintertime radar images of the same scenes. The date, satellite, and approximate elevation [*Howat et al.*, 2014] of each 10 × 10 km scene are shown; elevations increase from right to left. (i) The locations of each (a–h) scene in colors corresponding to the image borders. The cyan square shows the location of Figure 4a; the 1958–2013 average ELA from RACMO2.3 is shown in magenta. Supraglacial features are labeled as follows: L = lake, FL = frozen-over lake, M = moulin, and SS = slush swamp.

persists, but distinct lakes give way to broad topographic lows with fuzzy boundaries. These "slush swamps" [*Bamber et al.*, 2007] occur because the firn absorbs much of the meltwater there, making the borders of water-filled basins more diffuse.

This analysis suggests that high-elevation frozen-over lakes can drain some of their water via overflow streams. Figure 4a shows the 312 major surface streams we identified using satellite imagery over a 6000 km^2 area spanning approximately 1100–1800 m elevation in southwestern Greenland (cyan box in Figure 3i). On average, the streams in this area are 10 km long and descend 60 m elevation, although this will vary in regions with different surface slopes, ice thicknesses, or other characteristics. The streams tend to lengthen at higher elevations, in agreement with stream mapping performed 300 km farther north [*Joughin et al.*, 2013]. For example, streams originating at 1200–1300 and 1700–1800 m elevation are 6 and 40 km long on average, respectively (Figure S2 in the supporting information). The highest-elevation stream termination (moulin) we identified was at 1580 m.

5. Variation of Strain Rate With Elevation

Hydrofracturing from the ice sheet surface to the bed requires both a crack and a sufficient input of meltwater to drive it through the ice sheet [*van der Veen*, 1998; *Krawczynski et al.*, 2009]. If new hydrofractures are to form in inland areas of the ice sheet where increased meltwater volumes are beginning to form supraglacial lakes [*Howat et al.*, 2013], cracks in these regions are required [*Alley et al.*, 2005]. These cracks can either (a) initiate directly beneath the lake water within the basin or (b) exist outside the basin. In the former case, it is sometimes

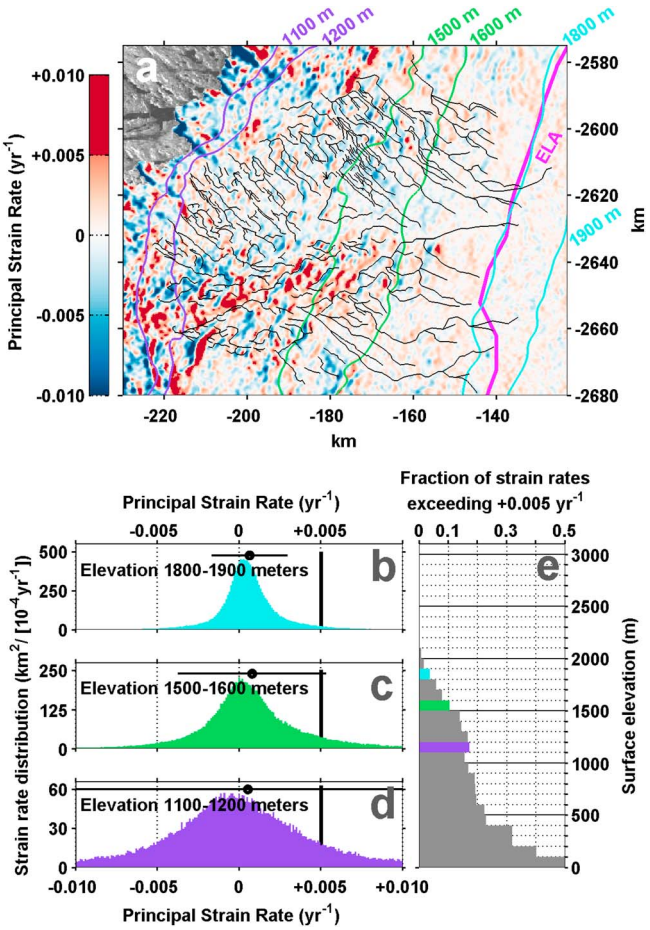

Figure 4. (a) Surface streams (black) identified from 24 June 2004 and 30 July 2014 Landsat images overlain on the principal strain rate field (colored). Positive strain rates indicate extension. Elevation contours from the GIMP DEM [*Howat et al.*, 2014] are labeled, and the 1958–2013 average ELA from RACMO2.3 is shown in magenta. (b–d) Histograms of the strain rates in western Greenland at various elevations: (Figure 4b) 1800–1900 m, (Figure 4c) 1500–1600 m, and (Figure 4d) 1100–1200 m. The approximate strain rate threshold for crevassing, +0.005/year, is shown as a vertical black bar. The mean strain rate (black dot) and one standard deviation (black horizontal line) for each elevation band are also indicated. (e) Bar graph showing the fraction of the entire western Greenland study region (Figure 1) where the tail of the strain rate distribution exceeds the +0.005/year fracture threshold, binned by elevation band. The results derived from the histograms (Figures 4b–4d) are color coded.

assumed that when a certain energy threshold or melt volume is reached, a lake can self-generate the crack necessary for drainage [*Georgiou et al.*, 2009; *Johansson et al.*, 2013]. However, whether lakes drain is not well correlated to their volume [*Fitzpatrick et al.*, 2014], implying that some other drainage initiation mechanism is required [*Selmes et al.*, 2013]. For drainage outside the basin (b), overflow channels deliver lake water into a preexisting moulin or a crevasse that, through hydrofracture, becomes a moulin [*Catania et al.*, 2008; *Das et al.*, 2008; *Tedesco et al.*, 2013]. Together, these studies suggest that without an existing crevasse, hydrofracture cannot initiate.

To constrain where on the ice sheet hydrofracture may initiate, we use surface strain rates as a proxy to identify where crevasses are likely to form. A survey of submeter-resolution imagery [*Joughin et al.*, 2013] indicated a general correspondence between areas with principal strain rates above +0.005/year and areas where crevasses are visible. More traditional methods of identifying where ice may fracture are stress thresholds or fracture toughness values [*van der Veen*, 1998], but these are difficult to observe remotely. Thus, while approximate, surface strain rates have the advantage that they are easily obtained from available velocity data. With this in mind, we use principal strain rates exceeding +0.005/year to indicate where crevassing is likely to occur.

We calculate principal strain rates on a 1×1 km grid from the average 2007–2010 wintertime ice sheet surface velocity [*Joughin et al.*, 2010] (see the supporting information) and examine their variation with elevation over our study region (Figure 1). Figures 4b–4e show the distribution of strain rates with elevation. These quantities are inversely correlated: higher elevations have lower magnitude, less variable strain rates. For example, at 1100–1200 m elevation (Figures 3a and 3b), the strain rates span from −0.01 to +0.01/year and exceed the +0.005/year threshold in 17% of the surface area (Figure 4d). At 1500–1600 m elevation (Figures 3c–3f and 4c), the distribution of strain rates is narrower and 10% of the ice sheet area is susceptible to fracture formation. At 1800–1900 m (Figures 3g, 3h, and 4b), only 3.6% of the area likely is susceptible to crevassing.

6. Discussion

As we show with our analyses of the RACMO2.3 output (Figure 2), the ice sheet surface has been melting farther inland (or, equivalently, at higher elevations) over the last several decades. This surface meltwater may

potentially reach the bed and seasonally accelerate ice flow at new inland locations, but for this to occur, the water must create new local hydrofractures that access the bed. Here we discuss the limits to inland expansion of hydrofracture and the likely consequences of new high-elevation surface melt reaching the bed.

6.1. Limitation to High-Elevation Hydrofracture

Our results and work by others [*Johansson et al.*, 2013] show that at low elevations (below ~1300 m; Figures 3a–3d), lakes are typically empty by the end of the melt season, draining either rapidly through hydrofractures [*Krawczynski et al.*, 2009] or more slowly through short (local) overflow streams. By contrast, higher-elevation lakes tend to drain incompletely (Figures 3e and 3f) through long overflow streams that carry the melt to distant (nonlocal) moulins (Figure 4a and Figure S1 in the supporting information) [*Johansson et al.*, 2013].

Figure 3 shows a general increase in the area of individual supraglacial lakes with elevation. Thicker ice dampens the surface expression of bedrock topography, passing only longer-wavelength basal undulations to the surface [*Gudmundsson*, 2003; *Lampkin and VanderBerg*, 2011]. Thus, higher-elevation lakes tend to be shallow and broad; accumulated meltwater can therefore sometimes overtop the lake basin. However, such overflow channels may not completely empty the lake; if the inflow of meltwater is slow, the turbulent outflow volume may be insufficient to incise a channel to lake-bottom level.

Water that is left in higher-elevation lakes after the melt season can form an ice cover, which sometimes superimposes onto the ice sheet ice (Figures 3c–3f) and is advected through and out of the lake basin. This process forms bands called lake ogives, which have been observed at several higher-elevation lakes [*Darnell et al.*, 2013]. The small width of lake ogives (~100 m) compared to that of the lakes (~2 km at 1600 m elevation) suggests that lake ogives may contribute only slightly to the water balance of a high-elevation lake.

The lake water that cannot drain into an in-basin hydrofracture or refreeze into lake ogives must eventually overflow the basin. At high elevations, this overflow often forms surface streams that extend tens of kilometers downglacier, sometimes cascading through multiple lakes (as seen between the two central lakes in Figures 3e and 3f and throughout Figure S1 in the supporting information) until the streams encounter a crevasse or moulin (Figures 4a and Figure S2 in the supporting information) and terminate. Such crevasses or moulins are likely to initiate in areas of tensile ice flow located near topographic highs [*Catania et al.*, 2008; *Das et al.*, 2008], yet streams flow toward topographic lows. This hydrologic characteristic is especially apparent at higher elevations, where short, efficient streams that connect lakes directly to nearby moulins are uncommon (Figures 3e–3h), and streams are generally longer (Figure S2 in the supporting information). Our data show that at 1600 and 1900 m elevation, the formation of surface crevasses is infrequent (8% of the ice sheet area) and rare (1.6%), respectively (Figure 4e). Thus, the seeding of moulins should be similarly infrequent and rare at these elevations, as *Selmes et al.* [2013] posited and observed. Our satellite imagery and previous observations [*Howat et al.*, 2013; *Johansson et al.*, 2013; *Selmes et al.*, 2013] indicate that although lakes exist above approximately 1600 m, many do not drain completely to moulins and tend to freeze over winter. *Catania et al.* [2008] also found a scarcity of moulins above the ELA despite the occurrence of lakes there.

The stream paths we identified do indicate that though rare, higher-elevation moulin formation does occur. Of the 134 stream termini (resulting from convergence of 312 total streams) we identified, 25 occurred above 1500 m. Thus, the spatial density of moulins in the 1600 km^2 area at 1500–1600 m (0.02/km^2) is a tenth or less of that observed at lower elevations [*Zwally et al.*, 2002; *Phillips et al.*, 2011].

In summary, relatively few high-elevation lakes drain their water to the bed locally. Instead, most high-elevation meltwater (originating above ~1600 m) appears to drain through surface streams into nonlocal, lower-elevation moulins (Figure 4a). Thus, we hypothesize that as climate change increases meltwater volumes at higher elevations (Figure 2), surface streams are likely to lengthen and transport that melt downglacier to where moulins are more likely to form. Consequently, in the coming decades, the effects of an increasing amount of high-elevation meltwater on ice sheet sliding velocity generally will be concentrated at lower elevations.

As the ice sheet evolves over the next hundreds to thousands of years, regions that are currently unlikely to hydrofracture (above ~1600 m) may thin enough to reach elevations (below ~1300 m) where hydrofracture is more common, as explored by *Leeson et al.* [2014]. This will bring water to these inland areas of the bed

and may eventually activate sliding in new areas, forming a feedback for ice sheet destabilization. However, this enhanced basal motion will be a consequence of a large drawdown of Greenland's ice—not its cause.

6.2. Effect of New Meltwater at the Bed

The results of our thermal model suggest that the boundary between frozen and melted basal areas likely lies at or above the 2000 m surface elevation contour (Figure 1), although this result is somewhat sensitive to the geothermal flux. If we take this elevation as a rough boundary between frozen and wet beds in western Greenland, then a wet bed underlies the areas where lakes currently form and where they may form in the next several decades. Our data indicate that at elevations above 2000 m, hydrofracture to the bed will be extremely rare (Figure 4e), so that surface melt thawing a frozen bed is unlikely.

Although our data suggest that hydrofracture becomes less frequent with elevation, there is evidence of surface meltwater affecting the flow of high-elevation ice through longitudinal coupling. Observations of speedup at a site at 1840 m elevation, where there was no evidence of moulins or surface uplift, suggest that melt reached the bed tens of kilometers downstream [*Doyle et al.*, 2014]. The speedup was greatest in 2012, when melt was well above the current climatic mean (Figure 2); this response may thus be representative of the mean behavior several decades in the future. Nonetheless, the consequent seasonal (~8%) and annual (~2%) high-elevation speedups were relatively small [*Doyle et al.*, 2014].

7. Conclusions

Our results indicate that the likelihood of crevassing and, consequently, lake drainage via local spillover into crevasses decreases substantially with elevation. Thus, despite the observed inland migration of the ELA and surface melt in western Greenland, creation of new hydrofractures at high elevations is unlikely. Instead, most high-elevation meltwater likely will flow downhill via an extended network of surface streams and drain through existing moulins at lower elevations. Strain rate data indicate that relatively little water should reach the bed at elevations above ~1600 m, and this should diminish almost completely by 2000 m elevation. Furthermore, results from numerical models indicate that the bed in western Greenland is generally melted below ~2000 m surface elevation. Thus, it is unlikely that surface melt will reach the bed in regions where it could thaw the bed and produce large changes in ice sheet velocity. Instead, new water that reaches the bed is likely to have a modest effect similar to that already observed [e.g., *Bartholomew et al.*, 2011b; *Doyle et al.*, 2014]. Overall, in the next several decades, the inland migration of melt is unlikely to produce large changes in flow due to increased basal lubrication or the thawing of a frozen bed.

Acknowledgments

National Science Foundation grants supported K.P. (CReSIS; ANT-0424589), I.J. (ARC-1023382), S.B.D., and M.D.B. (ARC-1023364). The Polar Program of the Netherlands Organisation for Scientific Research supported J.T.M.L. and M.R.v.d.B. Velocity data are available through NASA MEaSUREs at http://nsidc.org/data/NSIDC-0478. Radar imagery will be available shortly at the NSIDC. Landsat imagery is publicly available at http://landsat.usgs.gov. All other data in this study are available at the University of Washington Library at http://hdl.handle.net/1773/27336. We thank Nick Selmes and an anonymous reviewer for their constructive comments.

The Editor thanks Nick Selmes and an anonymous reviewer for their assistance in evaluating this paper.

References

Alley, R. B., T. K. Dupont, B. R. Parizek, and S. Anandakrishnan (2005), Access of surface meltwater to beds of sub-freezing glaciers: Preliminary insights, *Ann. Glaciol.*, *40*(1), 8–14, doi:10.3189/172756405781813483.

Bamber, J. L., R. B. Alley, and I. Joughin (2007), Rapid response of modern day ice sheets to external forcing, *Earth Planet. Sci. Lett.*, *257*(1–2), 1–13, doi:10.1016/j.epsl.2007.03.005.

Bartholomew, I. D., P. Nienow, A. Sole, D. Mair, T. Cowton, S. Palmer, and J. Wadham (2011a), Supraglacial forcing of subglacial drainage in the ablation zone of the Greenland ice sheet, *Geophys. Res. Lett.*, *38*, L08502, doi:10.1029/2011GL047063.

Bartholomew, I. D., P. Nienow, A. Sole, D. Mair, T. Cowton, M. A. King, and S. Palmer (2011b), Seasonal variations in Greenland Ice Sheet motion: Inland extent and behavior at higher elevations, *Earth Planet. Sci. Lett.*, *307*(3–4), 271–278, doi:10.1016/j.epsl.2011.04.014.

Catania, G. A., T. A. Neumann, and S. F. Price (2008), Characterizing englacial drainage in the ablation zone of the Greenland ice sheet, *J. Glaciol.*, *54*(187), 567–578, doi:10.3189/002214308786570854.

Darnell, K. N., J. M. Amundson, L. M. Cathles, and D. R. MacAyeal (2013), The morphology of supraglacial lake ogives, *J. Glaciol.*, *59*(215), 533–544, doi:10.3189/2013JoG12J098.

Das, S. B., I. Joughin, M. D. Behn, I. M. Howat, M. A. King, D. Lizarralde, and M. P. Bhatia (2008), Fracture propagation to the base of the Greenland Ice Sheet during supraglacial lake drainage, *Science*, *320*(5877), 778–781, doi:10.1126/science.1153360.

Doyle, S. H., A. Hubbard, A. Fitzpatrick, D. van As, A. B. Mikkelsen, R. Pettersson, and B. Hubbard (2014), Persistent flow acceleration within the interior of the Greenland ice sheet, *Geophys. Res. Lett.*, *41*, 899–905, doi:10.1002/2013GL058933.

Fitzpatrick, A., A. Hubbard, J. E. Box, D. J. Quincey, D. Van As, A. P. B. Mikkelsen, S. H. Doyle, C. F. Dow, B. Hasholt, and G. A. Jones (2014), A decade (2002–2012) of supraglacial lake volume estimates across Russell Glacier, West Greenland, *Cryosphere*, *8*(1), 107–121, doi:10.5194/tc-8-107-2014.

Fox Maule, C., M. E. Purucker, N. Olsen, and K. Mosegaard (2005), Heat flux anomalies in Antarctica revealed by satellite magnetic data, *Science*, *309*(5733), 464–467, doi:10.1126/science.1106888.

Georgiou, S., A. Shepherd, M. McMillan, and P. Nienow (2009), Seasonal evolution of supraglacial lake volume from ASTER imagery, *Ann. Glaciol.*, *50*(52), 95–100, doi:10.3189/172756409789624328.

Gudmundsson, G. H. (2003), Transmission of basal variability to a glacier surface, *J. Geophys. Res.*, *108*(B5), 2253, doi:10.1029/2002JB002107.

Hoffman, M. J., G. A. Catania, T. A. Neumann, L. C. Andrews, and J. A. Rumrill (2011), Links between acceleration, melting, and supraglacial lake drainage of the western Greenland Ice Sheet, *J. Geophys. Res.*, *116*, F04035, doi:10.1029/2010JF001934.

Howat, I. M., S. de la Peña, J. H. van Angelen, J. T. M. Lenaerts, and M. R. van den Broeke (2013), Expansion of meltwater lakes on the Greenland Ice Sheet, *Cryosphere*, *7*(1), 201–204, doi:10.5194/tc-7-201-2013.
Howat, I. M., A. Negrete, and B. E. Smith (2014), The Greenland Ice Mapping Project (GIMP) land classification and surface elevation data sets, *Cryosphere*, *8*(4), 1509–1518, doi:10.5194/tc-8-1509-2014.
Jeffries, M. O., K. Morris, W. F. Weeks, and H. Wakabayashi (1994), Structural and stratigraphie features and ERS 1 synthetic aperture radar backscatter characteristics of ice growing on shallow lakes in NW Alaska, winter 1991–1992, *J. Geophys. Res.*, *99*(C11), 22,459–22,471, doi:10.1029/94JC01479.
Johansson, A. M., P. Jansson, and I. A. Brown (2013), Spatial and temporal variations in lakes on the Greenland Ice Sheet, *J. Hydrol.*, *476*, 314–320, doi:10.1016/j.jhydrol.2012.10.045.
Joughin, I., S. B. Das, M. A. King, B. E. Smith, I. M. Howat, and T. Moon (2008), Seasonal speedup along the western flank of the Greenland Ice Sheet, *Science*, *320*(5877), 781–783, doi:10.1126/science.1153288.
Joughin, I., B. E. Smith, I. M. Howat, T. Scambos, and T. Moon (2010), Greenland flow variability from ice-sheet-wide velocity mapping, *J. Glaciol.*, *56*(197), 415–430.
Joughin, I., S. B. Das, G. E. Flowers, M. D. Behn, R. B. Alley, M. A. King, B. E. Smith, J. Bamber, M. R. van den Broeke, and J. H. van Angelen (2013), Influence of supraglacial lakes and ice-sheet geometry on seasonal ice-flow variability, *Cryosphere*, *7*, 1185–1192, doi:10.5194/tc-7-1185-2013.
Koenig, L. S., et al. (2014), Wintertime storage of water in buried supraglacial lakes across the Greenland Ice Sheet, *Cryosphere Discuss.*, *8*(4), 3999–4031, doi:10.5194/tcd-8-3999-2014.
Krawczynski, M. J., M. D. Behn, S. B. Das, and I. Joughin (2009), Constraints on the lake volume required for hydrofracture through ice sheets, *Geophys. Res. Lett.*, *36*, L10501, doi:10.1029/2008GL036765.
Lampkin, D. J. (2011), Supraglacial lake spatial structure in western Greenland during the 2007 ablation season, *J. Geophys. Res.*, *116*, F04001, doi:10.1029/2010JF001725.
Lampkin, D. J., and J. VanderBerg (2011), A preliminary investigation of the influence of basal and surface topography on supraglacial lake distribution near Jakobshavn Isbrae, western Greenland, *Hydrol. Processes*, *25*(21), 3347–3355, doi:10.1002/hyp.8170.
Leeson, A. A., A. Shepherd, K. Briggs, I. Howat, X. Fettweis, M. Morlighem, and E. Rignot (2014), Supraglacial lakes on the Greenland ice sheet advance inland under warming climate, *Nat. Clim. Change*, *5*(1), 51–55, doi:10.1038/nclimate2463.
Lemke, P., et al. (2007), Observations: Changes in snow, ice and frozen ground, in *Climate Change 2007: The Physical Science Basis, Contribution of Working Group I to the Fourth Assessment Report of the Intergovernmental Panel on Climate Change*, edited by S. Solomon et al., Cambridge Univ. Press, Cambridge, U. K., and New York.
Palmer, S., A. Shepherd, P. Nienow, and I. Joughin (2011), Seasonal speedup of the Greenland Ice Sheet linked to routing of surface water, *Earth Planet. Sci. Lett.*, *302*(3–4), 423–428, doi:10.1016/j.epsl.2010.12.037.
Parizek, B. R., and R. B. Alley (2004), Implications of increased Greenland surface melt under global-warming scenarios: Ice-sheet simulations, *Quat. Sci. Rev.*, *23*, 1013–1027, doi:10.1016/j.quascirev.2003.12.024.
Phillips, T., S. Leyk, H. Rajaram, W. Colgan, W. Abdalati, D. McGrath, and K. Steffen (2011), Modeling moulin distribution on Sermeq Avannarleq glacier using ASTER and WorldView imagery and fuzzy set theory, *Remote Sens. Environ.*, *115*(9), 2292–2301, doi:10.1016/j.rse.2011.04.029.
Schoof, C. (2010), Ice-sheet acceleration driven by melt supply variability, *Nature*, *468*(7325), 803–806, doi:10.1038/nature09618.
Selmes, N., T. Murray, and T. D. James (2011), Fast draining lakes on the Greenland Ice Sheet, *Geophys. Res. Lett.*, *38*, L15501, doi:10.1029/2011GL047872.
Selmes, N., T. Murray, and T. D. James (2013), Characterizing supraglacial lake drainage and freezing on the Greenland Ice Sheet, *Cryosphere Discuss.*, *7*(1), 475–505, doi:10.5194/tcd-7-475-2013.
Seroussi, H., M. Morlighem, E. Rignot, and A. Khazendar (2013), Dependence of century-scale projections of the Greenland ice sheet on its thermal regime, *J. Glaciol.*, *59*(218), doi:10.3189/2013JoG13J054.
Shapiro, N. M., and M. H. Ritzwoller (2004), Inferring surface heat flux distributions guided by a global seismic model: Particular application to Antarctica, *Earth Planet. Sci. Lett.*, *223*, 213–224.
Sundal, A. V., A. Shepherd, P. Nienow, E. Hanna, S. Palmer, and P. Huybrechts (2009), Evolution of supra-glacial lakes across the Greenland Ice Sheet, *Remote Sens. Environ.*, *113*(10), 2164–2171, doi:10.1016/j.rse.2009.05.018.
Sundal, A. V., A. Shepherd, P. Nienow, E. Hanna, S. Palmer, and P. Huybrechts (2011), Melt-induced speed-up of Greenland Ice Sheet offset by efficient subglacial drainage, *Nature*, *469*(7331), 521–524, doi:10.1038/nature09740.
Surdu, C. M., C. R. Duguay, L. C. Brown, and D. Fernández Prieto (2014), Response of ice cover on shallow lakes of the North Slope of Alaska to contemporary climate conditions (1950–2011): Radar remote sensing and numerical modeling data analysis, *Cryosphere*, *8*, 167–180, doi:10.5194/tc-8-167-2014.
Tedesco, M., I. C. Willis, M. J. Hoffman, A. F. Banwell, P. Alexander, and N. S. Arnold (2013), Ice dynamic response to two modes of surface lake drainage on the Greenland ice sheet, *Environ. Res. Lett.*, *8*(3), 034007, doi:10.1088/1748-9326/8/3/034007.
van de Wal, R. S. W., W. Boot, M. R. van den Broeke, C. J. P. P. Smeets, C. H. Reijmer, J. J. A. Donker, and J. Oerlemans (2008), Large and rapid melt-induced velocity changes in the ablation zone of the Greenland Ice Sheet, *Science*, *321*(5885), 111–113, doi:10.1126/science.1158540.
van de Wal, R. S. W., W. Boot, C. J. P. P. Smeets, H. Snellen, M. R. van den Broeke, and J. Oerlemans (2012), Twenty-one years of mass balance observations along the K-transect, West Greenland, *Earth Syst. Sci. Data*, *4*, 31–35, doi:10.5194/essd-4-31-2012.
van der Veen, C. J. (1998), Fracture mechanics approach to penetration of surface crevasses on glaciers, *Cold Reg. Sci. Technol.*, *27*(1), 31–47.
Zwally, H. J., W. Abdalati, T. Herring, K. Larson, J. Saba, and K. Steffen (2002), Surface melt-induced acceleration of Greenland Ice-Sheet flow, *Science*, *297*(5579), 218–222, doi:10.1126/science.1072708.

Geophysical Research Letters

Supporting Information for

Limits to future expansion of surface-melt-enhanced ice flow into the interior of western Greenland

Kristin Poinar[1], Ian Joughin[1], Sarah B. Das[2],
Mark D. Behn[2], Jan T. M. Lenaerts[3], and Michiel R. van den Broeke[3]

[1]*Polar Science Center, Applied Physics Lab, University of Washington, Seattle, USA*
[2]*Dept. of Marine Geology and Geophysics, Woods Hole Oceanographic Inst., Woods Hole, MA, USA*
[3]*Institute for Marine and Atmospheric Research, Utrecht University, Utrecht, Netherlands*

Corresponding author: K. Poinar, `kpoinar@apl.washington.edu`

Contents of this file

- Supplementary Text
  - Methods
  - Model for the thermal state of the bed
  - Climatological analysis of the change in surface melt extent
  - Inland migration distance of the ELA
  - Identification of surface features
  - Strain rate dataset
- Figures S1 and S2
- Supplementary References

Supplementary Text

Methods

We use four remotely sensed datasets to examine the observed and expected behavior of supraglacial lakes with elevation in western Greenland. We use satellite imagery from Landsat and RADARSAT to identify the current spatial distribution of supraglacial lakes, moulins, and streams in a 420,000-km^2 study area (the size of Sweden) in western Greenland. We also analyze surface-velocity-derived strain rates (Joughin et al., 2010) as a function of surface elevation (Howat et al., 2014; Joughin et al., 2010). The study area runs from approximately 63.0°N (south of Sermilik Glacier; -3000 km polar stereographic) to 70.5°N (north of Swiss Camp; -2000 km polar stereographic), and from the west coast inland to the divide. It is shown in Figure 1 of the main paper.

Model for the thermal state of the bed

We use a two-dimensional thermal model for ice sheets to calculate the basal temperatures and consequent thermal state along 27 flowlines spanning our study area. The model is unique because it is thermal rather than thermo-mechanical: that is to say, it uses the present-day ice-sheet geometry as a rigid domain, rather than spinning up in a way chosen to best match the current ice sheet. We use surface and basal elevations from Bamber et al. (2013) smoothed with a 20-km window and present-day surface velocity (Joughin et al., 2010). The model is also constrained by a climate history from the Summit ice core (Cuffey and Clow, 1997) scaled to present-day climate parameters (Ettema et al., 2009). We use one of two geothermal flux maps for the basal boundary condition: Shapiro and Ritzwoller (2004), which is seismically derived, and Fox Maule et al. (2005), which is based on magnetic data. We use two different geothermal flux datasets because

basal temperature is highly sensitive to this parameter (Rogozhina et al., 2012), which is not well validated due to a paucity of direct measurements in boreholes.

The model solves the heat equation, including multi-phase (polythermal) ice physics based on MacAyeal (1997), in a series of one-dimensional vertical columns that are linked to one another along a present-day flowline. Twenty-seven independent flowlines are interpolated to fill the study area. The spatial resolution of this product is approximately 50 km north-south and 5 km east-west. This asymmetry is because we wish to detect, along each east-west flowline, the inland frozen-thawed basal boundary, which we do not expect to vary greatly in the latitudinal direction (between adjacent flowlines). Our thermal model does not include surface-sourced water at the bed; that is, our basal heat sources are exclusively deformational, frictional, and geothermal.

Comparison of our model results with those of Seroussi et al. (2013) shows that they find a considerably larger area with a frozen bed. This likely results from refinements that Seroussi et al. (2013) made to the geothermal flux map to reflect the low heating rates observed at the bottom of the Dye-3 borehole. In particular, their model predicts a small, mid-elevation area with a frozen bed in the southern portion of our study region, at approximately y = -2800 km (Figure 1c). This area lies directly underneath freezing lakes and is therefore vulnerable, in theory, to the incursion of latent heat from surface meltwater. (The ice here has a surface elevation of approximately 1600–1800 meters, however, so we assert that it is at low risk of hydrofracture.)

We also compare our model results to those of Aschwanden et al. (2012). They used a spatially constant geothermal flux of 50 mW/m^2, which is somewhat lower than the average values in our study area given by Shapiro and Ritzwoller (2004) and Fox Maule et al. (2005). However, they find a wet bed extending inland to approximately the 2200-meter contour in the southern portion of our study area, and increasingly farther inland with latitude, to the 3000-meter contour in the northernmost portions of our study area.

They also find a mid-elevation frozen-bed area near the southern border of our study area, similar to but north of that detected by Seroussi et al. (2013). The frozen-bedded area of Aschwanden et al. (2012) spans approximately 400 kilometers and encompasses roughly 1800–2200 meters; many frozen-over lakes overly this area. If the bed is in fact frozen here, this area would be vulnerable to occasional basal speedup in the coming decades. For example, in the 2012 extreme melt year, Doyle et al. (2014) saw evidence of seasonalspeedup at 1840 meters elevation in this area of the ice sheet, although this speedup was likely caused by longitudinal coupling to lower-elevation regions where surface melt reached the bed.

A third modeling study (Rogozhina et al., 2012) did not detect any mid-elevation frozen-bedded areas. Because they used unadjusted geothermal flux from Shapiro and Ritzwoller (2004) and Fox Maule et al. (2005), this third study is most similar in nature to ours. They find a wet bet extending inland to approximately the 2400-meter contour.

In sum, because our model uses, in some places, a slightly higher geothermal flux than these previous studies, we consider our model results to be an upper bound on the melt extent. Our choice to use the 2000-meter contour as the approximate inland extent of a melted bed is conservative, as our results and the others discussed here find that the wet bed extends farther inland than that in most places within our study area.

Climatological analysis of the change in surface melt extent

We used RACMO2.3 output (updated from RACMO2.1 used by van Angelen et al. (2013)) of surface melt and surface mass balance (SMB) to study the changes in these quantities since 1958 in western Greenland. RACMO2.3 output is posted at 11 km. To study the changes in surface melt and SMB as a function of elevation, we resample the surface elevation (Howat et al., 2014) to this grid, then bin the melt and SMB model output into 100- and 200-meter elevation bands that span 0 to 3000 meters elevation. Higher elevation

bands (e.g., the 1900–2000 m band), which are wider (∼20 km), have more RACMO2.3 pixels than lower elevation bands (e.g., the 900–1000 m band), which can be as narrow as 3 km. To address this issue while still resolving the steep gradients in surface melt at lower elevations, we used 200-meter elevation bands at low elevations (surface elevations $s < 900$ m) and 100-meter bands at higher elevations ($s \geq 900$ m).

We test whether two populations of melt (or SMB) at each given elevation band are different at the 95% confidence level. Population 1 spans 1958–1987 (N_1 = 30 years) and Population 2 spans 1988–2013 (N_2 = 26 years). The test calculates the true mean of each population by considering the observed interannual variability over each period. We do not consider errors present in the RACMO output in this analysis.

For each elevation band, we run a two-tailed Student's t-test to determine the significance of the observed inland migration of melt (or the ELA). For this test, the t-statistic is given by

$$t = \frac{\bar{x}_1 - \bar{x}_2}{S_p \sqrt{1/N_1 + 1/N_2}},$$

$$\text{where } S_p = \sqrt{\frac{(N_1 - 1)s_1^2 + (N_2 - 1)s_2^2}{N_1 + N_2 - 2}},$$

where an overbar indicates the sample mean, N is sample size, s is sample standard deviation, and the subscripts 1 and 2 indicate each population (Devore, 1982). For 54 degrees of freedom (56 years minus the two means being calculated) in a two-tailed t-test, $t > 2.0049$ indicates that the two populations within a given elevation band are different at the 95% confidence level. Because each population contains measurements within 26 distinct elevation bands, we run this significance test 26 quasi-independent times. (The tests are not truly independent because of the coarseness of the melt model output, 11 km,

relative to the finer spacing, e.g. 3 km, in some lower elevation bands.) At 95% confidence, we would expect one or two bands to fail this test even if Populations 1 and 2 were truly different within those bands.

Our analysis of the surface melt model output shows that 23 of 26 elevation bands (88%) pass the t-test; the melt in these elevation bands has significantly changed since the earlier climatological period. (The RACMO 2.3 output in Figure 2 in the main paper shows that, at all elevations, this change is an increase.) The three bands that fail the t-test are s=200–400 m, 2600–2700 m, and 2700–2800 m; we cannot confidently say that melt has changed at these elevations. The low-elevation failed band (s=200–400 m) contained substantially fewer pixels than other bands (14 pixels compared to the average of 104 pixels) due to the steepness of terrain at low elevations, which may have caused it to fail. Furthermore, all three of these failed bands lie toward the ends of our tested elevations (0–3000 m). At the higher-elevation failed bands (2600–2800 m), our results indicate that surface melt may not be increasing; however, these elevations are substantially higher than both our identified upper limit of moulin formation ($\sim$1600 meters) and the frozen bed – wet bed transition ($\sim$2000 meters), so we do not analyze this further.

Our analysis of the SMB model output shows that only ten of the 26 elevation bands pass the t-test. In general, the elevation bands without a significant change in SMB span 1800–2800 meters elevation. In most elevation bands below 1800 meters elevation, which is roughly equivalent to the ELA (1630 meters averaged over the entire 56-year time period), there is a significant decrease in SMB. This suggests that the increased melt observed in the RACMO2.3 output at all elevations is, at high elevations, being at least partially offset by increased snowfall. Indeed, this is the expected behavior of an ice sheet in a warming climate (Cuffey and Paterson, 2010). Furthermore, the variation in SMB reflects changes in runoff rather than melt. Although melt is increasing at all elevations, increased melt rates also bring increased refreezing rates; thus, the change in runoff will

be less than the changes in melt, and overall, the change in SMB will be dampened compared to changes in surface melt. This may manifest in areas with little to no runoff: for example, the highest elevation bands studied (2800–3000 m). These bands showed a significant decrease in SMB between the two periods.

Inland migration distance of the ELA

Between the two periods of melt studied, the ELA rose 110 meters, from 1580 meters to 1690 meters. The average surface slopes in our study area at this elevation (Howat et al., 2014) indicate that this corresponds to an inland migration of 12 km. Because we are studying the average of two thirty-year periods, this migration distance represents the average migration over a thirty-year period. These distances differ from that found by Leeson et al. (2014), who studied the inland migration of the uppermost supraglacial lakes since 1971, i.e., over a 43-year period. Their result, 53 km, as well as that of Howat et al. (2013), 56 km over the same period, scale to 37 and 39 km over a thirty-year period, respectively. These distances are significantly longer than those revealed by our analysis of the ELA. However, when restricting the RACMO2.3 output to the smaller, more shallowly sloped study area of Leeson et al. (2014), we find an inland migration of the ELA of 38 km over the 30-year time period, which agrees well with the inland migration of the uppermost supraglacial lakes found by these two separate studies.

Identification of surface features

We used Landsat and radar images (from RADARSAT and ALOS-PALSAR) within our study area to identify surface streams and supraglacial lakes that do not drain completely by the end of each summer. Lakes with frozen lake ice lids visible in summertime Landsat imagery were identified as lakes that had formed the previous summer and overwintered

without draining (Darnell et al., 2013). Lake locations were confirmed with wintertime radar images, which highlight the contrast between lake ice caps and the surrounding ice sheet. We used images from 2000, 2010, and 2013 to identify frozen-over lakes because the greatest number of cloud-free Landsat images were available for these years. We use the presence of lake ice as the sole indicator that a lake overwintered without fully draining that year.

We used two visible-spectrum Landsat images (24 June 2004 and 30 July 2014) and radar images (an L-band ALOS-PALSAR mosaic from winter 2009-2010 as well as C-band RADARSAT mosaics from winters spanning 2000–2006) to identify and digitize the major surface streams in a smaller, centrally located area of approximately 6,000 km^2 (the size of Delaware). This region spans approximately 1100–1800 meters elevation (Figure 3a). We digitized a total of 312 major stream channels in this area. Though the width of the streams (approximately two meters or less) is less than the pixel size of the Landsat (30–70 meters) or radar (20 meters) data, the streams are nonetheless quite discernible; this is due to their long lengths ($\sim$10 km corresponds to $\sim$150–500 pixels), which allow the eye to identify adjacent pixels that are part of a linear feature. In most cases, the streams terminated into lakes or moulins that were conspicuous in the radar data as meter-scale bright spots, some of which were hundreds of meters downstream from lakebeds.

Visual inspection shows more complex surface water flow than we have digitized; Figure S1 illustrates the diversity of streams in the area over time (2004 and 2014) and space. While we digitized the major stream channels (red) from the 2004 image, the image clearly shows that these are fed by smaller, undigitized streams that we missed in 2004 (Figure S1a) and/or that intensified by 2014 (Figure S1d). Comparing the red digitized 2004 streams to the 2014 image they are overlain on also shows the slight migration of stream channels over time.

The lengths of these 312 streams tend to increase with elevation, as shown in Figure S2.

We find one long stream (35 km) originating at 1591 meters elevation; all other streams that originate at elevations <1600 meters (267 streams) are shorter than 30 km. By contrast, 70% (30 out of 44) of the streams originating above 1600 meters elevation are longer than 30 km. Stream length also becomes more variable with elevation, however: at 1200–1300 meters elevation, for example, the 39 identified streams are 6 $\pm$ 1 km long (95% confidence) on average, while at 1700–1800 meters elevation, the 15 identified streams average 40 $\pm$ 6 km in length. Despite the variability, this is a six-fold increase in stream length. Lower surface slopes likely play a role in the degree of stream lengthening. For example, surface slopes decrease by a factor of two to three, from 0.033 to 0.012, between 1200–1300 meters and 1700–1800 meters elevation in this area. This is markedly less than the factor-of-six increase in stream length observed for these same elevation bands, however. We therefore suggest that the absence of moulins at higher elevations is the primary explanation for the increased stream lengths there.

Strain rate dataset

We calculated the principal strain rate from wintertime velocity data averaged over 2007–2010 (Joughin et al., 2010). These data are posted at 500-meter resolution. We differenced these data to calculate the strain rates $\frac{\partial \vec{u}_i}{\partial \vec{r}_j}$, which therefore have 1-km resolution. We then used these strain rates to calculate the principal strain rate, following Cuffey and Paterson (2010):

$$\dot{\epsilon} = \frac{\partial u}{\partial x}\cos^2\theta + \frac{\partial v}{\partial y}\sin^2\theta,$$

$$\text{where } \theta = \frac{1}{2}\,\text{Tan}^{-1}\left(\frac{\dfrac{\partial u}{\partial y} + \dfrac{\partial v}{\partial x}}{\dfrac{\partial u}{\partial x} + \dfrac{\partial v}{\partial y}}\right)$$

These wintertime velocity data do not reflect higher summer velocities, which in land-terminating sectors of the ice sheet can be more than 50% greater due to meltwater-induced sliding enhancement (Joughin et al., 2008). Extensional strain rates thus reach their maximum in summer, when the differential seaward motion of the lower (below $\sim$1000 meters) and upper (above $\sim$1000 meters) parts of the ice sheet is at its peak. This is a direct result of surface meltwater reaching the bed. However, this effect lessens higher on the ice sheet: Palmer et al. (2011) observed only a 0.2% speedup at their station at 1716 meter elevation. At this elevation, the abundance of frozen-over lakes and the relative absence of moulins suggest that meltwater is not reaching the bed. Thus, we take wintertime data to be representative of summertime conditions higher on the ice sheet, where the implications of our study of strain rates are focused.

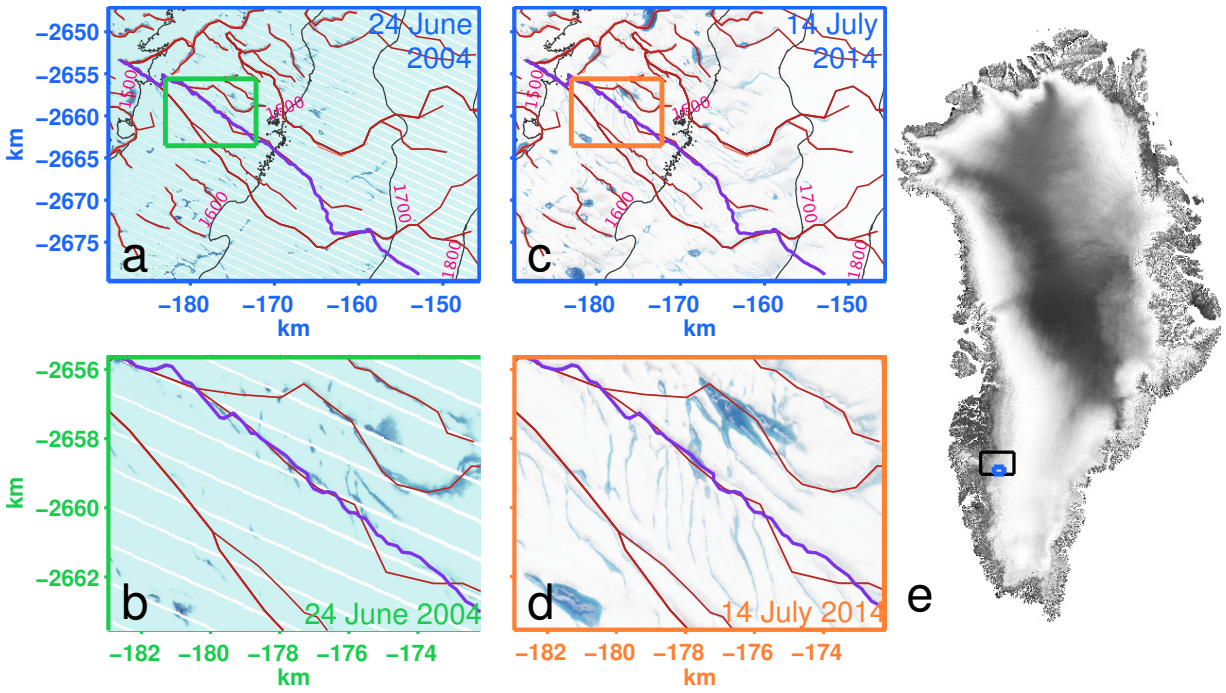

Figure S1

Landsat images (a–d) showing lakes and streams in southwestern Greenland. The black box in (e) indicates the location of Figure 4a in the main text, while the small blue box in (e) shows the location of panels (a) and (c) here (each sized 1400 km^2, the size of Rio de Janeiro). Panels (b) and (d) are 90-km^2 sub-areas of (a) and (c). The surface in June 2004 (a–b) and July 2014 (c–d) is shown, along with a subset of the 312 digitized streams (red) that span this area. Also shown is a long (~47 km) surface stream that appears clearly in the 2014 imagery (purple diagonal line). Surface elevation contours from the GIMP DEM (Howat et al., 2014) are shown in black and labeled in pink. The black streams shown in Figure 4a were identified from the 2004 Landsat image shown here in panels (a–b) and updated with information from the 2014 Landsat image in panels (c–d).

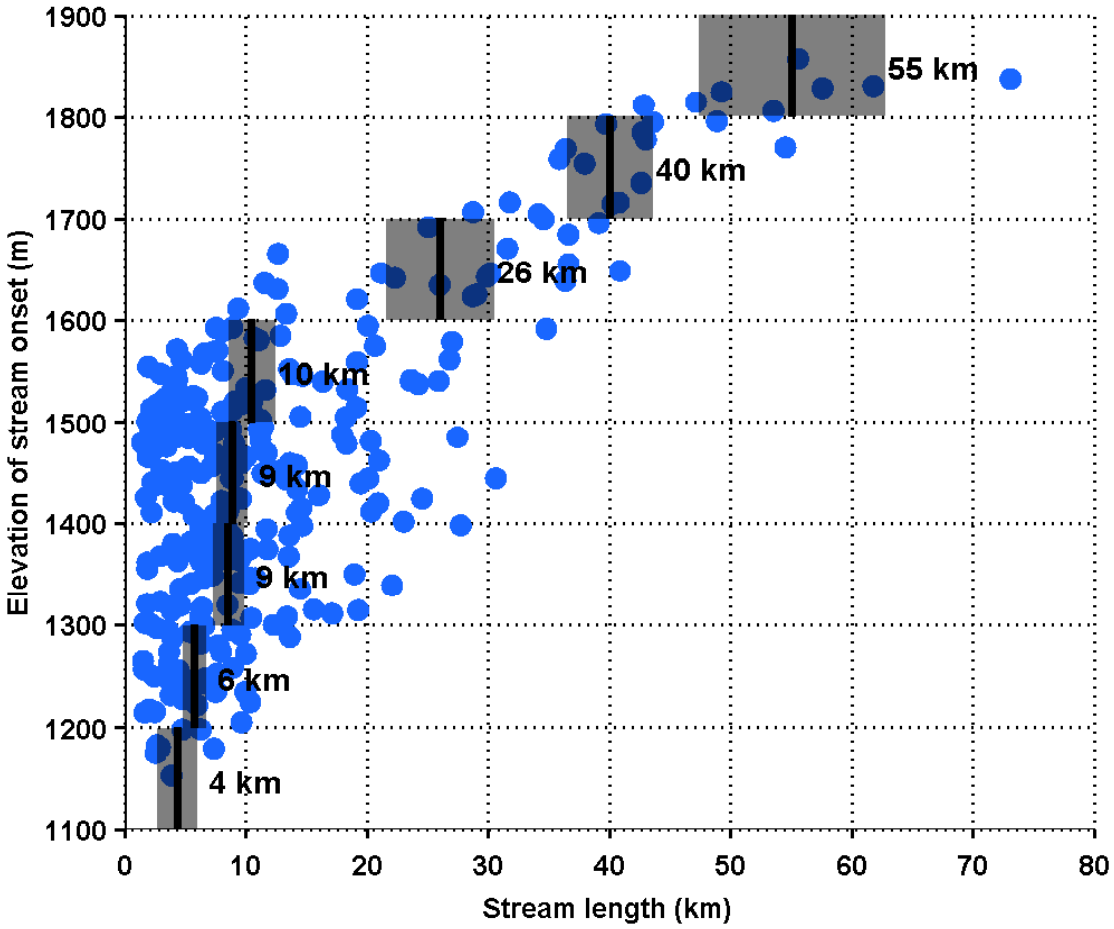

Figure S2

Stream length as a function of elevation, where the elevation of each stream is measured from the GIMP DEM (Howat et al., 2014) at the onset, or highest elevation, of the stream. Blue dots show the 312 streams we digitized; black lines show the mean stream length in each 100-meter elevation bin, with the 95% confidence interval shaded.

References

Aschwanden, A., E. Bueler, C. Khroulev, and H. Blatter (2012). An enthalpy formulation for glaciers and ice sheets. *Journal of Glaciology 58*(209), 441–457.

Bamber, J. L., J. A. Griggs, R. T. W. L. Hurkmans, J. A. Dowdeswell, S. P. Gogineni, I. Howat, J. Mouginot, J. Paden, S. Palmer, E. Rignot, and D. Steinhage (2013). A new bed elevation dataset for Greenland. *The Cryosphere 7*(2), 499–510.

Cuffey, K. M. and G. D. Clow (1997). Temperature, accumulation, and ice sheet elevation in central Greenland through the last deglacial transition. *Journal of Geophysical Research 102*(C12), 26383–26–396.

Cuffey, K. M. and W. S. B. Paterson (2010). The Physics of Glaciers.

Darnell, K. N., J. M. Amundson, L. M. Cathles, and D. R. MacAyeal (2013, July). The morphology of supraglacial lake ogives. *Journal of Glaciology 59*(215), 533–544.

Devore, J. L. (1982). *Probability & Statistics for Engineering and the Sciences*. California Polytechnic State University: Brooks/Cole Publishing Company.

Doyle, S. H., A. Hubbard, and A. Fitzpatrick (2014). Persistent flow acceleration within the interior of the Greenland ice sheet. *Geophysical Research Letters*.

Ettema, J., M. R. van den Broeke, E. van Meijgaard, W. J. van de Berg, J. L. Bamber, J. E. Box, and R. C. Bales (2009, June). Higher surface mass balance of the Greenland ice sheet revealed by high-resolution climate modeling. *Geophysical Research Letters 36*(12), L12501.

Fox Maule, C., M. E. Purucker, N. Olsen, and K. Mosegaard (2005, July). Heat flux anomalies in Antarctica revealed by satellite magnetic data. *Science 309*(5733), 464–467.

Howat, I. M., S. de la Peña, J. H. van Angelen, J. T. M. Lenaerts, and M. R. van den Broeke (2013). Expansion of meltwater lakes on the Greenland Ice Sheet. *The Cryosphere 7*(1), 201–204.

Howat, I. M., A. Negrete, and B. E. Smith (2014). The Greenland Ice Mapping Project (GIMP) land classification and surface elevation data sets. *Cryosphere 8*(4), 1509–1518.

Joughin, I., I. M. Howat, M. Fahnestock, B. Smith, W. Krabill, R. B. Alley, H. Stern, and M. Truffer (2008, October). Continued evolution of Jakobshavn Isbrae following its rapid speedup. *Journal of Geophysical Research 113*(F4), F04006.

Joughin, I., B. E. Smith, I. M. Howat, T. Scambos, and T. Moon (2010). Greenland flow variability from ice-sheet-wide velocity mapping. *Journal of Glaciology 56*(197), 415–430.

Leeson, A. A., A. Shepherd, K. Briggs, I. Howat, X. Fettweis, M. Morlighem, and E. Rignot (2014, December). Supraglacial lakes on the Greenland ice sheet advance inland under warming climate. *Nature Climate Change 5*(1), 51–55.

MacAyeal, D. R. (1997). EISMINT: Lessons in ice-sheet modeling. Technical report.

Palmer, S., A. Shepherd, P. Nienow, and I. Joughin (2011, February). Seasonal speedup of the Greenland Ice Sheet linked to routing of surface water. *Earth and Planetary Science Letters 302*(3-4), 423–428.

Rogozhina, I., J. M. Hagedoorn, Z. Martinec, K. Fleming, O. Soucek, R. Greve, and M. Thomas (2012, May). Effects of uncertainties in the geothermal heat flux distribution on the Greenland Ice Sheet: An assessment of existing heat flow models. *Journal of Geophysical Research 117*(F2), F02025.

Seroussi, H., M. Morlighem, E. Rignot, and A. Khazendar (2013). Dependence of century-scale projections of the Greenland ice sheet on its thermal regime. *Journal of Glaciology*.

Shapiro, N. M. and M. H. Ritzwoller (2004). Inferring surface heat flux distributions guided by a global seismic model: particular application to Antarctica. *Earth and Planetary Science Letters*.

van Angelen, J. H., M. R. van den Broeke, B. Wouters, and J. T. M. Lenaerts (2013, November). Contemporary (1960–2012) Evolution of the Climate and Surface Mass Balance of the Greenland Ice Sheet. *Surveys in Geophysics 35*(5), 1155–1174.

Chapter 6

SYNTHESIS AND CONCLUSION

6.1 Summary of research contributions

My work applies models and remote sensing analysis toward current topics in understanding the ablation and percolation zones of the Greenland Ice Sheet. The major contributions of this thesis are as follows:

Contribution 1 Cryo-hydrologic warming can affect ice temperatures substantially (up to $\sim$10°C warmer), but alters ice velocities in Pâkitsoq by less than 10%.

Importance: Cryo-hydrologic warming is a relatively new idea as applied to ice sheets (circa 2010). Since then, it has received much press, but little investigation outside of the research group who first applied it to Greenland and coined the term (Phillips et al., 2010). My work (Chapter 3) is just the second independent model for this process, and the first to apply it to all available boreholes in the Jakobshavn region. It also corrects a misinterpretation of the observed velocity record (Phillips et al., 2013), which erroneously claimed that ice velocities had increased due to this process.

Contribution 2 Most ice in Greenland (>60%) flows too quickly through the ablation zone to cryo-hydrologically warm by more than $\sim$3°C.

Importance: The fifth IPCC (2014) report acknowledged the occurrence of cryo-hydrologic warming, but did not include the process in its projections of sea-level rise because it had not been evaluated on an ice-sheet-wide scale. My work (Chapter 3) was the first to do this. It shows that cryo-hydrologic warming is limited to slow-flowing regions that usually terminate on land and lose mass primarily through ablation. Thus, the majority of the ice flux coming off of the island is not subject to the threat of cryo-hydrologic warming.

I evaluated the cryo-hydrologic warming potential of the entire ice sheet. The areas that likely host significantly warmer ice due to their slower flow are limited to a

well-studied swath in central western Greenland and a few small pockets of land-terminating ice in Northeast and Northwest Greenland. While these latter regions likely have minimal important to the overall mass balance of the ice sheet, they may be interesting places to monitor as melt rates, which are currently just 20–30% of those in central western Greenland, continue to increase.

Contribution 3 Meltwater can persist in crevasse fields for decades without refreezing englacially or draining to the bed. Such water-filled crevasses typically occupy the top $\sim$300 meters of the ice sheet.

Importance: Crevasse fields have sometimes been seen as a "distributed network" for carrying surface meltwater to the bed (Colgan et al., 2011); that is, meltwater in crevasses would slowly "trickle through" the vertical thickness of the ice sheet. In contrast, cold ice might refreeze the meltwater faster than the timescales of such trickles (Alley et al., 2005). My work (Chapter 4) found that high-melt-influx cases could indeed form such a distributed network (i.e., moulins can form on decadal timescales). However, for more likely melt influxes, the englacial refreezing rates roughly balance the meltwater input rates, and liquid water persists englacially for multiple decades. The depths of these crevasses ($\sim$300 meters) agrees with my independent findings from Chapter 3. Englacial water at these depths may have been observed in radar in the western Greenland ablation zone (Catania et al., 2008).

Contribution 4 High-elevation meltwater is unlikely to penetrate the ice sheet in areas where the bed is frozen.

Importance: This directly addresses an item in the fifth IPCC (2014) report: "the potential of latent-heat effects in the future" to enhance ice flow in frozen-bedded regions of the ice sheet. The likelihood of such latent-heat incursions was not well constrained at the time. Previous observations (Howat et al., 2013) and model-based analyses (Leeson et al., 2014) suggested that the zone of supraglacial lakes has been

expanding inward and may soon overlie frozen beds. My work (Chapter 5) shows that although this may be true, these lakes are unlikely to create new hydrofractures in situ because of a lack of crevasses at high elevations. Instead, the high-elevation meltwater is more likely to run down across the surface of the ice sheet, where it will enter preëxisting moulins and have a limited effect on ice flow.

Contribution 5 The surface boundary condition of an ice-sheet model can be used to efficiently represent the effects of surface meltwater that refreezes within the percolation zone. We found that such refreezing warms the upper ∼200 meters of the ice column by 3–5°C.

Importance: Most large-scale ice-sheet models do not incorporate this process because doing so physically is computationally intensive and somewhat spatially unconstrained. Our use of firn temperatures calculated by the subsurface routine of the RACMO2 climate model demonstrates the efficacy and ease of implementation of incorporating thermal processes in the percolation zone.

6.2 Generalization and pattern of my scientific contributions

The work I present in this thesis was based on testing ideas that others have conceived. Will high-elevation melt reach a frozen bed? Will cryo-hydrologic warming accelerate ice flow around Greenland? Can meltwater seep through a crevasse field and reach the bottom of the ice sheet? These questions motivated me to develop and apply two new process-scale models to the ablation zone of the Greenland Ice Sheet. My work added rigor to these young topics, which is a complement to the creative nature of these questions and early speculations. Both aspects of science – envisioning the unknowns that may soon become knowable, and crafting tractable approaches to probe those open questions – are important. As I continue to grow as a scientist, my work will expand from the second category, where I feel comfortable working now, into the first as well.

My work on these questions has uncovered a number of side topics, interesting puzzles, and future topics of inquiry. Firstly, the physical systems I studied have a number of parallels elsewhere in geophysics; I describe a few such cases in the next section. Next, I outline a handful of interesting questions for future research, some with a narrow focus and others with a broader vision. Finally, I summarize my contributions to my specific sub-field, englacial hydrology.

6.3 Application of methods to other geophysical research areas

Many earth systems have similar behavior to one another. The atmosphere and ocean are fluids that differ in their viscosities and compressibilities. Aeolian dunes and ripples on a sandy river bottom differ in their scale. The two-phase thermodynamic system of ice and water, which forms the basis of this thesis, is similar to magma flow near mid-ocean ridges. The crucial difference between these two systems is merely a frame of reference: due to the relative densities of the phases involved, magma flow is analogous to crevasse propagation or basal temperate ice layers, but turned upside-down.

6.3.1 Thermodynamics of mantle melts

As polar ice is relatively near its melting point, the mantle is relatively near its freezing point, the solidus. In the deep mantle, the pressure is high and the material exists in its solid form. Near mid-ocean ridges, the mantle substance rises and decompresses. It also cools as it rises (Figure 6.1), but eventually reaches a pressure low enough that it will melt. This occurs approximately 60 km below the surface, although the depth can vary (Sparks and Parmentier, 1991). This phase transition is akin to cold ice crossing downward through the CTS: a solid crossing a freezing front where a phase change *can* occur, but is not required.

Once at its melting point, the mantle melts are able to physically separate from the solid component. The melts, which are less dense, rise with a faster velocity than the

solid component. The right-hand panel of Figure 6.1 illustrates temperatures of two distinct materials: a mantle melt (dotted line) and a solid-rock component (dashed line). This is distinctive from temperate ice, where the liquid water is largely trapped at grain boundaries. (Some models allow freer motion; for example, Aschwanden et al. (2012).)

The greatest similarity between a polythermal ice sheet and a mid-ocean ridge occurs at the freezing front, the point where the fluid temperature again intersects the solidus, and the mantle melts recombine with the solid rock. This occurs at depths of $\sim$10 km or less (Sparks and Parmentier, 1991). This phase transition, where all liquid *must* refreeze, is analogous to temperate ice moving upward through the CTS.

This thermal problem is more complex than the one in polythermal ice sheets. For one, the vertical motion of the ice is due to ablation and pressure from the flow of ice upstream, not because of a density contrast. Furthermore, the density of liquid water is *greater* than that of the solid, so liquid water would actually descend, relative to solid ice, in a density-driven flow.

6.3.2 Mechanics of mantle plumes and dikes

In some places, mantle chambers coalesce magma into a buoyant body that can rise through the surrounding solid rock. This generally occurs at mid-ocean ridges and hot spots, and is often called a mantle plume, I think. The rising magma displaces its solid surroundings elastically, just as a descending water-filled crevasse opens elastically. The mantle surrounding the plume should also deform viscously, leading to pinch-off (Figure 6.2), although pinch-off can also occur purely elastically (Weertman, 1996). Finally, the magma is also subject to re-solidication along the walls of the plume, where it is in contact with cooler solid rock. These three processes are precisely the same as in water-filled crevasses, except with different substances, and upside-down because of the solid-liquid density difference.

When a mantle plume reaches the surface, it outcrops, solidifies, and becomes a dike.

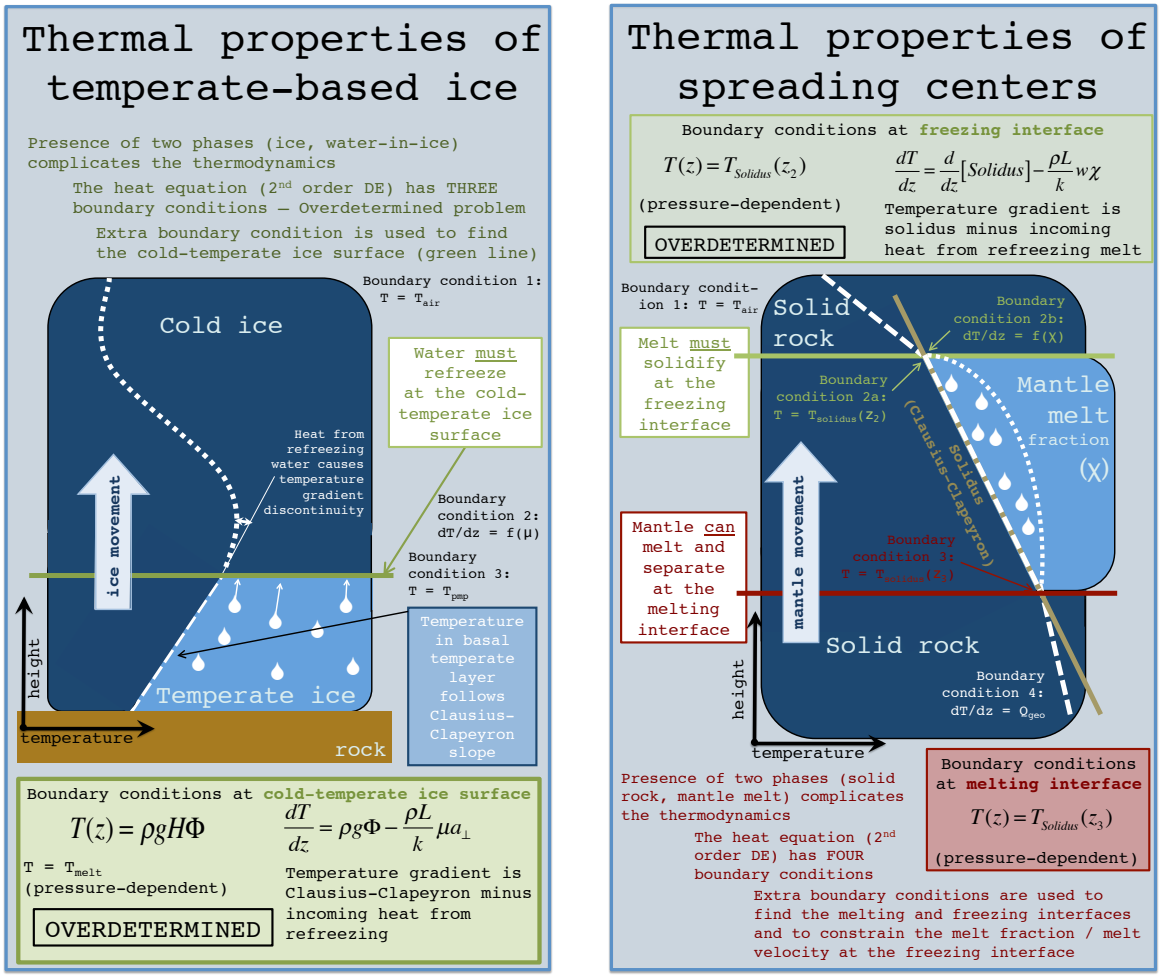

Figure 6.1: Similarities between the multi-phase thermal problems in polythermal ice sheets (left) and mid-ocean ridge spreading centers (right). Both are multi-phase systems with phase changes taking place at specific locations determined by the energy of the system.

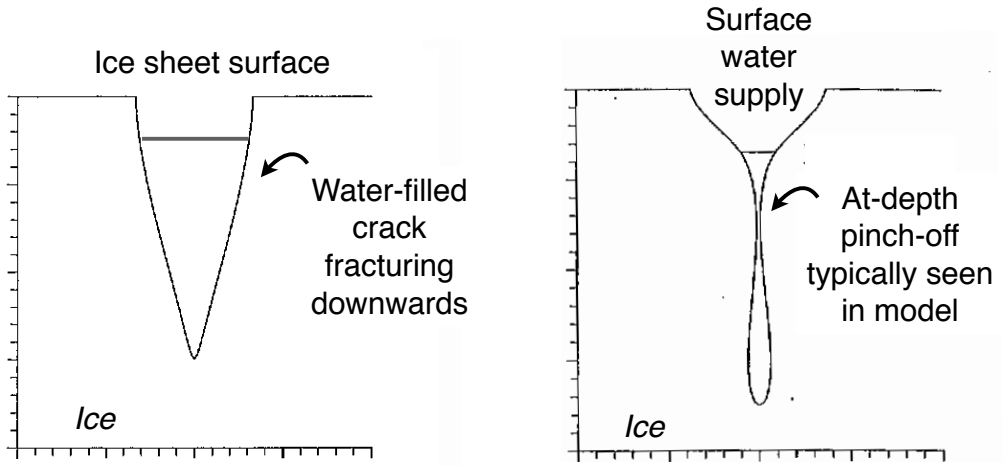

Figure 6.2: Schematic of a water-filled crevasse fracturing through an ice sheet. (Left), early in the evolution of the crevasse, it has a clear connection to the ice-sheet surface and its melt supply. (Right), after multiple years of evolution, pinch-off begins, and disconnection from the surface water supply eventually occurs. Adapted from Weertman (1996).

This is analogous to a fully healed crevasse, one that has frozen shut entirely. Solitary dikes can be observed, but they also occur in dike swarms, which are of course analogous to crevasse fields.

6.3.3 Phase changes in permafrost

Permanently frozen ground (permafrost) is another geophysical system that incorporates the solid and liquid phases of water. Like the mantle melts problem, it features two phase boundaries: a freezing front a few hundred meters below the surface and a thawing front within the top ten meters (the active layer). The phases are inverted with respect to the mantle melts, though: liquid may exist within the uppermost and lowest areas, while the

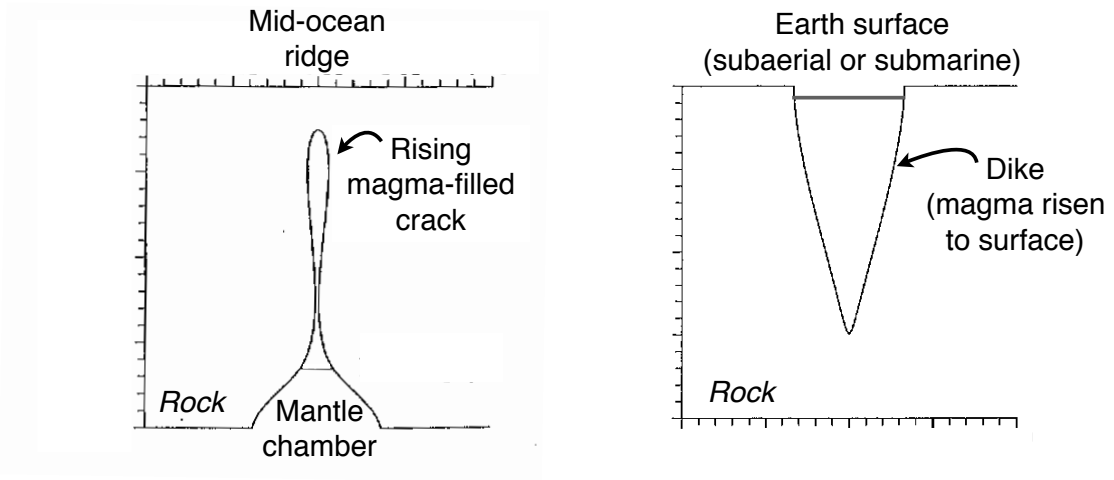

Figure 6.3: Schematic of a buoyant-magma-filled crack rising through the surrounding rock near a mid-ocean ridge. (Left), the crack is initially connected to the magma chamber, which supplies the fluid, but pinch-off eventually occurs. (Right), the magma continues to rise and, if it outcrops onto the surface, forms a dike. Adapted from Weertman (1996).

solid phase (permafrost) occupies the middle region.

Ice wedges can also form in regions of permafrost. These are analogous to water-filled crevasses, except the host material is a different substance: soil, not ice. Thus, although the water refreezes each winter, it does not "rejoin" the host material, as it does in my crevasse model. Ice wedges tend to be smaller (meter-scale) than crevasses, perhaps because they are initiated by tension through, counterintuitively, thermal contraction. Ice-wedge polygons, which are the surface expression of ice wedges, are observed on Mars.

6.4 Potential questions for further research

In the course of applying my models to the research questions outlined in this thesis, I uncovered new questions within these topics, alternative lines of investigation, and complementary research by other workers. These topics form the basis for possible research directions in the near future.

6.4.1 Explanation of warm basal ice in Southwest Greenland

Recent observational work by Harrington et al. (2015) on Russell Glacier, Southwest Greenland indicated the presence of thick layers ($\sim$100 m) of temperate ice beneath that glacier. To investigate the source of this warm ice, they applied a simple temperature model to the area and concluded that basal crevassing explained the warm ice temperatures: basal meltwater had evidently refrozen within sizable crevasses, warming the bottom $\sim$100 m of ice to the melting point.

While I do not suppose that basal crevassing is absent in this region, I suspect that other, more simple processes may explain the observations of warm basal ice. Specifically, the thermal model that Harrington et al. (2015) used to diagnose the area lacked a number of standard terms: horizontal advection, vertical advection, latent heat effects, and a water-content-dependent flow-law parameter were all missing from this model. While horizontal advection would tend to cool the ice, the latter three terms would tend

to warm the basal ice, potentially enough to create a temperate layer comparable to that observed.

My model (Chapter 2) includes the above terms that the Harrington et al. (2015) model lacked. A simple application of my model to the Russell Glacier area could elucidate whether the field observations do, in fact, imply extensive basal crevassing and basal water storage in that area.

If my thermal model *does* indicate that meltwater is refreezing within basal crevasses, a pertinent question becomes *how much* water. The volumes of meltwater that are held englacially or subglacially is a current open question in Greenland Ice Sheet hydrology (Chu, 2013; Rennermalm et al., 2013; Smith et al., 2015). Subglacial storage is also a central topic in the hydrology of surge glaciers (Lingle and Fatland, 2003; Sevestre et al., 2015). My model for the growth of a water-filled crevasse and its thermal effects on the ice surrounding it (Chapter 4) could have direct application to the basal hydrologic system.

6.4.2 The timescale of cryo-hydrologic warming

The two other published models that treat cryo-hydrologic warming quantify this process in different ways. Phillips et al. (2013) construct the source term around the difference between the melting point and the ambient ice temperature. This may be $\sim$20°C at, for instance, the TD5 borehole near Swiss Camp. This creates a relatively high temperature gradient ($\sim$0.2–1°C/m for water-filled crevasses spaced by 20–100 meters) over a large length scale. In reality, the large length scale implies a slow timescale: diffusion times of 10–1,000 years in this case. Yet the model of Phillips et al. (2013) discounts horizontal diffusion, presumably because of the increased computational time it usually adds. Their source term also allows heat to spread to the center of thick ice blocks immediately. Thus, this approach would appear to overestimate true warming rates.

The setup of my model for crevasse propagation (Chapter 4) treats this problem more

precisely than does Phillips et al. (2013) through more complete physics (it includes horizontal diffusion) and higher spatial resolution (5 meters, which corresponds to a diffusion time of one year). Because my model calculates temperature gradients over a smaller spatial scale, they are initially steeper than represented by Phillips et al. (2013): $\sim$3°C/m at 300 meters depth, and $\sim$1.5°C/m at 100 meters depth, after 7 years. Over time, these decrease to $\sim$0.1°C/m at 300 meters depth and $\sim$0.003°C/m at 100 meters depth after 50 years. Over very long timescales, my model and that of Phillips et al. (2013) incorporate similar quantities of refrozen water and thus should find the same equilibrium ice temperature. However, as described above, my thermal model should more accurately determine the temporal evolution of the warming.

In terms relevant to society, although the *magnitude* of the temperature change of the ice will affect the amount of sea-level rise, we also need information on the *timescale* over which such warming will occur. Previous models parameterized the cryo-hydrologic warming process simply, in a way that correctly identifies the ultimate magnitude but obscures the timescale. My model, on the other hand, incorporates more detailed physics that affect the rates of temperature change. Thus, one potential contribution is to better inform us of the rates of englacial warming and the consequent sea-level rise.

6.4.3 Moulin formation on a drastically different Greenland Ice Sheet

In Chapter 5, I examined whether high-elevation moulin formation could activate wholesale ice-sheet thinning across western Greenland. Though the evidence suggests that this will not occur, it *is* likely that the ice sheet will thin, due to other causes, considerably in this area in the coming centuries (IPCC, 2014). Such thinning will increase surface slopes, which will increase driving stress and thus also increase longitudinal strain rates and ice speeds.

Any given location on the present-day ice-sheet surface, then, will be atop thinner ice and will experience higher strain rates in this future scenario. Recall that thick ice

suppresses crevasse formation by masking bedrock obstacles (Gudmundsson, 2003). At the same time, thick ice *can* crevasse if extensional strain rates are high enough: Jakobshavn Isbræ is an extreme example (H >2000 meters of heavily crevassed ice). So while crevasses may not form at a location currently at 1600 meters elevation, in the future, they may form in the now-thinner ice at this grid point. At some places, this will be a moot point: the hypothesized thinning may melt frozen beds, so that moulin formation in these areas may not substantially affect melt-driven ice flow. However, are there marginal cases where modest thinning, or an increase in strain rates due to longitudinal coupling to fast-thinning ice downstream, can increase the likelihood of crevassing *above* the frozen–wet transition?

Answering these questions requires (1) better knowledge of where the frozen–wet basal boundary is, and (2) an ice-flow model underlain by (3) a realistic basal topography map. These tools exist (2–3) or are areas of active research (1), and assembly of them would constrain the possibility of this hypothesis.

6.4.4 Why do moulins form where they do?

Formation of a moulin requires both a large volume of meltwater and a crack or crevasse in the ice sheet into which that water can flow. However, as shown in Figure 6.4, the natures of sites that can typically host each feature are mutually exclusive: lakes collect in topographic lows, while crevasses form on highs. If the lake level rises high enough to access the nearest crevasse, as shown in the figure, then a moulin can form.

If this conceptual model for moulin formation is correct, then moulins should form in regions of only slightly extensive flow. This contrasts with my assumption in Chapter 5 that moulins require high strain rates (>0.005 yr^{-1}) to form. In fact, strain rates at the 134 stream terminations that I identified (and assumed to be moulins) averaged substantially less than this value, and <10 stream terminations occurred in areas with strain rates above the >0.005 yr^{-1} threshold.

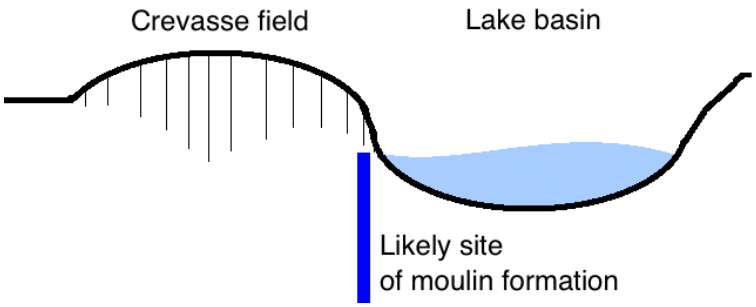

Figure 6.4: Schematic of a region in which a moulin may form. Supraglacial lakes pool water in local topographic lows, while neighboring high regions (usually immediately downstream) in tension form crevasses. If water from the lake can access a crevasse, moulin formation is possible. Thus, moulins are commonly observed downstream of their respective lakes.

Vena Chu (University of California, Berkeley) has found a similar result with her moulin dataset, which is based on high-resolution WorldView imagery and is far more extensive (1236 moulins) than mine. Furthermore, while my dataset is limited to stream-fed moulins readily identifiable in lower-resolution Landsat imagery, hers includes both stream-fed and lakeside moulins. Thus, the discrepancy between moulin location and expected strain rate likely is not due to any bias in formation mechanism.

The pertinent question is why moulins do not seem to occur in areas of high strain rate. Ongoing research by Vena Chu is likely to give further insight, but I present some hypotheses here.

Many moulins stay active for multiple years, during which they advect downstream from their formation regions. Thus, when we correlate moulin locations with strain rates, we are not capturing the strain rates associated with moulin formation. As shown in Figure 6.4, though, moulins usually move farther into crevasse fields as they age, where strain rates are yet higher. This is at odds with what we observe.

Stevens et al. (2015) showed that moulins can form in the center of lake basins, despite

the compressional regime there, if other local fractures have allowed meltwater to the bed. Additional water at the bed would produce local basal stress transients that can temporarily push the ice-sheet surface into a tensional regime, allowing moulin formation. Indeed, observations of lake drainage events clustered in time (Doyle et al., 2013; Fitzpatrick et al., 2014) support this idea, although the spatial scale of coupling remains unconstrained. It is possible that one moulin formed as illustrated in Figure 6.4 may be enough to trigger the drainage of other nearby supraglacial lakes, even those with long-term strain rates below the hypothetical threshold for crevassing.

The high-resolution moulin dataset (Vena Chu) also features a number of high-elevation moulins ($\sim$1800 meters). Interestingly, the strain rates at those locations are low, and no regions of high strain rate exist upstream of these features. There is a high-strain-rate ($\sim$0.005 yr^{-1}) area 5 km downstream of the moulins, although that crevasse field has no visible moulins. The nearest high-strain-rate area *with* moulins is 20 km downstream, at an elevation of 1670 meters. This is similar to, though modestly longer than, the length scale of longitudinal coupling ($\sim$12 km) identified by Price et al. (2008). Thus, might it be possible for moulin formation to progress steadily higher on the ice sheet, as moulins at lower elevations trigger the drainage of lakes $\sim$20 km upstream?

6.4.5 What is the subsurface character of a moulin?

Said another way, this is a question of semantics: "What is a moulin?" Is it the point at which the water leaves the ice-sheet surface, or is it better defined englacially? For instance, a high-resolution moulin dataset (Vena Chu, University of California, Berkeley) identifies 6 surface-entry points within a 0.25-km^2 area along the shore of a single lake. It is clear that separate surface streams terminate into these multiple entry points, but perhaps they feed a common englacial fracture. That fracture, if it exists, would imply that meltwater from the separate entry points reaches the bed at a common location.

My crevasse propagation model (Chapter 4) suggests that individual surface cracks

can regularly reach depths of 300 meters and hold considerable water volumes for decadal periods. If an oblique fracture ran through multiple such cracks, the water in them could readily combine and form an englacial surface-to-bed connection. This moulin would likely retain its multiple surface entry points and could look similar to the observed moulin complex described above.

Though it seems rather technical, this point should be considered by those conducting analyses of "moulin density." A few such studies (e.g., Banwell et al., 2012; Phillips et al., 2011) have been conducted in western Greenland, and with the scientific potential and ready availability of high-resolution imagery for this area, such quantitative mapping projects are becoming popular.

6.5 Thesis summary

This thesis described mechanisms through which liquid water may affect present-day or near-future ice flow on the Greenland Ice Sheet. First, liquid water exists at the grain boundaries of temperate ice, which enhances the ability of these grains to slid past each other and deform the ice sheet. Second, surface meltwater can access the englacial system through crevasses. The water can refreeze in crevasses, in which case the latent heat warms and softens the ice, enhancing deformational motion. Third, surface meltwater can also access the bed through moulins, which can also form from seed crevasses. If introduced to new areas, basal meltwater may allow the ice sheet to slide, increasing its speed. For each mechanism, I chose a local study area where the nature of the ice sheet highlighted that particular aspect of ice-sheet flow or fracture.

My findings highlight differences among local areas. Jakobshsavn Isbræ moves primarily through basal sliding, but deformation of soft temperate ice also contributes hundreds of meters per year (15–40%) of motion. This is in contrast to the neighboring Pâkitsoq region, which also moves primarily by basal sliding, but at much slower speeds. The ice here spends centuries or longer in the ablation zone, collecting melt in crevasses. Through two independent models, I found that crevasses typically extend to depths of

$\sim$300 meters and warm the ice, through the latent heat of refreezing, by up to $\sim$7–10°C. This has only a small effect on overall ice motion, though: $<$10% in slow-moving regions, and an imperceptible effect in the fast-moving Jakobshavn Isbræ. Slow-moving regions drain $<$40% of the ice flux leaving Greenland, though, so crevasse-based refreezing likely has less importance to ice-sheet mass balance than has previously been suggested.

Higher on the ice sheet, where the ice is colder, aggregate melt volumes can form moulins. However, a crucial component of moulin inception is a crevasse, which are sparse at high elevations: 80% rarer, on average, at elevations of 1800–1900 meters than they are at 1100–1200 meters elevation.While supraglacial lakes in the lower elevation range commonly drain rapidly through nearby moulins, lakes in the higher elevation range rarely appear to behave in this way. Instead, high-elevation lakes appear to overflow into long surface streams that carry the water tens of kilometers downstream, to elevations hundreds of meters lower, where they access crevasses or preëxisting moulins.

6.6 Relevance to Greenland Ice Sheet hydrology

I developed process-scale models relevant to the ablation and percolation zones of the Greenland Ice Sheet. I combined these models with remote-sensing and field-based observations to study multiple aspects of how meltwater from the ice-sheet surface may interact with the flow of the ice sheet. Two particular interactions that I studied had been directly addressed in the fifth IPCC (2014) report as outstanding processes with unknown effects on the mass balance of the ice sheet. While quantifying the role of these specific processes on sea-level rise would require incorporating them into a systemic ice-sheet model, which is beyond the scope of this thesis, I have provided quantitative guidelines for those ice-sheet modelers:

- Meltwater is unlikely to reach the bed underlying elevations above $\sim$1600 meters
- Cryo-hydrologic warming affects ice temperatures in the top $\sim$300 meters in locations that have experienced $>\sim$250 years of melt in the ablation zone

My findings have contributed to our understanding of how specific processes that link melt and ice dynamics are likely to affect sea-level rise sourced from the Greenland Ice Sheet. This work joins the body of scientific literature that helps policymakers and stakeholders make informed decisions on the growing number of issues that climate change and sea-level rise affect.

BIBLIOGRAPHY

Alley, R. B., T. K. Dupont, B. R. Parizek, and S. Anandakrishnan (2005). Access of surface meltwater to beds of sub-freezing glaciers: preliminary insights. *Annals of Glaciology 40*(1), 8–14.

Aschwanden, A., E. Bueler, C. Khroulev, and H. Blatter (2012). An enthalpy formulation for glaciers and ice sheets. *Journal of Glaciology 58*(209), 441–457.

Bamber, J. L., R. B. Alley, and I. Joughin (2007). Rapid response of modern day ice sheets to external forcing. *Earth and Planetary Science Letters 257*(1-2), 1–13.

Bamber, J. L., J. A. Griggs, R. T. W. L. Hurkmans, J. A. Dowdeswell, S. P. Gogineni, I. Howat, J. Mouginot, J. Paden, S. Palmer, E. Rignot, and D. Steinhage (2013). A new bed elevation dataset for Greenland. *The Cryosphere 7*(2), 499–510.

Banwell, A. F., N. S. Arnold, I. C. Willis, M. Tedesco, and A. P. Ahlstrøm (2012). Modeling supraglacial water routing and lake filling on the Greenland Ice Sheet - Banwell - 2012 - Journal of Geophysical Research: Earth Surface (2003–2012) - Wiley Online Library. *Journal of Geophysical Research 117*(F4), F04012.

Bartholomew, I., P. Nienow, A. Sole, D. Mair, T. Cowton, S. Palmer, and J. Wadham (2011). Supraglacial forcing of subglacial drainage in the ablation zone of the Greenland ice sheet. *Geophysical Research Letters 38*(8).

Bartholomew, I. D., P. Nienow, A. Sole, D. Mair, T. Cowton, M. A. King, and S. Palmer (2011). Seasonal variations in Greenland Ice Sheet motion: Inland extent and behaviour at higher elevations. *Earth and Planetary Science Letters 307*(3-4), 271–278.

Bennartz, R., M. D. Shupe, D. D. Turner, V. P. Walden, K. Steffen, C. J. Cox, M. S. Kulie, N. B. Miller, and C. Pettersen (2013). July 2012 Greenland melt extent enhanced by low-level liquid clouds. *Nature 496*(7443), 83–86.

Benson, C. S. (1962). Stratigraphic studies in the snow and firn of the Greenland ice sheet. Technical report.

Block, A. E. and R. E. Bell (2011). Geophysical evidence for soft bed sliding at Jakobshavn Isbrae, West Greenland. *The Cryosphere Discussions 5*(1), 339–366.

Bougamont, M., J. L. Bamber, and W. Greuell (2005). A surface mass balance model for the Greenland Ice Sheet. *Journal of Geophysical Research 110*(F4), F04018.

Catania, G. A. and T. A. Neumann (2010). Persistent englacial drainage features in the Greenland Ice Sheet. *Geophysical Research Letters 37*(2).

Catania, G. A., T. A. Neumann, and S. F. Price (2008). Characterizing englacial drainage in the ablation zone of the Greenland ice sheet. *Journal of Glaciology 54*(187), 567–578.

Chu, V. W. (2013). Greenland ice sheet hydrology: A review. *Progress in Physical Geography 38*(1), 1–36.

Clarke, T. S. and K. A. Echelmeyer (1996). Seismic-reflection evidence for a deep subglacial trough beneath Jakobshavns Isbrae, West Greenland. *Journal of Glaciology 43*(141).

Clason, C. C., D. Mair, P. Nienow, I. Bartholomew, A. Sole, S. Palmer, and W. Schwanghart (2015). Modelling the transfer of supraglacial meltwater to the bed of Leverett Glacier, southwest Greenland. *The Cryosphere 9*, 123–128.

Colgan, W., K. Steffen, W. S. McLamb, W. Abdalati, H. Rajaram, R. Motyka, T. Phillips, and R. Anderson (2011). An increase in crevasse extent, West Greenland: Hydrologic implications. *Geophysical Research Letters 38*(18).

Cook, J. C. (1956). Some Observations in a Northwest Greenland Crevasse. *Eos 37*, 715–718.

Csatho, B. M., A. F. Schenk, C. J. van der Veen, G. Babonis, K. Duncan, S. Rezvanbehbahani, M. R. van den Broeke, S. B. Simonsen, S. Nagarajan, and J. H. van Angelen (2014). Laser altimetry reveals complex pattern of Greenland Ice Sheet dynamics. *Proceedings of the National Academy of Sciences of the United States of America*, 201411680.

Cuffey, K. M. and G. D. Clow (1997). Temperature, accumulation, and ice sheet elevation in central Greenland through the last deglacial transition. *Journal of Geophysical Research 102*(C12), 26–383–26–396.

Cuffey, K. M. and W. S. B. Paterson (2010). The Physics of Glaciers.

Dansgaard, W. and S. J. Johnsen (1969). A flow model and a time scale for the ice core from Camp Century, Greenland. *Journal of Glaciology 8*, 215–223.

Darnell, K. N., J. M. Amundson, L. M. Cathles, and D. R. MacAyeal (2013). The morphology of supraglacial lake ogives. *Journal of Glaciology 59*(215), 533–544.

Das, S. B., I. Joughin, M. D. Behn, I. M. Howat, M. A. King, D. Lizarralde, and M. P. Bhatia (2008). Fracture Propagation to the Base of the Greenland Ice Sheet During Supraglacial Lake Drainage. *Science 320*(5877), 778–781.

Devore, J. L. (1982). *Probability & Statistics for Engineering and the Sciences*. California Polytechnic State University: Brooks/Cole Publishing Company.

Doyle, S. H., A. Hubbard, and A. Fitzpatrick (2014). Persistent flow acceleration within the interior of the Greenland ice sheet. *Geophysical Research Letters 41*, 899–905.

Doyle, S. H., A. L. Hubbard, C. F. Dow, G. A. Jones, A. Fitzpatrick, A. Gusmeroli, B. Kulessa, K. Lindback, R. Pettersson, and J. E. Box (2013). Ice tectonic deformation dur-

ing the rapid in situ drainage of a supraglacial lake on the Greenland Ice Sheet. *The Cryosphere 7*(1), 129–140.

Echelmeyer, K. and W. D. Harrison (1990). Jakobshavns Isbrae, West Greenland: Seasonal Variations in Velocity - Or Lack Thereof. *Journal of Glaciology 36*(122).

Enderlin, E. M., I. M. Howat, S. Jeong, M. J. Noh, J. H. Angelen, and M. R. Broeke (2014). An improved mass budget for the Greenland ice sheet. *Geophysical Research Letters 41*(3), 866–872.

Ettema, J., M. R. van den Broeke, E. van Meijgaard, W. J. van de Berg, J. L. Bamber, J. E. Box, and R. C. Bales (2009). Higher surface mass balance of the Greenland ice sheet revealed by high-resolution climate modeling. *Geophysical Research Letters 36*(12), L12501.

Fahnestock, M. (2001). High Geothermal Heat Flow, Basal Melt, and the Origin of Rapid Ice Flow in Central Greenland. *Science 294*(5550), 2338–2342.

Fitzpatrick, A. A. W., A. L. Hubbard, J. E. Box, D. J. Quincey, D. van As, A. P. B. Mikkelsen, S. H. Doyle, C. F. Dow, B. Hasholt, and G. A. Jones (2014). A decade (2002-2012) of supraglacial lake volume estimates across Russell Glacier, West Greenland. *Cryosphere 8*(1), 107–121.

Forster, R. R., J. E. Box, M. R. van den Broeke, C. Miège, E. W. Burgess, J. H. van Angelen, J. T. M. Lenaerts, L. S. Koenig, J. Paden, C. Lewis, S. P. Gogineni, C. Leuschen, and J. R. McConnell (2013). Extensive liquid meltwater storage in firn within the Greenland ice sheet. *Nature Geoscience*, –.

Fountain, A. G., R. W. Jacobel, R. Schlichting, and P. Jansson (2005). Fractures as the main pathways of water flow in temperate glaciers. *Nature 433*(7026), 618–621.

Fudge, T. J., E. D. Waddington, H. Conway, J. M. D. Lundin, and K. Taylor (2014). Interpolation methods for Antarctic ice-core timescales: application to Byrd, Siple Dome and Law Dome ice cores. *Climate of the Past 10*(3), 1195–1209.

Funk, M., K. Echelmeyer, and A. Iken (1994). Mechanisms of fast flow in Jakobshavns Isbrae, West Greenland: Part II. Modeling of englacial temperatures. *Journal of Glaciology 40*(136), 569–585.

Georgiou, S., A. Shepherd, M. McMillan, and P. Nienow (2009). Seasonal evolution of supraglacial lake volume from ASTER imagery. *Annals of Glaciology 50*(52), 95–100.

Gogineni, S. P., J. B. Yan, J. Paden, C. Leuschen, J. Li, F. Rodriguez-Morales, D. BraaTEN, K. Purdon, Z. Wang, W. Liu, and J. Gauch (2014). Bed topography of Jakobshavn Isbræ, Greenland, and Byrd Glacier, Antarctica. *Journal of Glaciology 60*(223), 813–833.

Greuell, W. and T. Konzelmann (1994). Numerical modelling of the energy balance and the englacial temperature of the Greenland Ice Sheet. Calculations for the ETH-Camp location (West Greenland, 1155 m asl). *Global and Planetary Change 9*(1), 91–114.

Greve, R. (1997). Application of a polythermal three-dimensional ice sheet model to the Greenland ice sheet: response to steady-state and transient climate scenarios. *Journal of Climate 10*(5), 901–918.

Gudmundsson, G. H. (2003). Transmission of basal variability to a glacier surface. *Journal of Geophysical Research: Solid Earth 108*.

Gusmeroli, A., T. Murray, P. Jansson, R. Pettersson, A. Aschwanden, and A. D. Booth (2010). Vertical distribution of water within the polythermal Storglaciären, Sweden. *Journal of Geophysical Research 115*(F4), F04002.

Harrington, J. A., N. F. Humphrey, and J. T. Harper (2015). Temperature distribution and thermal anomalies along a flowline of the Greenland ice sheet. *Annals of Glaciology 56*(70), 98–104.

Hoffman, M. J., G. A. Catania, T. A. Neumann, L. C. Andrews, and J. A. Rumrill (2011). Links between acceleration, melting, and supraglacial lake drainage of the western Greenland Ice Sheet. *Journal of Geophysical Research: Solid Earth 116*(F4).

Howat, I. M., Y. Ahn, I. Joughin, M. R. van den Broeke, J. T. M. Lenaerts, and B. Smith (2011). Mass balance of Greenland's three largest outlet glaciers, 2000-2010. *Geophysical Research Letters 38*(12).

Howat, I. M., S. de la Peña, J. H. van Angelen, J. T. M. Lenaerts, and M. R. van den Broeke (2013). Expansion of meltwater lakes on the Greenland Ice Sheet. *The Cryosphere 7*(1), 201–204.

Howat, I. M., A. Negrete, and B. E. Smith (2014). The Greenland Ice Mapping Project (GIMP) land classification and surface elevation data sets. *Cryosphere 8*(4), 1509–1518.

Humphrey, N. (1991). Estimating ice temperature from short records in thermally disturbed boreholes. *Journal of Glaciology 37*(127), 414–419.

Humphrey, N. F., J. T. Harper, and W. T. Pfeffer (2012). Thermal tracking of meltwater retention in Greenland's accumulation area. *Journal of Geophysical Research 117*(F1), F01010.

Hutter, K., H. Blatter, and M. Funk (1988). A Model Computation of Moisture-Content in Polythermal Glaciers. *Journal of Geophysical Research 93*(B10), 12205–12214.

Iken, A., K. Echelmeyer, W. Harrison, and M. Funk (1993). Mechanisms of fast flow in Jakobshavns Isbræ, West Greenland. I: Measurements of temperature and water level in deep boreholes. *Journal of Glaciology 39*(131), 15–25.

IPCC (2007). *Climate Change 2007: The Physical Science Basis. Contribution of Working Group I to the Fourth Assessment Report of the Intergovernmental Panel on Climate Change*. Cambridge, United Kingdom and New York, NY, USA: Cambridge University Press.

IPCC (2014). *Climate Change 2013: The Physical Science Basis. Contribution of Working Group I to the Fifth Assessment Report of the Intergovernmental Panel on Climate Change*. Cambridge, United Kingdom and New York, NY, USA: Cambridge University Press.

Jarvis, G. T. and G. K. Clarke (1974). Thermal effects of crevassing on Steele glacier, Yukon Territory, Canada. *Journal of Glaciology 13*, 243–254.

Jeffries, M. O., K. Morris, W. F. Weeks, and H. Wakabayashi (1994). Structural and stratigraphie features and ERS 1 synthetic aperture radar backscatter characteristics of ice growing on shallow lakes in NW Alaska, winter 1991–1992. *Journal of Geophysical Research 99*(C11), 22459–22471.

Johansson, A. M., P. Jansson, and I. A. Brown (2013). Spatial and temporal variations in lakes on the Greenland Ice Sheet. *Journal of Hydrology 476*, 314–320.

Joughin, I., S. B. Das, G. E. Flowers, M. D. Behn, R. B. Alley, M. A. King, B. E. Smith, J. Bamber, M. R. van den Broeke, and J. H. van Angelen (2013). Influence of supraglacial lakes and ice-sheet geometry on seasonal ice-flow variability. *The Cryosphere 7*, 1185–1192.

Joughin, I., S. B. Das, M. A. King, B. E. Smith, I. M. Howat, and T. Moon (2008). Seasonal Speedup Along the Western Flank of the Greenland Ice Sheet. *Science 320*(5877), 781–783.

Joughin, I., B. E. Smith, I. M. Howat, D. Floricioiu, R. B. Alley, M. Truffer, and M. Fahnestock (2012). Seasonal to decadal scale variations in the surface velocity of Jakobshavn Isbrae, Greenland: Observation and model-based analysis. *Journal of Geophysical Research 117*(F2), F02030.

Joughin, I., B. E. Smith, I. M. Howat, T. Scambos, and T. Moon (2010). Greenland flow variability from ice-sheet-wide velocity mapping. *Journal of Glaciology 56*(197), 415–430.

Joughin, I., B. E. Smith, D. E. Shean, and D. Floricioiu (2014). Further summer speedup of Jakobshavn Isbræ. *The Cryosphere 8*, 209–214.

Koenig, L. S., D. J. Lampkin, L. N. Montgomery, S. L. Hamilton, J. B. Turrin, C. A. Joseph, S. E. Moutsafa, B. Panzer, K. A. Casey, J. D. Paden, C. Leuschen, and P. Gogineni (2014).

Wintertime storage of water in buried supraglacial lakes across the Greenland Ice Sheet. *The Cryosphere Discussions 8*(4), 3999–4031.

Krawczynski, M. J., M. D. Behn, S. B. Das, and I. Joughin (2009). Constraints on the lake volume required for hydro-fracture through ice sheets. *Geophysical Research Letters 36*(10), L10501.

Lampkin, D. J. (2011). Supraglacial lake spatial structure in western Greenland during the 2007 ablation season. *Journal of Geophysical Research 116*.

Lampkin, D. J. and J. VanderBerg (2011). A preliminary investigation of the influence of basal and surface topography on supraglacial lake distribution near Jakobshavn Isbrae, western Greenland. *Hydrological Processes 25*(21), 3347–3355.

Leeson, A. A., A. Shepherd, K. Briggs, I. Howat, X. Fettweis, M. Morlighem, and E. Rignot (2014). Supraglacial lakes on the Greenland ice sheet advance inland under warming climate. *Nature Climate Change 5*(1), 51–55.

Lemke, P., J. Ren, R. B. Alley, I. Allison, J. Carrasco, G. Flato, Y. Fujii, G. Kaser, P. Mote, and R. H. Thomas (2007). Observations: Changes in snow, ice and frozen ground. *Titel: Climate change 2007: the physical science basis; summary for policymakers, technical summary and frequently asked questions. Part of the Working Group I contribution to the Fourth Assessment Report of the Intergovernmental Panel on Climate Change*, 337–383.

Lingle, C. S. and D. R. Fatland (2003). Does englacial water storage drive temperate glacier surges? *Annals of Glaciology, Vol 36 36*, 14–20.

Lüthi, M., M. Funk, A. Iken, S. Gogineni, and M. Truffer (2002). Mechanisms of fast flow in Jakobshavn Isbræ, West Greenland: Part III. Measurements of ice deformation, temperature and cross-borehole conductivity in boreholes to the bedrock. *Journal of Glaciology 48*(162), 369–385.

Lüthi, M. P., C. Ryser, L. C. Andrews, G. A. Catania, M. Funk, R. L. Hawley, M. J. Hoffman, and T. A. Neumann (2015). Excess heat in the Greenland Ice Sheet: dissipation, temperate paleo-firn and cryo-hydrologic warming. *The Cryosphere 9*, 245–253.

MacAyeal, D. R. (1997). EISMINT: Lessons in ice-sheet modeling. Technical report.

Meierbachtol, T. W., J. T. Harper, J. V. Johnson, N. F. Humphrey, and D. J. Brinkerhoff (2015). Thermal boundary conditions on western Greenland: Observational constraints and impacts on the modeled thermomechanical state. *Journal of Geophysical Research: Earth Surface 120*.

Mock, S. J. and W. F. Weeks (1965). The distribution ten-meter snow temperatures on the Greenland ice sheet. *Journal of Glaciology 6*(43), 23–41.

Morlighem, M., E. Rignot, J. Mouginot, H. Seroussi, and E. Larour (2014). Deeply incised submarine glacial valleys beneath the Greenland ice sheet. *Nature Geoscience 7*(6), 418–422.

Munneke, P. K., S. M. Ligtenberg, M. R. van den Broeke, J. H. van Angelen, and R. R. Forster (2014). Explaining the presence of perennial liquid water bodies in the firn of the Greenland Ice Sheet. *Geophysical Research Letters*.

Nye, J. F. (1955). Comments on Dr Loewe's letter and notes on crevasses. *Journal of Glaciology 2*, 512–514.

Nye, J. F. (1957). The Distribution of Stress and Velocity in Glaciers and Ice-Sheets. *Proceedings of the Royal Society A: Mathematical, Physical and Engineering Sciences 239*(1216), 113–133.

Nye, J. F. (1989). The Geometry of Water Veins and Nodes in Polycrystalline Ice. *Journal of Glaciology 35*(119), 17–22.

Palmer, S., A. Shepherd, P. Nienow, and I. Joughin (2011). Seasonal speedup of the Greenland Ice Sheet linked to routing of surface water. *Earth and Planetary Science Letters 302*(3-4), 423–428.

Parizek, B. R. and R. B. Alley (2004). Implications of increased Greenland surface melt under global-warming scenarios: ice-sheet simulations. *Quaternary Science Reviews*.

Phillips, T., S. Leyk, H. Rajaram, W. Colgan, W. Abdalati, D. McGrath, and K. Steffen (2011). Modeling moulin distribution on Sermeq Avannarleq glacier using ASTER and WorldView imagery and fuzzy set theory. *Remote Sensing of Environment 115*(9), 2292–2301.

Phillips, T., H. Rajaram, W. Colgan, K. Steffen, and W. Abdalati (2013). Evaluation of cryohydrologic warming as an explanation for increased ice velocities in the wet snow zone, Sermeq Avannarleq, West Greenland. *Journal of Geophysical Research: Earth Surface 118*(3), 1241–1256.

Phillips, T., H. Rajaram, and K. Steffen (2010). Cryo-hydrologic warming: A potential mechanism for rapid thermal response of ice sheets. *Geophysical Research Letters 37*(20).

Poinar, K. and I. Joughin (2016). The contribution of englacial latent heat transfer to seaward ice flux in western Greenland. *Journal of Glaciology* (in prep).

Polashenski, C., Z. Courville, C. Benson, A. Wagner, J. Chen, G. Wong, R. Hawley, and D. Hall (2014). Observations of Pronounced Greenland Ice Sheet Firn Warming and Implications for Runoff Production. *Geophysical Research Letters*, n/a–n/a.

Price, S. F., A. J. Payne, G. A. Catania, and T. A. Neumann (2008). Seasonal acceleration of inland ice via longitudinal coupling to marginal ice. *Journal of Glaciology 54*(185), 213–219.

Reeh, N. (1989). Parameterization of Melt Rate and Surface Temperature on the Greenland Ice Sheet. *Polarforschung 59*(3), 113–128.

Rennermalm, A. K., L. C. Smith, V. W. Chu, J. E. Box, R. R. Forster, M. R. van den Broeke, D. van As, and S. E. Moustafa (2013). Evidence of meltwater retention within the Greenland ice sheet. *The Cryosphere 7*(5), 1433–1445.

Rogozhina, I., J. M. Hagedoorn, Z. Martinec, K. Fleming, O. Soucek, R. Greve, and M. Thomas (2012). Effects of uncertainties in the geothermal heat flux distribution on the Greenland Ice Sheet: An assessment of existing heat flow models. *Journal of Geophysical Research 117*(F2), F02025.

Ryser, C., M. Lüthi, L. Andrews, M. J. Hoffman, G. A. Catania, R. L. Hawley, T. A. Neumann, and S. S. Kristensen (2014). Sustained high basal motion of the Greenland ice sheet revealed by borehole deformation. *Journal of Glaciology 60*(222), 647–660.

Schäfer, M., F. Gillet-Chaulet, R. Gladstone, R. Pettersson, V. A Pohjola, T. Strozzi, and T. Zwinger (2014). Assessment of heat sources on the control of fast flow of Vestfonna ice cap, Svalbard. *The Cryosphere 8*(5), 1951–1973.

Schoof, C. (2010). Ice-sheet acceleration driven by melt supply variability. *Nature 468*(7325), 803–806.

Schøtt, C., E. D. Waddington, and C. F. Raymond (1992). Predicted time-scales for GISP2 and GRIP boreholes at Summit, Greenland. *Journal of Glaciology*.

Selmes, N., T. Murray, and T. D. James (2011). Fast draining lakes on the Greenland Ice Sheet. *Geophysical Research Letters 38*.

Selmes, N., T. Murray, and T. D. James (2013). Characterizing supraglacial lake drainage and freezing on the Greenland Ice Sheet. *The Cryosphere Discussions 7*(1), 475–505.

Sergienko, O. V., T. T. Creyts, and R. C. A. Hindmarsh (2014). Similarity of organized patterns in driving and basal stresses of Antarctic and Greenland ice sheets beneath extensive areas of basal sliding. *Geophysical Research Letters*.

Seroussi, H., M. Morlighem, E. Rignot, A. Khazendar, E. Larour, and J. Mouginot (2013). Dependence of century-scale projections of the Greenland ice sheet on its thermal regime. *Journal of Glaciology 59*(218), 1024–1034.

Sevestre, H., D. I. Benn, and N. Hulton (2015). Thermal structure of Svalbard glaciers and implications for thermal switch models of glacier surging. *Journal of Geophysical Research*.

Shapero, D. R., I. R. Joughin, K. Poinar, M. Morlighem, and F. Gillet-Chaulet (2015). Basal Resistance for Three of the Largest Greenland Outlet Glaciers. *(in review)*, 1–48.

Shapiro, N. M. and M. H. Ritzwoller (2004). Inferring surface heat flux distributions guided by a global seismic model: particular application to Antarctica. *Earth and Planetary Science Letters 223*(1-2), 213–224.

Smith, L. C., V. W. Chu, K. Yang, C. J. Gleason, L. H. Pitcher, A. K. Rennermalm, C. J. Legleiter, A. E. Behar, B. T. Overstreet, S. E. Moustafa, M. Tedesco, R. R. Forster, A. L. LeWinter, D. C. Finnegan, Y. Sheng, and J. Balog (2015). Efficient meltwater drainage through supraglacial streams and rivers on the southwest Greenland ice sheet. *Proceedings of the National Academy of Sciences of the United States of America*, 201413024.

Sparks, D. W. and E. M. Parmentier (1991). Melt Extraction From the Mantle Beneath Spreading Centers. *Earth and Planetary Science Letters 105*(4), 368–377.

Stevens, L. A., M. D. Behn, J. J. McGuire, S. B. Das, I. Joughin, T. Herring, D. E. Shean, and M. A. King (2015). Greenland supraglacial lake drainages triggered by hydrologically induced basal slip. *Nature 522*(7554), 73–76.

Sundal, A. V., A. Shepherd, P. Nienow, E. Hanna, S. Palmer, and P. Huybrechts (2009). Evolution of supra-glacial lakes across the Greenland Ice Sheet. *Remote Sensing of Environment 113*(10), 2164–2171.

Sundal, A. V., A. Shepherd, P. Nienow, E. Hanna, S. Palmer, and P. Huybrechts (2011). Melt-induced speed-up of Greenland ice sheet offset by efficient subglacial drainage. *Nature 469*(7331), 521–524.

Tedesco, M., P. Alexander, J. E. Box, J. Cappelen, T. Mote, K. Steffen, R. S. W. van de Wal, J. Wahr, and B. Wouters (2013). [Arctic] Greenland ice sheet [in "State of the Climate in 2012"]. *Bulletin of the American Meteorological Society 94*, S121–S123.

Tedesco, M., I. C. Willis, M. J. Hoffman, A. F. Banwell, P. Alexander, and N. S. Arnold (2013). Ice dynamic response to two modes of surface lake drainage on the Greenland ice sheet. *Environmental Research Letters 8*(3), 034007.

Thomsen, H. H. (1988). Mass balance, ice velocity and ice temperature at the inland ice margin north-east of Jakobshavn, central West Greenland. *Rapp. Gronl. Geol. Unders 140*, 111–114.

Thomsen, H. H. and O. B. Olesen (1990). Continued glaciological investigations with respect to hydropower and ice–climate relationships, at Pâkitsoq, Jakobshavn, West Greenland. *Rapp. Grønl. Geol. Undersøgelse 148*, 83–86.

Thomsen, H. H., O. B. Olesen, R. J. Braithwaite, and C. E. Boggild (1991). Ice drilling and mass balance at Pakitsoq, Jakobshavn, central West Greenland. *Report of the Geological Survey of Greenland 152*, 80–84.

van Angelen, J. H., M. R. van den Broeke, B. Wouters, and J. T. M. Lenaerts (2013). Contemporary (1960–2012) Evolution of the Climate and Surface Mass Balance of the Greenland Ice Sheet. *Surveys in Geophysics 35*(5), 1155–1174.

van de Wal, R. S. W., W. Boot, C. J. P. P. Smeets, H. Snellen, M. R. van den Broeke, and J. Oerlemans (2012). Twenty-one years of mass balance observations along the K-transect, West Greenland. *Earth Syst Sci Data 4*, 31–35.

van de Wal, R. S. W., W. Boot, M. R. van den Broeke, C. J. P. P. Smeets, C. H. Reijmer, J. J. A. Donker, and J. Oerlemans (2008). Large and rapid melt-induced velocity changes in the ablation zone of the Greenland Ice Sheet. *Science 321*(5885), 111–113.

van den Broeke, M., J. Bamber, J. Ettema, E. Rignot, E. Schrama, W. J. van de Berg, E. van Meijgaard, I. Velicogna, and B. Wouters (2009). Partitioning Recent Greenland Mass Loss. *Science 326*(5955), 984–986.

van der Veen, C. J. (1998). Fracture mechanics approach to penetration of surface crevasses on glaciers. *Cold regions science and technology 27*(1), 31–47.

van der Veen, C. J. (2007). Fracture propagation as means of rapidly transferring surface meltwater to the base of glaciers. *Geophysical Research Letters*.

Vaughan, D. G. (1995). Tidal Flexure at Ice Shelf Margins. *Journal of Geophysical Research: Solid Earth 100*(B4), 6213–6224.

Vaughan, D. G., J. C. Comiso, I. Allison, J. Carrasco, G. Kaser, R. Kwok, P. Mote, T. Murray, F. Paul, J. Ren, E. Rignot, O. Solomina, K. Steffen, and T. Zhang (2013). Observations: Cryosphere. Technical report.

Vorkauf, M. (2014). *Modeling the influence of moulins and temperate firn on the vertical temperature profile of the Greenland Ice Sheet*. Ph. D. thesis, ETH Zurich.

Wang, W. L., H. J. Zwally, W. Abdalati, and S. Luo (2002). Modeling of ice flow and internal layers along a flowline through Swiss Camp, West Greenland. *Annals of Glaciology 34*(1), 303–308.

Weertman, J. (1973). Can a water-filled crevasse reach the bottom surface of a glacier? *IASH Publ*, 139–145.

Weertman, J. (1996). *Dislocation based fracture mechanics*. London: World Scientific.

Zdanowicz, C., A. S. Sowa, D. Fisher, N. Schaffer, L. Copland, J. Eley, and F. Dupont (2012). Summer melt rates on Penny Ice Cap, Baffin Island: Past and recent trends and implications for regional climate. *Journal of Geophysical Research: Earth Surface*.

Zwally, H. J., W. Abdalati, T. Herring, K. Larson, J. Saba, and K. Steffen (2002). Surface Melt-Induced Acceleration of Greenland Ice-Sheet Flow. *Science 297*(5579), 218–222.